

ORIGINAL ARTICLE

New insights into marine group III Euryarchaeota, from dark to light

Jose M Haro-Moreno^{1,3}, Francisco Rodriguez-Valera¹, Purificación López-García², David Moreira² and Ana-Belen Martin-Cuadrado^{1,3}

¹Evolutionary Genomics Group, Departamento de Producción Vegetal y Microbiología, Universidad Miguel Hernández, Alicante, Spain and ²Unité d'Ecologie, Systématique et Evolution, UMR CNRS 8079, Université Paris-Sud, Orsay Cedex, France

Marine Euryarchaeota remain among the least understood major components of marine microbial communities. Marine group II Euryarchaeota (MG-II) are more abundant in surface waters (4–20% of the total prokaryotic community), whereas marine group III Euryarchaeota (MG-III) are generally considered low-abundance members of deep mesopelagic and bathypelagic communities. Using genome assembly from direct metagenome reads and metagenomic fosmid clones, we have identified six novel MG-III genome sequence bins from the photic zone (Epi1–6) and two novel bins from deep-sea samples (Bathy1–2). Genome completeness in those genome bins varies from 44% to 85%. Photic-zone MG-III bins corresponded to novel groups with no similarity, and significantly lower GC content, when compared with previously described deep-MG-III genome bins. As found in many other epipelagic microorganisms, photic-zone MG-III bins contained numerous photolyase and rhodopsin genes, as well as genes for peptide and lipid uptake and degradation, suggesting a photoheterotrophic lifestyle. Phylogenetic analysis of these photolyases and rhodopsins as well as their genomic context suggests that these genes are of bacterial origin, supporting the hypothesis of an MG-III ancestor that lived in the dark ocean. Epipelagic MG-III occur sporadically and in relatively small proportions in marine plankton, representing only up to 0.6% of the total microbial community reads in metagenomes. None of the reconstructed epipelagic MG-III genomes were present in metagenomes from aphotic zone depths or from high latitude regions. Most low-GC bins were highly enriched at the deep chlorophyll maximum zones, with the exception of Epi1, which appeared evenly distributed throughout the photic zone worldwide.

The ISME Journal advance online publication, 13 January 2017; doi:10.1038/ismej.2016.188

Introduction

Marine archaea are important marine microbes in terms of their metabolic activity and abundance (Karner *et al.*, 2001; Li *et al.*, 2015). Ammonia-oxidizing Thaumarchaeota (Brochier-Armanet *et al.*, 2008) are the most abundant archaeal phylum in the oceans and have a key role in the marine nitrogen cycle (Konneke *et al.*, 2005; Qin *et al.*, 2014). Studies have also identified three major groups of marine Euryarchaeota: (i) group II (MG-II) (DeLong, 1992; Fuhrman *et al.*, 1992; Fuhrman and Davis, 1997; Massana *et al.*, 2000), (ii) group III (MG-III) (Fuhrman and Davis, 1997; Lopez-Garcia *et al.*, 2001a), and (iii) group IV (MG-IV) (Lopez-Garcia *et al.*, 2001b). So far,

there are no cultured representatives of marine Euryarchaeota and little is known about their physiology and ecological role in the oceans. MG-II are widely distributed within the euphotic zone of temperate waters. MG-II are the dominant archaeal community not only in the surface and in the deep chlorophyll maximum (DCM) (Massana *et al.*, 2000; Karner *et al.*, 2001; Herndl *et al.*, 2005; DeLong *et al.*, 2006; Galand *et al.*, 2010; Belmar *et al.*, 2011; Martin-Cuadrado *et al.*, 2015) but have also been found in deep-sea waters (Lopez-Garcia *et al.*, 2001a; Martin-Cuadrado *et al.*, 2008; Li *et al.*, 2015). The other two marine Euryarchaeota groups, MG-III and MG-IV, are considered to be rare components of deep-sea communities (Lopez-Garcia *et al.*, 2001a,b; Galand *et al.*, 2009).

MG-III were first described by Fuhrman and Davis, 1997 from deep marine plankton samples and have subsequently been found in 16S-rRNA gene surveys from most deep oceanic regions, albeit at very low abundance (Massana *et al.*, 2000; Lopez-Garcia *et al.*, 2001a,b), and by metagenomics throughout the water column in the central Pacific gyre (DeLong *et al.*, 2006).

Correspondence: A-B Martin-Cuadrado, Departamento de Producción Vegetal y Microbiología, Universidad Miguel Hernández, APARTADO 18, CAMPUS SAN JUAN, CP. 03550, San Juan de Alicante, Alicante 03550, Spain.
E-mail: amartin@umh.es

³These authors contributed equally to this work.

Received 9 May 2016; revised 25 November 2016; accepted 5 December 2016

However, occasionally, they have been identified at much higher proportions. For instance, 16S-rRNA sequences from MG-III represented one of the largest archaeal groups in the deep Arctic Ocean (>40% of tag sequences) (Galand *et al.*, 2009) and between 30% and 50% of the archaeal sequences from a deep (500–1250 m) Marmara Sea metagenome (Quaiser *et al.*, 2011). They were also relatively abundant (ca.18% of the total archaeal population) in the oxygen minimum zone (50–400 m) in the Eastern tropical South Pacific (Belmar *et al.*, 2011). Only a few studies report the presence of MG-III in the photic zone. They represented 0.4% of all the archaeal sequences obtained in surface Arctic waters (Galand *et al.*, 2009) and up to 10% in samples recovered along 4.5 years in the Mediterranean DCM (Galand *et al.*, 2010).

The initial analysis of three MG-III fosmid from deep-sea metagenomic libraries allowed a first glance at their metabolic potential (Martin-Cuadrado *et al.*, 2008). The presence of some fermentation-related genes led to the hypothesis that they could be facultative anaerobes. In a recent study, up to 3% of the single amplified genomes of archaea recovered from mesopelagic waters from South-Atlantic and North-Pacific gyres belonged to MG-III (Swan *et al.*, 2014). However, only two single amplified genomes classified as MG-III, SCGC-AAA-007-O11 (isolated at 800 m in the South-Atlantic sub-tropical gyre) and SCGC-AAA-288-E19 (from 770 m in the North-Pacific sub-tropical gyre), have been deposited in GenBank. Only the SCGC-AAA-288-E19 partial genome had ribosomal RNA genes that corresponded to MG-III, but contig annotation showed contamination with *Chloroflexi* (32 genome fragments out of the 102). Complete archaeal fosmids (452 adding up to 16 Mb of sequence) from deep Mediterranean samples belonging to MG-II/III have been published (Deschamps *et al.*, 2014) and five MG-III partial genomes (31–65% completeness) were assembled from metagenomes from the Guaymas basin (1993 m, Gulf of California) and the Mid-Cayman Rise (2040–2238 m and 4869–4946 m, Caribbean Sea) (Li *et al.*, 2015). Based on the genes present in these genomes, it was proposed that the microbes they represented are motile heterotrophs with different mechanisms for scavenging organic matter.

Binning the assembled fragments by oligonucleotide frequencies, GC content and differential recruitment in metagenomes is a successful strategy for the discovery of novel microbial lineages (Tyson *et al.*, 2004; Ghai *et al.*, 2012; Iverson *et al.*, 2012; Narasingarao *et al.*, 2012; Martin-Cuadrado *et al.*, 2015; Li *et al.*, 2015; Vavourakis *et al.*, 2016). We applied this approach to recover MG-III sequences using several metagenomic fosmid libraries from the Mediterranean Sea (collections KM3, AD1000 (Martin-Cuadrado *et al.*, 2008) and MedDCM-OCT2007 (Ghai *et al.*, 2010)) and from the assemblies of 16 metagenomes (four collections from the Mediterranean: MedDCM-JUL2012 (Martin-Cuadrado *et al.*, 2015), MedDCM-SEP2014 (this work),

Med-IO7–77mDCM and Med-Ae2–600mDeep (Mizuno *et al.*, 2016) and 12 from TARA microbiomes (Sunagawa *et al.*, 2015)). We obtained a total of eight different MG-III genome bins. Six of them belong to novel surface MG-III lineages distantly related to the previously described deep MG-III sequence bins (Li *et al.*, 2015). They are the first near-complete genomes of MG-III living in the photic zone. Some of them appear to be widespread in the ocean; their distribution in different water masses has been analyzed.

Materials and methods

Sampling and sequencing

A fosmid metagenomic library of ca. 13 000 clones was constructed with biomass recovered in October 2007 (50 m deep) at the Mediterranean DCM (38°4'6.64"N 0°13'55.18"W). Partial results of almost 7000 fosmid sequences have been described previously in Ghai *et al.* (2010) and Martin-Cuadrado *et al.* (2015). Metagenomes were also sequenced from samples recovered at the same location and at a similar depth the following years (MedDCM-JUL2012 (Martin-Cuadrado *et al.*, 2015) and MedDCM-SEP2014) from one sample recovered at the DCM from the Ionian Sea (Med-IO7–77mDCM) and from a sample collected from the deep Aegean Sea (Med-Ae2–600mDeep) (Mizuno *et al.*, 2016). For these metagenomes, sea water was collected and sequentially filtered on-board using a positive pressure system through a 20 µm pore filter followed by a 5 µm pore size polycarbonate filter and, finally, 0.22 µm pore size Sterivex filters (Durapore; Millipore, Billerica, MA, USA). Filters were frozen on dry ice and kept at –80 °C until processed in the laboratory. Filters were thawed on ice and then treated with 1 mg ml⁻¹ lysozyme and 0.2 mg ml⁻¹ proteinase K (final concentrations). Nucleic acids were extracted with phenol–chloroform–isoamyl alcohol and chloroform–isoamyl alcohol. Sequencing was carried out using Illumina HiSeq2000 (PE, 100 bp) (Macrogen, Seoul, Korea and BGI, Hong Kong).

'De novo' assembly, gene annotation and binning of the MG-III sequences

A schematic of the assembly pipeline is shown in Supplementary Figure S1. The assembly of the fosmids from the MedDCM-OCT2007, KM3 and AD1000 metagenomic fosmid libraries has been previously described (Ghai *et al.*, 2010; Deschamps *et al.*, 2014; Martin-Cuadrado *et al.*, 2015). Sequences from metagenomes MedDCM-JUL2012, MedDCM-SEP2014, Med-IO7–77mDCM and Med-Ae2–600mDeep were quality trimmed and assembled independently using IBDA-UD (Peng *et al.*, 2012) with the following parameters: –mink 70, –maxk 100, –step 10, –pre_correction. Gene predictions on the assembled sequences were carried out using Prodigal (Hyatt *et al.*, 2010). Ribosomal genes were identified using ssu-align (Nawrocki, 2009) and meta_rna (Huang *et al.*, 2009). Functional annotation was performed by comparing predicted protein

Table 1 General features of the MG-III bins and the composite genomes CG-MGIII

MG-III bin	No. of contigs	%GC ± s.d.	No. of Mb	% Genome (1) (2) (3) ^a	No. of genomes	Largest contig (Kb)	No. of CDS/nr CDS ^b	Intergenic region (bp)	Median gene size (bp)	CheckM ^c % contamination
Epi1	136	36.6 ± 0.9	2.95	80.0/35.1/83.0	2	120.8	3058/1307	42	752	—
CG-Epi1	25	36.6 ± 0.8	1.18	85.7/34.2/84.9	1	135.9	—/1106	40	792	2
Epi2A	34	36.0 ± 0.9	0.54	54.3/16.2/45.3	1	27.4	519/—	41	765	—
Epi2B	26	36.2 ± 0.9	0.56	57.1/18.0/54.7	1	79.1	525/—	40	768	—
Epi2C	10	36.1 ± 0.9	0.31	5.7/4.5/5.7	1	92.8	282/—	40	807	—
CG-Epi2	43	36.1 ± 1.1	1.22	80.0/30.6/75.5	1	101.9	—/1182	42	777	25
Epi3	35	35.9 ± 1.2	0.71	48.6/19.8/45.3	1	55.8	675/673	37	798	—
CG-Epi3	30	35.9 ± 1.2	0.79	62.9/24.3/62.3	1	71.7	—/741	40	786	0.8
Epi4	31	36.5 ± 0.8	0.66	34.3/15.3/39.6	1	47.2	612/610	37	794	—
CG-Epi4	24	36.4 ± 0.7	0.71	34.3/16.2/43.4	1	80	—/666	37	786	0
Epi5	18	36.1 ± 0.8	0.26	2.9/3.6/7.6	1	23.4	242/221	36	767	—
CG-Epi5	22	36.3 ± 0.8	0.39	2.9/4.5/9.4	1	47.6	—/370	38	804	0
Epi6	26	36.6 ± 0.9	0.88	51.4/15.3/54.7	1	111.1	854/594	47	705	—
CG-Epi6	26	36.3 ± 1.1	0.54	57.1/21.6/60.4	1	50.3	—/542	47	714	1.6
Bathy1	39	36.9 ± 0.9	1.2	54.3/23.4/60.4	1	94.7	1143/1007	46	807	—
CG-Bathy1	22	37.5 ± 1.8	1.04	60.0/26.1/64.2	1	211.7	—/988	46	792	4.8
Bathy2	37	64.6 ± 1.8	1.06	68.6/18.9/58.5	1	41.7	1023/654	40	771	—
CG-Bathy2	18	64.4 ± 1.5	0.77	68.6/21.6/58.5	1	130.1	—/704	41	816	2.4

Abbreviations: CDS, Coding DNA sequence; nr-CDS, non-redundant CDS.

^a(1) Raes et al. (2007); (2) Albersen et al. (2013); (3) Narasingarao et al. (2012).

^bnr-CDS; non-redundant CDS clustered at 80% similarity and 70% coverage.

^cParks et al., 2014.

sequences against the NCBI-nr database, Pfam (Bateman et al., 2004), arCOGS (Makarova et al., 2015) and TIGRFams (Haft et al., 2001) (cutoff *E*-value 10⁻⁵). Based on sequence similarity against the non-redundant NCBI database, the best hit for each gene was determined and used to bin to top-level taxa. *Bona fide* Euryarchaeota genome fragments were defined as having >50% of the predicted open reading frames with best hits to other Euryarchaeota genes. The resulting sequences were used to screen for their presence in several metagenomes (in subsets of 20 million reads, where applicable): the TARA data sets (Sunagawa et al., 2015), the GOS collection (Rusch et al., 2007), the depth profiles collections from the subtropical gyres of North Atlantic (Bermuda Atlantic Time Series, BATS) and North Pacific (Hawaii Ocean Time-Series, HOT) (DeLong, 2006; Coleman and Chisholm, 2010), several Mediterranean Sea metagenomes at different depths (Ghai et al., 2010; Quaiser et al., 2011; Smedile et al., 2012; Martin-Cuadrado et al., 2015), and a number of deep ocean and cold waters metagenomes (Alonso-Saez et al., 2012; Larsson et al., 2014). The collections coming from the surroundings of hydrothermal vents published in Li et al. (2015) were also included. The screening was performed using Usearch6 (Edgar, 2010), with a cutoff of 95% identity over an alignment length of at least 50 bp (approximately species-level divergence, Konstantinidis and Tiedje, 2005). To compare the results among different data sets, the number of reads was normalized to the metagenome size and the sequence length. The final coverage results were expressed as the number of reads per kilobase of the fragment per gigabase of metagenome collection (rpkg). Only metagenomes in which any of the MG-III sequences recruited reads at over 3 rpkg, a total of 33 metagenomes, were used for genome assembly (Supplementary Table S1).

All the sequences obtained from these assemblies were binned together in order to cluster them by their tetranucleotide frequencies, GC content and coverage values (Supplementary Figure S2 and Supplementary Table S1). Tetranucleotide frequencies were computed using the 'wordfreq' program from the EMBOSS package (Rice et al., 2000) and the coverage values were calculated as rpkg as described before. Only those clusters with >10 sequences and containing at least one gene marker with a clear affiliation to MG-III were retained. The phylogenetic assignment to MG-III was determined by the presence of at least one housekeeping gene in the same bin (see below). Following this method, a total of 375 genomic fragments >10 Kb could be classified into 10 different MG-III bins of sequences, Epi1, Epi2A, Epi2B, Epi2C, Epi3, Epi4, Epi5, Epi6, Bathy1 and Bathy2. We also considered 16 MG-III sequences that contained a ribosomal or a housekeeping gene but that could not be included in any of the bins by the criteria used (Supplementary Table S2).

In order to improve the completeness and remove the redundancy present in the initial MG-III bins,

Table 2 Environmental collections from where MG-III sequences were assembled

	Depth (m)	Fraction size (µm)	Epi1	Epi3	Epi4	Epi5	Epi6	Epi2A	Epi2B	Epi2C	Bathy1	Bathy2
Total, Kb			2950.4	707.0	631.3	259.7	848.7	542.7	564.7	305.0	1196.5	1061.4
ERR598993 (TARA_18) ^a	5	0.22–1.6	658.3									
ERR599073 (TARA_18) ^a	60	0.22–1.6	54.6									
ERR315859 (TARA_023) ^a	55	0.22–0.1.6					11.7					
ERR594297 (TARA_068) ^a	5	0.45–0.8	25.3									
ERR594294 (TARA_068) ^a	50	0.22–0.45	367.2				47.4					
ERR594348 (TARA_068) ^a	50	0.45–0.8	159.3									
ERR594335 (TARA_070) ^a	5	0.45–0.8	41.9									
ERR598942 (TARA_133) ^a	45	0.22–3		707.0		60.9						
ERR598983 (TARA_145) ^a	5	0.22–3				198.8		422.4	305.0			
ERR598996 (TARA_150) ^a	40	0.22–3	128.0									
ERR598976 (TARA_151) ^a	5	0.22–3	264.7									
ERR598986 (TARA_151) ^a	80	0.22–3	216.5									
MedDCM-OCT2007 ^b	60	0.22–5	1034.7		34.5		733.8					
MedDCM-JUL2012 ^c	75	0.22–5						542.7	142.3			
MedDCM-SEP2014 ^d	60	0.22–5			596.7							
AD1000 ^e	1000	0.22–5									38.7	
Med-Ae2–600mDeep ^f	600	0.22–5									1017.6	
Med-Io7–77mDCM ^f	77	0.22–5					55.8					
KM3 ^e	3000	0.22–5									140.1	1059.6

^aSunaguawa *et al.* (2015). ^bGhai *et al.* (2010). ^cMartin-Cuadrado *et al.* (2015). ^dThis work. ^eMartin-Cuadrado *et al.* (2008). ^fMizuno *et al.* (2016).

a second assembly was performed combining the sequences >10 Kb with the short paired-end Illumina reads of the metagenomes from where they were assembled (Tables 1 and 2 and Supplementary Figure S3). For each of the MG-III sequence bins, we used the BWA aligner (Li and Durbin, 2009; default parameters) to recover the short pair-reads that mapped onto the >10 Kb contigs. For each bin, these reads were then pooled and assembled together with the large DNA contigs previously assembled using SPAdes (Bankevich *et al.*, 2012). The final assemblies were termed ‘composite genomes’ (CGs), as they belong to similar MG-III cellular lineages (defined by the MG-III bins) but from different samples (Supplementary Table S3). The completeness of the reconstructed archaeal genomes was estimated by three different criteria and based on the presence of essential/core genes using HMMER (35, 112 and 53 genes (Raes *et al.*, 2007; Narasingarao *et al.*, 2012; Albertsen *et al.*, 2013)). An *E*-value <10⁻⁵ and an alignment coverage >65% were used as cutoffs to define homologs of the essential/core genes. Analysis of the contamination within the CGs was performed using CheckM (Parks *et al.*, 2014) (Table 1). Average nucleotide identity (ANI) and conserved DNA fraction between reconstructed and/or reference genomes were calculated based on the whole-genome sequence as in Goris *et al.* (2007) (Supplementary Figure S4). GC content was calculated using the ‘geecee’ tool from the emboss package (Rice *et al.*, 2000).

Phylogenetic analysis

16S-rRNA and 23S-rRNA gene sequences detected in the MG-III genomic fragments were used to retrieve rRNA gene sequences from the most closely related euryarchaeal genomes and selected genome

fragments in GenBank using BLAST (Altschul *et al.*, 1990). 16S-rRNA sequences from metagenome collections were screened and trimmed using ssu-align (Nawrocki, 2009). Archaeal 16S-rRNA and 23S-rRNA gene sequences were then aligned using MUSCLE (Edgar, 2004). Phylogenetic reconstructions were conducted by maximum likelihood using MEGA6-v.0.6 (Tamura-Nei model, 100 bootstraps, gamma distribution with (five discrete categories), all positions with <80% site coverage were eliminated) (Tamura *et al.*, 2013) (Supplementary Figure S5). For the protein trees of RecA, RpoB, SecY, geranylgeranyl glyceryl phosphate synthase, DnaK, GyrA, GyrB, photolyase and rhodopsin (Supplementary Figures S6–S14), sequences were selected based on existing literature. Sequences were aligned using MUSCLE (Edgar, 2004) and a maximum likelihood tree was constructed using MEGA6-v.0.6 (Jones-Taylor-Thornton model, 100 bootstraps, gamma distribution with five discrete categories, positions with <80% site coverage were eliminated). Taxonomic affiliation of the selected bins was also determined by a phylogenomic tree based on concatenates of several ribosomal proteins (L13, S9, L5, S8, L6, S5, S12, S7, L11, L3, L4, L2, L22, S3, L14, S17, L15 and L18). A balanced taxonomic representation of other archaeal genomes was included as reference. Shared proteins were concatenated and aligned using Kalign (Lassmann and Sonnhammer, 2005) and a maximum likelihood tree was made using MEGA6-v.0.6.

Genome comparisons

Synteny among the CG-MGIII was examined with CIRCOS (Krzywinski *et al.*, 2009) and defined as arrays of contiguous genes in tracts of DNA >5 Kb and having >70% of identity. For each of the MG-III bins, non-redundant protein databases were

constructed clustering the coding DNA sequences with UCLUST (Edgar, 2010) (cutoff: 80% similarity in 70% of their length). These subsets of proteins were compared among themselves using a reciprocal best-hit analysis of putative homologs by BLASTP. Reciprocal relations were plotted using CYTOSCAPE (Shannon *et al.*, 2003). In order to identify the unique proteins of each of the bins, UCLUST was used with a cutoff of 30% similarity along 70% of their length.

Accession numbers

Mediterranean metagenomes used for recruitment are available at NCBI-BioProjects: PRJNA257723 (MedDCM-SEP2014, MedDCM-JUL2012 and MedDCM-OCT2007), PRJNA305355 (Med-Io7–77mDCM, Med-Io16–70mDCM, Med-Io17–3500mDeep, Med-Ae1–75mDCM and Med-Ae2–600mDeep). Sequences >10 Kb and the reconstructed CGs genomes have been deposited in BioProject number: PRJNA335308. TARA metagenomes were downloaded from the European-Bioinformatics-Institute (<http://www.ebi.ac.uk/services/tara-oceans-data>).

Results and Discussion

General features of MG-III archaeal genomes

Following assembly and binning, we obtained 375 genomic fragments that clustered into 8 MG-III bins (Supplementary Figure S1). Six bins, Epi1–Epi6, were from epipelagic origin (photic zone) and contained a total of 386 genomic fragments with a total of 8.3 Mb. Two bins, Bathy1 and Bathy2, were from deep marine samples (aphotic zone) and contained 76 fragments for a total of 2.3 Mb. Manual inspection of the differential coverage of the sequences in each bin identified three subsets of Epi2, referred to as Epi2A, Epi2B and Epi2C. Further genomic comparisons indicated that these bins were very similar to each other (93–96% ANI, Supplementary Figure S4) and represent genomes from related species, likely within the same genus.

Remarkably, seven genome bins were formed by sequences primarily from a single sampling site (Table 2). The exception was Epi1, which includes sequences retrieved from nine different sites in the Mediterranean Sea, Atlantic and North-Pacific oceans. These findings suggest that the organisms represented by Epi1 are cosmopolitan in temperate epipelagic waters, whereas the other groups are only abundant enough to assemble from metagenomes at specific sites (endemic) or under transient environmental conditions causing significant growth (for example, blooms; see below).

To improve the analysis of each genome bin, a second assembly was performed and CGs were reconstructed using sequences from different samples and geographic origins (Supplementary Figure S1). These CGs are non-redundant and consist of genomic fragments from similar lineages of MG-III cells but not necessarily from the same sample. In this further

assembly, subsets Epi2A, 2B and 2C were condensed into a single bin, CG-Epi2. Genomic features of the genome bins can be found in Tables 1 and 2 and the complete list of the MG-III contigs and the CGs are given in Supplementary Tables S2 and S3. Using the criteria of Narasingarao *et al.* (2012), the genome bins with highest degree of completeness were CG-Epi1 (85%), followed by CG-Epi2 (75%) and the mesopelagic CG-Bathy1 (64%). Based on the number of different variants of single copy genes in each bin, all our CGs contained a single microbial species each (Supplementary Table S4).

All MG-III bins had low GC content (36–36.8%) with the exception of Bathy2 (64.2%). Previously described MG-III sequences from different bathypelagic samples were all high GC (62.8%–65.4%) except for Guaymas32 (36.8%) (Li *et al.*, 2015). It has been noted that GC content tends to increase with depth (Romero *et al.*, 2009; Mizuno *et al.*, 2016). Selection for less nitrogen demand has been proposed as the main drive toward low genomic GC content in free-living marine bacterioplankton. In epipelagic waters, nitrogen is more likely to be the limiting nutrient, in contrast to the dark, energy-limited but relatively nitrogen-rich, deep ocean (Dufresne *et al.*, 2005; Swan *et al.*, 2013; Batut *et al.*, 2014; Giovannoni and Nemergut, 2014). Nevertheless, Bathy1 and Guaymas32 have similar low GC content to surface MG-III bins, suggesting that other factors might be also important.

In general, epipelagic MG-III bins were more genetically heterogeneous. Among the low GC-MGIII bins, the ANI varied from 68% to 85.4%, whereas the high GC-MGIII bins (Bathy2 is 90.8% similar to Cayman92) showed higher degrees of conservation, with ANIs ranging 89.5% to 96.2% (Supplementary Figure S4). This apparently higher diversity of the epipelagic groups may reflect the chemical and physical heterogeneity of surface water layers, which are submitted to stronger hydrodynamic, seasonal and geographical variations (Bryant *et al.*, 2015). In contrast, MG-III representatives from the deep ocean inhabit a more stable environment and might consequently be less diverse, with more homogeneous genomes.

Phylogenetic affiliation of the genomic bins

Genes coding for rRNA are difficult to bin because (i) rRNA genes assemble poorly due to their conservation and duplication in genomes and (ii) they recruit metagenomic reads at much higher levels making coverage-based approaches impractical. Most of the rRNA sequences came from fosmid-libraries (Km3 and AD1000) and did not cluster within any of the bins described here. The only assigned 16S-rRNA sequence (372 bp) belonged to Bathy1 and it appears distantly related to the previously described OTU-D (Galand *et al.*, 2009) and DH148-W24 clusters (Lopez-Garcia *et al.*, 2001a,b) (Supplementary Figure S5a). A similar result was obtained with the 23S-rRNA gene identified in Bathy1 (Supplementary Figure S5b). Therefore, we

looked for other housekeeping genes that might be helpful to define the phylogenetic relationships of the novel MG-III with other archaea. We identified and constructed phylogenetic trees for RecA, RpoB, SecY, the geranylgeranylglyceryl phosphate synthase, DnaK and the two gyrase subunits, GyrA and GyrB (Supplementary Figures S6–S12). Although DnaK, GyrA and GyrB have a complex history of horizontal gene transfer (HGT) (Gribaldo *et al.*, 1999; Petitjean *et al.*, 2012; Raymann *et al.*, 2014), their phylogenetic analysis clearly showed the split between MG-II and MG-III sequences. The MG-III housekeeping genes retrieved from epipelagic waters clustered into two groups, one represented only by Epi2 and the other including Epi1, 3, 4, 5 and 6. Bathy2 appeared as a separate cluster from the epipelagic MG-III, and Bathy1 sequences appeared as the most divergent and basal branch. The phylogenomic analysis of the concatenated ribosomal proteins revealed a similar topology (Figure 1). The two epipelagic clusters shared similar GC content. Accordingly, they were named LowGC-MGIII (comprising two subclades: LowGC1-MGIII

(Epi1, 3, 4 and 6) and LowGC2-MGIII (Epi2 and Guaymas32)), and a separate clade, containing bins exclusively of bathypelagic origin (Bathy2, Cayman92 and Guaymas31), was named HighGC-MGIII. Bin Epi5 lacks the ribosomal operon, but it was included into the LowGC1-MGIII based on the phylogenetic analysis of the other housekeeping genes (Supplementary Figures S11 and S12). Bathy1 consistently appeared as a separate basal branch, which might reflect the intermediate depth (600 m), location (Aegean Sea) and physicochemical conditions (highly saline, relatively warm and extremely oligotrophic) of the samples contributing sequences to this genomic bin. The position of Guaymas32 (retrieved from 1993 m), which clusters with Epi2 (5–75 m), might be explained by the presence of two different microbial species in the Guaymas32 bin (Li *et al.*, 2015). One appears to be most similar to the surface Epi2 sequences (80.8% ANI), while the other is closer to the deeper Bathy1 sequences (72.9% ANI) (also observed in the synteny plot of Figure 2a) (see below). Another plausible explanation is that Guaymas32 might be a surface

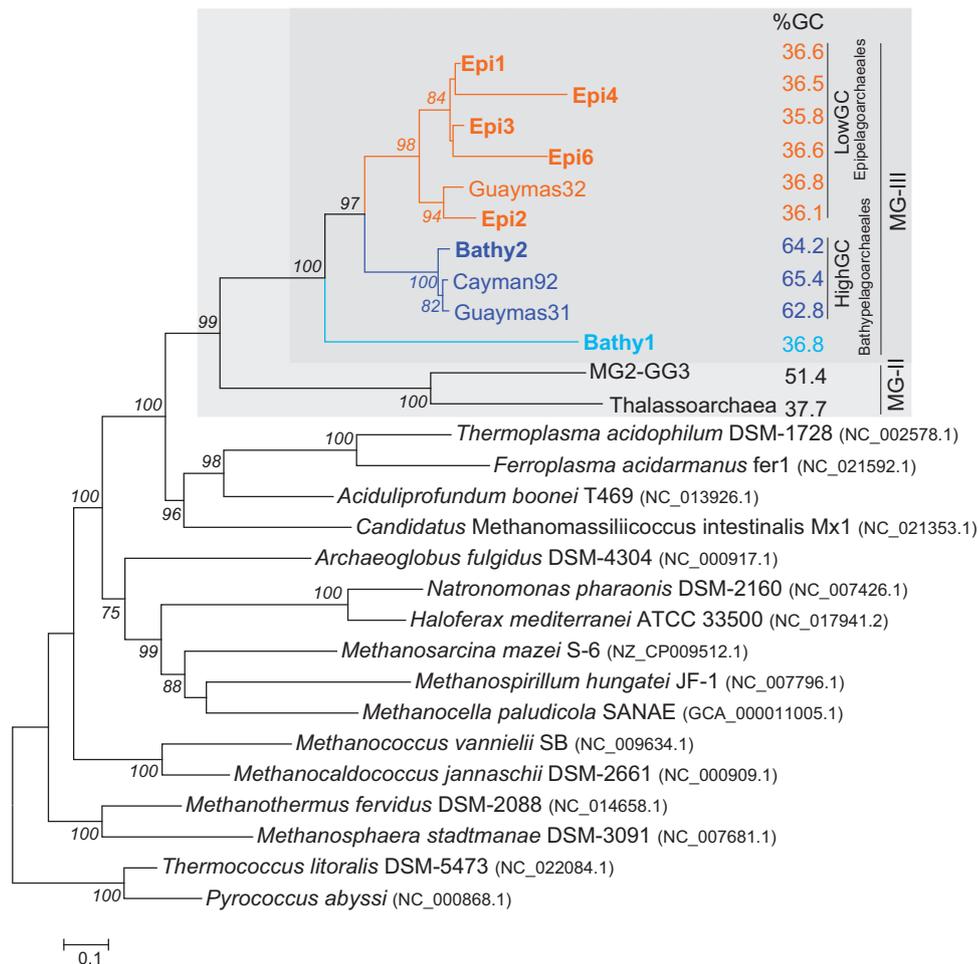


Figure 1 Maximum likelihood tree based on 18 ribosomal proteins concatenated present in draft MG-III archaeal genomes reconstructed from epipelagic and deep-sea metagenomes. Archaeal genomes from major orders of Euryarchaeota were included as references (accession number in brackets). Novel sequences from this work are shown in bold. Average GC content is shown on the right and colored depending on whether it is high or low GC. Only bootstrap values over >50% are shown.

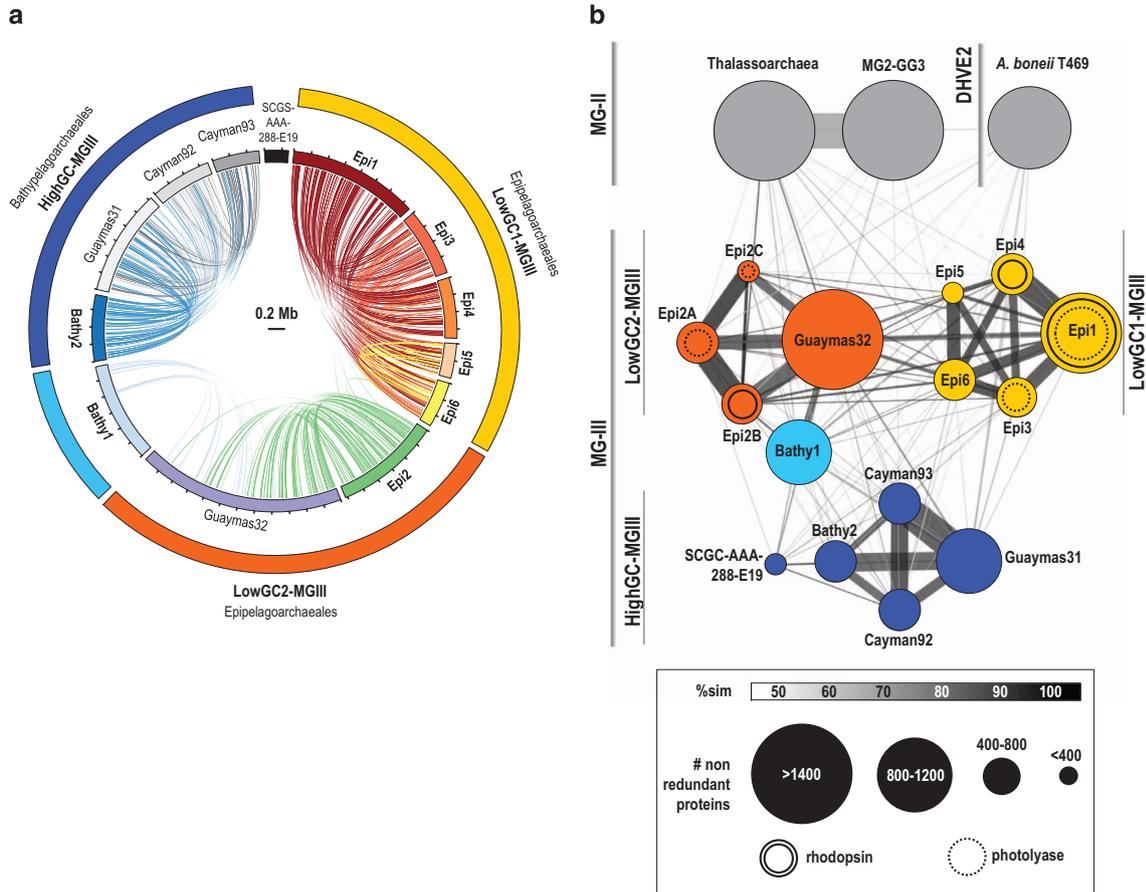


Figure 2 (a) Overview of genomic conserved synteny among the CG-MGIII genomes. Alignments > 5 Kb over 70% identity are shown. A color code is used for each MG-III bin. (b) Amino-acid comparison among the MG-III bins. Sets of non-redundant proteins (cutoff of 80% similarity over 70% of their length) were compared through reciprocal BLASTP and the average amino-acid similarity was plotted. Each circle represents a genome bin. Circles are interconnected as a function of the percentage of shared proteins and colored in accordance with their similarity. Size of the bins and width of the lines are explained in the legend. Proteins of the MG-II MG2-GG3 (Iverson *et al.*, 2012), Thalassoarchaea (Martin-Cuadrado *et al.*, 2015) and the deep-sea hydrothermal vent Euryarchaeota (DHVE2) *Aciduliprofundum boneii* T469 were included in the analysis.

organism dragged to the bottom by the continuous flux of surface microbes and particles into the deep. Indeed, Guaymas sediments are surprisingly enriched in surface planktonic microbes (Edgcomb *et al.*, 2002) when compared with other deep-sea sediments (Lopez-Garcia *et al.*, 2003). However, the lack of rhodopsins and photolyases (discussed below), together with higher recruitments from deep data sets, would suggest that Guaymas32 is a *bona fide* deep inhabitant.

Synteny and gene content

To examine the conservation of synteny across the different genome bins, we performed an all-versus-all genome comparisons with the available sequences of MG-III (Figure 2a). Within the two groups of LowGC-MGIII bins, large fragments have the same genomic context while synteny blocks are not conserved between LowGC-MGIII and HighGC-MGIII. In the case of LowGC-MGIII, the highest synteny was found between Epi1 and Epi4 (54 block alignments, 62% of Epi4 genome size). For LowGC-MGIII, only Epi2 and

Guaymas32 showed a significant synteny (56 block alignments, 38% of CG-Epi2). The low level of synteny between Bathy1 and other bins confirms that the microbes represented by this bin are very distant to the other LowGC-MGIII. Among the HighGC-MGIII bins, the highest synteny was found between Bathy2 and Guaymas31 (40 block alignments, 42% of CG-Bathy2) followed closely by Cayman92 and Guaymas31 (42 block alignments, 40.8% of the Cayman92 genome).

Non-redundant sets of proteins were obtained for each of the bins, including MG-II relatives, and compared between bins, retaining only the best hit for each protein and using a threshold of 80% similarity. The relationships between bins were then plotted in the similarity network showed in Figure 2b. This protein content analysis supported the clustering observed in the phylogenomic tree (Figure 1). Bathy1 and SCGC-AAA-288-E19 appeared distantly associated with Guaymas32 and Guaymas31, respectively. MG-III bins Epi1 with Epi4 had the largest percentage of shared proteins (34.8%), followed by Epi2B and Guaymas32 (24%) and then Bathy2 and Guaymas31

(25%). Only 8% of Epi1 proteins were conserved in Epi2 and 0.5% in Bathy2. Although these numbers may be biased owing to the incomplete nature of the bins, they suggest that marine Euryarchaeota are very diverse and contain very different gene pools. Similar results were obtained by Deschamps *et al.* (2014) who found that the core genome of the MGII/III Euryarchaeota was only 15.6% of their pangenome, while their flexible genome was almost triple that of the Thaumarchaeota.

Metabolic functional inference

Several studies have suggested that marine Euryarchaeota have a significant role in the degradation of dissolved organic matter in marine waters, for example, dissolved amino acids (Ouverney and Fuhrman, 2000) or carbohydrates (Boutrif *et al.*, 2011). The presence of large peptidases related to protein degradation, together with enzymes for the use of fatty acids in the MG2-GG3 genome suggested that particles might be a habitat for MG-II Euryarchaeota (Iverson *et al.*, 2012; Orsi *et al.*, 2015). MG-II shared various features with the deep MG-III described by Li *et al.* (2015), suggesting that they might be aerobic heterotrophs that use proteins and polysaccharides as major energy source. In order to infer different lifestyles, the predicted open reading frames were functionally classified according to the arCOG categories and their frequencies in the different genomes compared (Supplementary Tables S5 and S6 and Supplementary Figure S15).

Central carbon metabolism

MG-III genomes harbored enzymes for glycolysis, the tricarboxylic acid cycle and oxidative phosphorylation, indicating aerobic respiration (Supplementary Table S7). However, owing to the incomplete nature of these genomes, not all genes could be found, and some predictions need to be taken cautiously, especially for Bathy2. We found genes for the complete tricarboxylic acid cycle in LowGC-MGIII but three genes were absent in Bathy1. Remarkably, only the aconitase and the fumarase were found in Bathy2. As was observed in some MG-II (Martin-Cuadrado *et al.*, 2015), MG-III appears to possess most of the enzymes of the Embden–Meyerhof–Parnas (EMP) pathway for metabolism of hexose sugars, with the exception of the first and the last enzymes of the pathway. We were unable to find any other enzyme that could serve as an alternative for the missing glucokinase. For the final step of the EMP, we propose that phosphoenolpyruvate synthase, found in all of our MG-III bins, might be able to function bi-directionally and substitute for the missing pyruvate kinase, allowing the EMP to function in both directions, gluconeogenic and glycolytic. Likewise, we found typical gluconeogenesis enzymes such as phosphoenolpyruvate carboxykinases in the LowGC-MGIII and Bathy1 bins, as well as subunits of

the pyruvate/oxaloacetate carboxyltransferase in all the MG-III bins. We were unable to find glucose 1-dehydrogenase, gluconolactonase and 2-keto-3-deoxy gluconate aldolase homologs, suggesting that the Entner–Duodoroff hexose catabolic pathway is not present in the MG-III, unlike findings in other Euryarchaea (Makarova *et al.*, 1999; Makarova and Koonin, 2003; Hallam *et al.*, 2006).

Only a small number of amino-acid synthases were found in MG-III: cysteine in Bathy1 and Bathy2, glutamine in LowGC-MGIII, and for glutamate in all MG-III bins. Remarkably, many enzymes for *de novo* biosynthesis were missing, including those for synthesizing methionine, arginine, threonine, histidine, aromatic amino acids and branched amino acids (Supplementary Table S7). However, we observed multiple genes related with the uptake and transformation of peptides or amino acids in our MG-III bins, indicating that these organisms are capable of taking up amino acids from the environment and incorporating them into their proteins. For example, we found genes for permeases for lysine/arginine (all bins), histidine (Bathy2), glutamine (LowGC-MGIII and Bathy1), proline (LowGC-MGIII and Bathy1) and polar amino acids (Bathy2). Also, several ABC-transporter-systems were found for peptides and oligopeptides; for example, Dpp-ABC-type dipeptide/oligopeptide transporters (in all) and Liv-ABC-type branch amino-acid transporters (LowGC-MGIII and Bathy1). Several enzymes involved in the degradation of amino acids were also found, including dehydrogenases for alanine (all bins), glutamate (all bins), threonine (LowGC-MGIII and Bathy2) and proline (LowGC-MGIII), as well as several aminotransferases for branched-chain amino acids (LowGC-MGIII and Bathy1) and aspartate/tyrosine/aromatic aminotransferases (LowGC-MGIII and Bathy1). These findings suggest that there may be differences in the substrates used by the different MG-III groups. Indeed, although several subtilase-family proteases (arCOG00702 and arCOG02553) were present in all bins, some peptidases had limited distributions: dipeptidyl-aminopeptidases (LowGC-MGIII and Bathy1), C1A-peptidases (LowGC-MGIII), C25-peptidases (Bathy1), Xaa-Pro aminopeptidases (Bathy2), and several AprE-like subtilisins (arCOG06823, present in LowGC-MGIII and arCOG03610 present in Bathy1) (Supplementary Table S6).

Carbohydrates can be important carbon sources and, with the exception of Bathy1, several proteins with sugar-binding domains were found in all the bins (lectin and laminin-like). In the Epi6 bin, a cutin-like hydrolase was found (37% similar to a hydrolase from the Bacterioidetes *Rufibacter* sp. DG15C). Cutin is a polyester composed of hydroxyl/hydroxyepoxy fatty acids present in plants, and cutinases are produced by pathogenic fungi as extracellular degradative enzymes (Chen *et al.*, 1997). Lipo-oligosaccharide transport systems (*nodI/J*-like genes) and phosphonate transporters were found exclusively in the LowGC-MGIII. As observed in MG-II Thalamoarchaea (Martin-Cuadrado

et al., 2015), multidrug and antimicrobial peptide transporters (ABC-type) together with several permeases for drug/metabolites (RhaT-like family) were also abundant in all MG-III bins. Although the nature of the substrates is difficult to ascertain, these transporters may be involved in coping with high environmental concentrations of toxins such as those produced by cyanobacterial and algal blooms.

Oxygen. The presence of superoxide dismutase in all MG-III bins, together with several genes for alkyl-hydroperoxide reductases in LowGC1-MGIII and Bathy1, suggests that these microbes must cope with oxygen radicals. Complete cytochrome-C and B-B6 oxidase subunits operons were also found in LowGC1-MGIII and Bathy1 and Bathy2 bins. Copper-binding proteins and haloarchaeal-like halocyanins were found in proximity of these operons, an arrangement similar to that described for MG-II Thalassoarchaea (Martin-Cuadrado *et al.*, 2015). It has been suggested that MG-II could be facultative anaerobes (Martin-Cuadrado *et al.*, 2008; Belmar *et al.*, 2011) and that sulfate could be used as terminal electron acceptor. Although no sulfate reductase-like proteins could be identified in our MG-III bins, several phosphate/sulfate permeases could be identified in Epi6 and Bathy2 and were also present in Guaymas31/32 and Cayman92. Pterin-based molybdenum enzymes (for example, sulfite oxidase, xanthine oxidase and dimethyl sulfoxide reductase) function under anaerobic conditions whereby their respective cofactors serve as terminal electron acceptors in respiratory metabolism (Schwarz *et al.*, 2009). For Bathy2 (fosmid Km3–43-F08), a novel operon for the molybdopterin biosynthesis, was found (catalytic domains, MOCS1/S2/S3, have <55% similarities in the nr-database). However, we could not find any of the pterin-based enzymes.

Light-related genes. The presence of photolyases/cryptochromes among the LowGC-MGIII bins supports our hypothesis that they are *bona fide* epipelagic microbes (Figure 3a). Photolyases are proteins capable of photorepairing ultraviolet-induced pyrimidine dimers in the presence of light (Essen, 2006; Essen and Klar, 2006). Cryptochromes are proteins structurally similar to photolyases that act as blue light photoreceptors or regulators of the circadian rhythm (Cashmore *et al.*, 1999) but that have lost the enzymatic photolyase activity (Chaves *et al.*, 2011). Up to now, seven major classes of photolyase/cryptochrome families have been found (Scheerer *et al.*, 2015). Interestingly, while the subunits found in Epi1 and Epi3 have similarity with eukaryotic cryptochromes (38–49%), the photolyases found in Epi2A and Epi2C bins have their highest similarities with Planctomyceales homologs (30–52%), suggesting potential inter-domain HGT events. Five related genes, a phytoene synthase, a phytoene-desaturase, an histidine kinase, a sugar-epimerase and one hypothetical protein, were found adjacent to the photolyase gene. At the equivalent genomic position, the aphotic Guaymas32

had neither the photolyase nor the associated genes mentioned above (downstream from a 23S-rRNA gene) (Figure 3a). The phylogenetic origin of the genes flanking the photolyases was analyzed and, in several cases, were most closely related to homologs from Bacteroidetes/Planctomycetes, again suggesting instances of HGT. These included a chaperone involved in protein secretion that was 76% similar to a *Rhodopirellula mairorica* homolog, a nitroreductase that was 75% similar to a *Gracilimonas tropica* homolog and a sugar-epimerase next to the photolyase that was 58% similar to a *Pirellula staley* protein. Likewise, a hypothetical protein adjacent to the photolyase in Epi1 and Epi3 was most closely related to eukaryotic genes, suggesting that this pair of genes may have been transferred together.

Epipelagic bins Epi1-2-3 all contained rhodopsins (Figure 2b) indicative of a photoheterotrophic lifestyle (Beja *et al.*, 2000; Fuhrman *et al.*, 2008; Inoue *et al.*, 2013). In contrast, and consistent with previous reports (Deschamps *et al.*, 2014; Li *et al.*, 2015), Bathy1 and Bathy2 did not have rhodopsins. Phylogenetically, MG-III rhodopsins cluster with bacterial proteorhodopsins rather than with the euryarchaeal rhodopsins previously described for MG-II (Iverson *et al.*, 2012; Martin-Cuadrado *et al.*, 2014), suggesting that they may have been acquired by HGT from bacteria (Supplementary Figure S14). The analysis of key residues showed that all of these MG-III rhodopsins are proton pumps (Inoue *et al.*, 2013) with a glutamine (Q) in the characteristic spectral tuning residue site indicating their ability to absorb light from the blue range (Supplementary Figure S16). In deeper waters (down to 300 m), only blue light remains available and blue rhodopsins are more suitable for generating energy. Therefore, epipelagic MG-III archaea seem to prefer low-light environments rather than the highly irradiated uppermost surface. Indeed, epipelagic MG-III bins recruited better from DCM or subsurface pelagic metagenomes (~50–70 m) than from surface (5 m) ones (see below). Genomic comparisons with MG-II rhodopsins (Martin-Cuadrado *et al.*, 2014) revealed two new genomic contexts for this gene (Figure 3b). Interestingly, one of the clusters also contains one of the photolyase genes previously mentioned (Figure 3, contig Epi3-ERR598942-C530). Downstream from the rhodopsin genes, a gene for an unknown GYD domain protein was present. In cyanobacteria, proteins containing GYD and KaiC domains are involved in generating circadian rhythms (Chang *et al.*, 2015). This raises the possibility that epipelagic MG-III Euryarchaeota may also have a circadian rhythm. A similar genome segment was found in two Guaymas32 sequences but, in these cases, the rhodopsin and the GYD domain-containing protein were absent.

The phylogenetic relationships of photolyases and rhodopsins, their proximity in at least one of the MG-III bins, together with the multiple putative HGT events observed in the nearby genes, leads us to

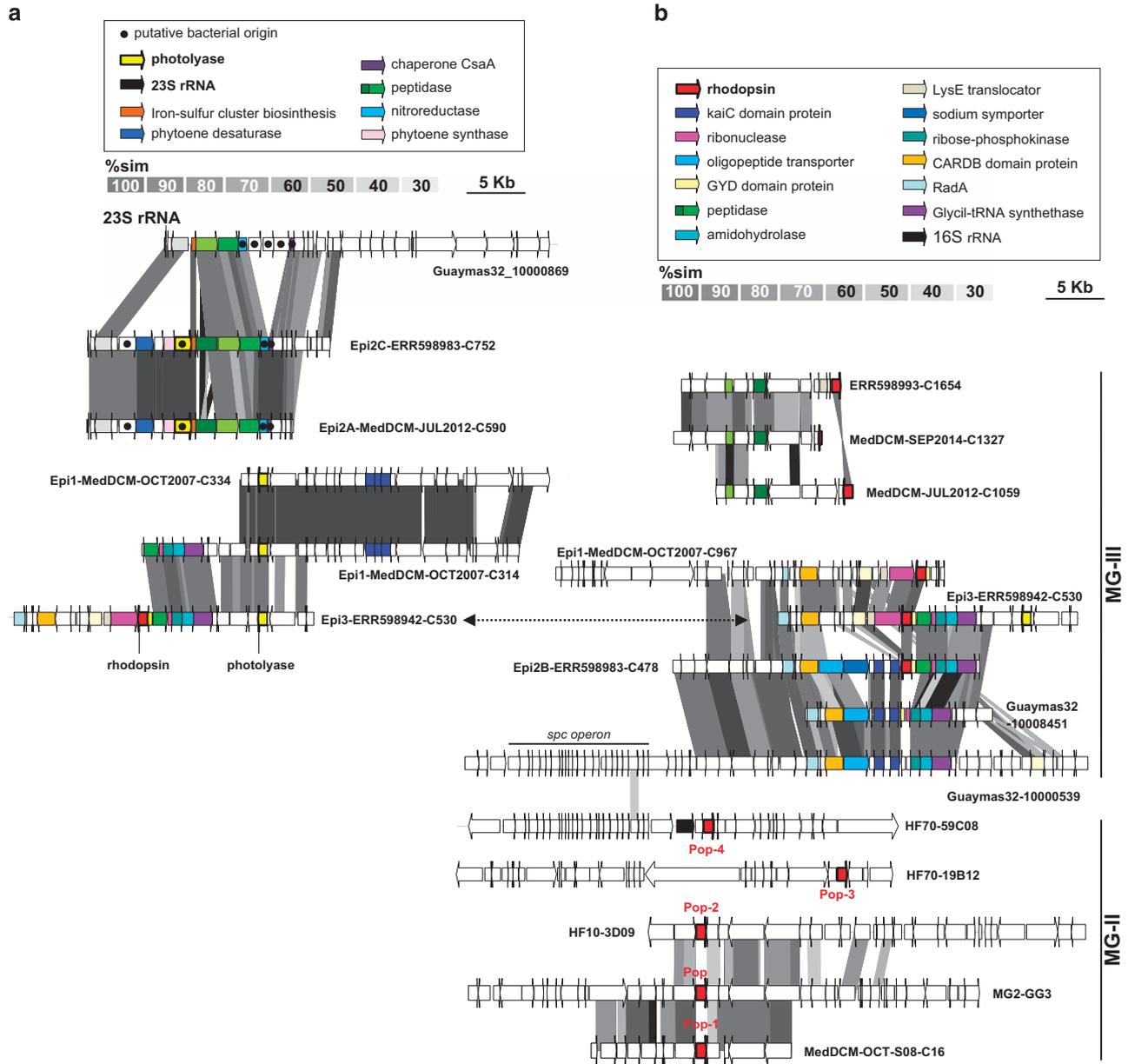


Figure 3 (a) Comparative genomic organization of MG-III sequences containing photolyases (in yellow). (b) Comparative genomic organization of MG-III sequences containing rhodopsins (in red) in context with other genomic fragments containing the MG-II Pop, Pop-1, Pop-2, Pop-3 and Pop-4 rhodopsins (bottom). Conserved genomic regions are indicated by gray shaded areas, gray intensity being a function of sequence similarity by TBLASTX. Particular open reading frames mentioned in the text are highlighted by a graphic code (see legend).

hypothesize an ancestral ‘dark nature’ for MG-III. These light-related genes would have been recently transferred from epipelagic bacteria to MG-III, probably long after the massive HGT events that have been detected prior to the diversification of several mesophilic archaeal clades, including MGII/III (Deschamps *et al.*, 2014; Lopez-Garcia *et al.*, 2016). The acquisition of proteorhodopsins, together with ultraviolet-protection photolyases, would have promoted a better adaptation to the oligotrophic surface waters allowing MG-III clades to expand into new photic niches.

Structural components

Cell envelope. One of the advantages of generating environmental fosmid sequences is that they allow the unequivocal assembly and detection of the so-called ‘metagenomic islands’ (Coleman *et al.*, 2006; Cuadros-Orellana *et al.*, 2007; Rodriguez-Valera *et al.*, 2009). These are clone-specific genome areas that, owing to their low coverage, are rarely assembled from metagenomic data sets but can be easily identified in reference-genome recruitment plots in the form of empty (or little populated) areas

with virtually no environmental homologs. One example can be observed in CG-Epi1. The area of the genome shown in Figure 4b (labeled with an

asterisk) is enriched in genes needed for cell wall biosynthesis and contains several glycosyltransferases (type I/IV), together with polysaccharide

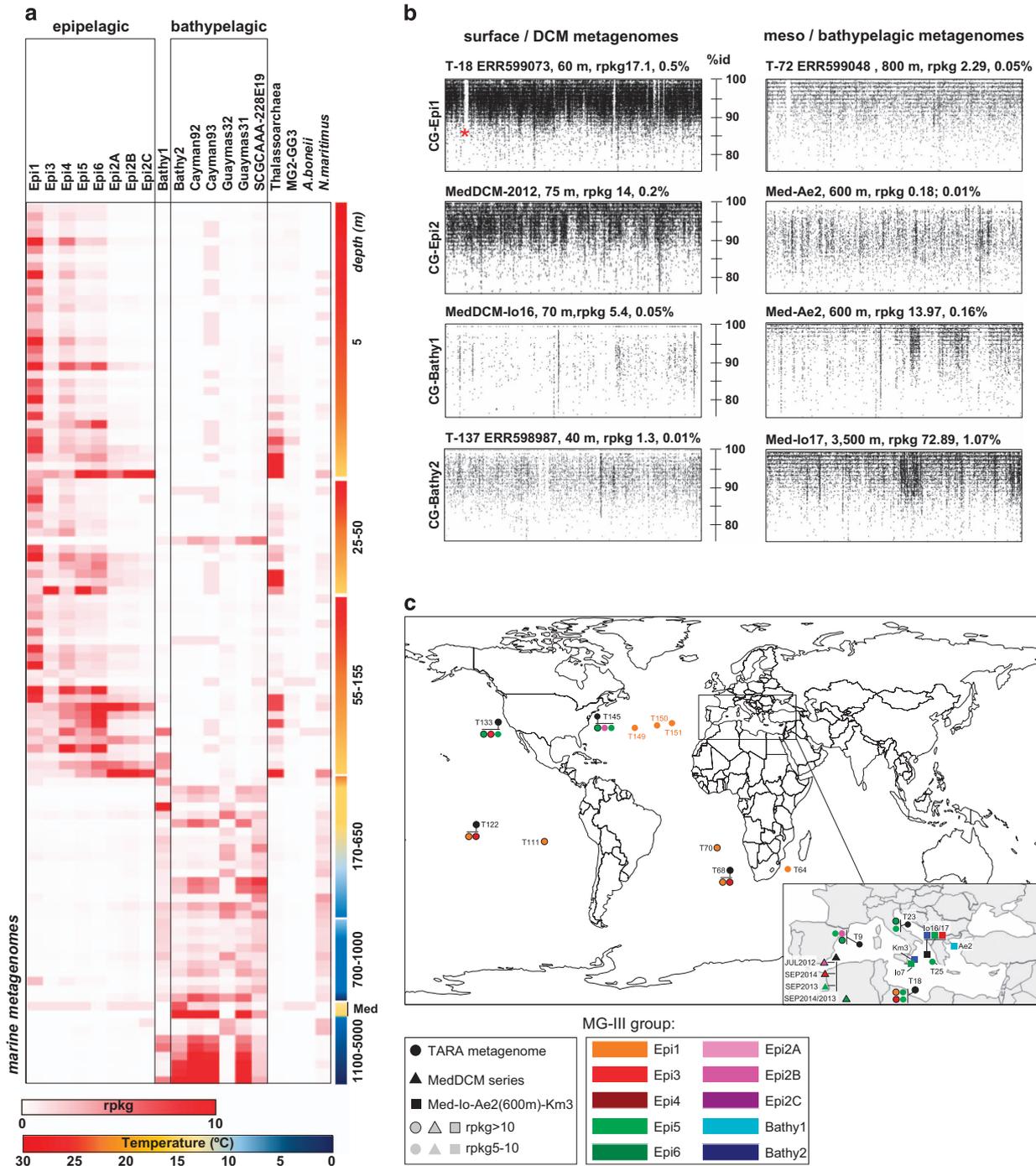


Figure 4 (a) Heat map of the number of rpkg of each CG-MGIII of this work together with the ones of Li *et al.* (2015), MG-II and other archaea genomes used as references in 106 different metagenomes from different geographical points and depths. Only those collections in which any of the MG-III sequences recruited rpkg > 1 were represented. (b) Recruitment plots of the CG-Epi1, CG-Epi2, CG-Bathy1 and CG-Bathy2 genomes in the metagenomes where they were better represented, from surface (<200 m) and bathypelagic (> 500 m) (BLASTN-based, see Methods section). Rpkg and the percentages of the total of the reads with an identity bigger than > 95% are indicated. (c) Worldwide distribution of the CG-MGIII determined by metagenomic fragment recruitment against public metagenomic databases. Only samples where the CGs recruited rpkg > 5 are indicated in the map (cutoff: %identity > 95% in > 50 bp coverage). TARA spots are indicated by T#station.

synthases and genes for carbohydrate modification (acyltransferases and aminotransferases). The presence of several lipopolysaccharide biosynthesis proteins in all MG-III bins suggests a more complex cell envelope than a protein layer (S-layer). Adjacent to the CG-Epi1 island, we found a giant protein of 7258 amino acids with no similarity in sequence databases. These types of proteins have previously been observed in several bacterial and archaeal genomes (Reva and Tummeler, 2008; Strom *et al.*, 2011) and have been hypothesized to have a role in defense against predation or in cell adhesion. Although we could not predict any function for it, the presence of lectin/glucanase domains (laminin_G3), glycosyl-transferase domains (RfaB), several beta-helix repeats and copper-binding domains (NosD) suggest an extracellular function. Large proteins (>5000 amino acids) with similar domains were also detected in other bins (Epi2-3-5). The similarity found between the giant proteins present in Guaymas31 and Bathy2 (90%) was remarkable.

Flagellum/Pili. Many archaeal surface structures are assembled by mechanisms related to the assembly of bacterial type IV pili (Lassak *et al.*, 2012). With the exception of Epi5, we found several sequences containing two concatenated *flaJ* genes (implicated in archaeal flagellum assembly) followed by a *flaI* gene (a transcriptional activator). Syntenic operons were also found among deep-MG-III in Li *et al.* (2015). However, these gene clusters are very different from the flagellar operon found in MG2-GG3 (Iverson *et al.*, 2012) or in any other Euryarchaeota described to date (Jarrell and McBride, 2008; Jarrell *et al.*, 2010). Although it has been claimed that the genes found might be enough to build a functional flagellum (Li *et al.*, 2015), the lack of a more complex gene cluster suggests that this operon might be involved in a secretion system translocating proteins rather than in cell motility.

Prevalence in the marine environment

To evaluate the relative abundance of the novel MG-III genomes, we used the non-redundant CGs to recruit reads from >200 metagenomic data sets that provide reasonably complete coverage of open-ocean waters from around the world. Among them, 106 gave values higher than one rpkg for any of the CGs tested (Figure 4 and Supplementary Table S1). Negative results are probably due to the small size of the data sets (for example, GOS) that may have poor representation of less abundant organisms. Although a considerable number of MG-III clones have been detected in cold waters such as the deep Atlantic layer of the central Arctic Ocean, (Galand *et al.*, 2009), the MG-III bins described here were not well represented in metagenomes from cold water regions such as polar regions (Alonso-Saez *et al.*, 2012), the Baltic (Larsson *et al.*, 2014) or the northeast subarctic Pacific (Allers *et al.*, 2013). This may suggest that there are other abundant MG-III

groups present in high latitudes that have yet to be discovered. Even in warmer latitudes, our LowGC-MG-III bins only represent a small fraction of the total prokaryotic population of photic marine habitats. The highest abundance we found was for CG-Epi1 that accounted for 0.5% of the reads in the samples from the Mediterranean station TARA-018 (ERR599073 collection) (Figure 4b). The deep MG-III bins recruited slightly more. For instance, CG-Bathy2 recruited up to 1% of the reads in the deep sample Med-Io17 (3500 m).

Figure 4 shows a clear correlation of the two MG-III groups with depth (as already suggested by the origin of the assembled bins). Most LowGC-MGIII bins are only present in epipelagic collections, while the HighGC-MGIII plus the LowGC Bathy1 and Guaymas32 were clearly bathy or mesopelagic. CG-Epi1 seemed to be evenly distributed throughout the photic zone, but CG-Epi3, 5 and 6 increased at deeper waters (25–155 m, including the DCM) and the three CG-Epi2 showed an increase in even deeper photic zone waters. Bathy1 has its maximum at mesopelagic waters (Adriatic Sea 600 m), but it was also detected in colder bathypelagic waters (for example, the metagenomes from the Cayman-Rise and Guaymas Basin). CG-Bathy2 together with the Cayman and Guaymas bins revealed a strong correlation with deeper waters with much higher abundance in metagenomic collections <1000 m. These bins were more abundant in the warmer (13 °C) and saltier Mediterranean deep samples (KM3, 3000 m and Io17, 3500 m deep), although the temperature in most bathypelagic waters, where these microbes were detected (global ocean), typically decreases down to <5 °C. Overall, these numbers indicate that MG-III cells are relatively minor components of the archaeal communities in the photic and aphotic zones.

Using the Mediterranean DCM time series data sets, we found significant temporal variation in the abundance of the different GC bins despite a relatively constant abundance of reads attributable to euryarchaeal 16S rRNA genes (Supplementary Figure S17). For example, CG-Epi2A predominated in 2012, whereas CG-Epi6 was dominant in 2013 and CG-Epi4 in 2014. In the case of MG-II, it has been experimentally demonstrated that eukaryotic phytoplankton additions stimulate their growth in bottle incubations (Orsi *et al.*, 2015). Also, MG-II became one of the most abundant organisms (up to 40% of prokaryotes) in a phytoplankton bloom where diatoms, small flagellates and picophytoplankton dominated consecutively (Needham and Fuhrman, 2016). In order to know whether MG-II and the genomes of MG-III described here respond to similar blooming patterns, we measured the recruitment of available MG-II genomes in the metagenomes from which MG-III were assembled. The results show very low numbers for MG-II genomes in these samples, close to 100 times less than for MG-III genomes (Supplementary Figure S18). These data indicate that, despite being closely related and using similar substrates, MG-II and MG-III do not bloom concurrently.

Using published plankton-interactome data (Lima-Mendez *et al.*, 2015), we constructed an interaction network for MG-III archaea (Supplementary Figure S19). The results showed that MG-III coexists mainly with Metazoa and Dinophyta, which represented 50.6% and 23.5% of the total of interactions observed. These findings may indicate that MG-III cells could be attached to other organisms and only sporadically be released to the environment.

Conclusions

The photic zone of the oligotrophic ocean, one of the largest microbial habitats on Earth, has been extensively explored by molecular and genomic approaches (DeLong, 1992; DeLong *et al.*, 1999; Venter *et al.*, 2004; Rusch *et al.*, 2007; Sunagawa *et al.*, 2015). Nevertheless, many epipelagic microbes remain to be characterized. Using metagenomics, we have uncovered eight new groups of planktonic marine Euryarchaeota that likely represent novel taxonomic orders or at least families. Based on differences in genome content and sequence identity, we propose the following nomenclature: Epipelagoarchaeales for the LowGC-MGIII and Bathypelagoarchaeales for the HighGC-MGIII. A separate and basal clade with low GC content but apparently living in the dark ocean (Bathy1) has also been uncovered. Genome comparisons between these new groups together and previously described MG-III genomes (Li *et al.*, 2015) showed a marked differentiation between MG-III from photic and aphotic layers. Genomic analysis indicates that at least some representatives Epipelagoarchaeales (Epi1–Epi6) are planktonic photoheterotrophs. Two other groups with the Epipelagoarchaeales, Bathy1 and Guaymas32, lack genes indicating photoheterotrophy and are likely mesopelagic microbes with diverse metabolic capabilities. We hypothesize that the low GC content characteristic of the Epipelagoarchaeales may be an adaptation to the nitrogen limitation of surface waters. It is remarkable that all marine Euryarchaeota appear to possess similar metabolic profiles based on heterotrophic degradation of polymers and proteins (Iverson *et al.*, 2012; Martin-Cuadrado *et al.*, 2014; Li *et al.*, 2015; Orsi *et al.*, 2015). The broad diversity of marine microbes exploiting this habitat is likely a reflection of the enormous diversity of metabolic substrates available. Our data suggest a possible interaction of MG-III with eukaryotic cells and, more specifically, with metazoa.

Conflict of Interest

The authors declare no conflict of interest.

Acknowledgements

We are thankful to José de la Torre for editing the manuscript. We are thankful to L Gasperini and G Bortoluzzi of the Instituto di Geologia Marina (ISMAR), CNR, Bologna (Italy) for allowing PLG to participate in the

Marmara2010 R/V Urania cruise during which part of the samples analyzed in this study were collected. This work was supported by projects MEDIMAX BFP2013–48007-P from the Spanish Ministerio de Economía y Competitividad, MaCuMBA Project 311975 of the European Commission FP7, project AQUAMET II/2014/012 from the Generalitat Valenciana and by the French Agence Nationale de la Recherche (ANR-08-GENM-024–001, EVOL-DEEP). JHM was supported with a PhD fellowship from the Spanish Ministerio de Economía y Competitividad.

References

- Albertsen M, Hugenholtz P, Skarshewski A, Nielsen KL, Tyson GW, Nielsen PH. (2013). Genome sequences of rare, uncultured bacteria obtained by differential coverage binning of multiple metagenomes. *Nat Biotechnol* **31**: 533–538.
- Alonso-Saez L, Waller AS, Mende DR, Bakker K, Farnelid H, Yager PL *et al.* (2012). Role for urea in nitrification by polar marine Archaea. *Proc Natl Acad Sci USA* **109**: 17989–17994.
- Altschul SF, Gish W, Miller W, Myers EW, Lipman DJ. (1990). Basic local alignment search tool. *J Mol Biol* **215**: 403–410.
- Allers E, Wright JJ, Konwar KM, Howes CG, Beneze E, Hallam SJ *et al.* (2013). Diversity and population structure of Marine Group A bacteria in the Northeast subarctic Pacific Ocean. *Isme J* **7**: 256–268.
- Bankevich A, Nurk S, Antipov D, Gurevich AA, Dvorkin M, Kulikov AS *et al.* (2012). SPAdes: a new genome assembly algorithm and its applications to single-cell sequencing. *J Comput Biol* **19**: 455–477.
- Bateman A, Coin L, Durbin R, Finn RD, Hollich V, Griffiths-Jones S *et al.* (2004). The Pfam protein families database. *Nucleic Acids Res* **32**(Database issue): D138–D141.
- Batut B, Knibbe C, Marais G, Daubin V. (2014). Reductive genome evolution at both ends of the bacterial population size spectrum. *Nat Rev Microbiol* **12**: 841–850.
- Beja O, Suzuki MT, Koonin EV, Aravind L, Hadd A, Nguyen LP *et al.* (2000). Construction and analysis of bacterial artificial chromosome libraries from a marine microbial assemblage. *Environ Microbiol* **2**: 516–529.
- Belmar L, Molina V, Ulloa O. (2011). Abundance and phylogenetic identity of archaeoplankton in the permanent oxygen minimum zone of the eastern tropical South Pacific. *FEMS Microbiol Ecol* **78**: 314–326.
- Boutrif M, Garel M, Cottrell MT, Tamburini C. (2011). Assimilation of marine extracellular polymeric substances by deep-sea prokaryotes in the NW Mediterranean Sea. *Environ Microbiol Rep* **3**: 705–709.
- Brochier-Armanet C, Boussau B, Gribaldo S, Forterre P. (2008). Mesophilic Crenarchaeota: proposal for a third archaeal phylum, the Thaumarchaeota. *Nat Rev Microbiol* **6**: 245–252.
- Bryant JA, Aylward FO, Eppley JM, Karl DM, Church MJ, DeLong EF. (2015). Wind and sunlight shape microbial diversity in surface waters of the North Pacific Subtropical Gyre. *ISME J* **10**: 1308–1322.
- Cashmore AR, Jarillo JA, Wu YJ, Liu D. (1999). Cryptochromes: blue light receptors for plants and animals. *Science* **284**: 760–765.

- Coleman ML, Chisholm SW. (2010). Ecosystem-specific selection pressures revealed through comparative population genomics. *Proc Natl Acad Sci USA* **107**: 18634–18639.
- Coleman ML, Sullivan MB, Martiny AC, Steglich C, Barry K, DeLong EF *et al.* (2006). Genomic islands and the ecology and evolution of *Prochlorococcus*. *Science* **311**: 1768–1770.
- Cuadros-Orellana S, Martin-Cuadrado AB, Legault B, D'Auria G, Zhaxybayeva O, Papke RT *et al.* (2007). Genomic plasticity in prokaryotes: the case of the square haloarchaeon. *ISME J* **1**: 235–245.
- Chang YG, Cohen SE, Phong C, Myers WK, Kim YI, Tseng R *et al.* (2015). Circadian rhythms. A protein fold switch joins the circadian oscillator to clock output in cyanobacteria. *Science* **349**: 324–328.
- Chaves I, Pokorny R, Byrdin M, Hoang N, Ritz T, Brettel K *et al.* (2011). The cryptochromes: blue light photoreceptors in plants and animals. *Annu Rev Plant Biol* **62**: 335–364.
- Chen S, Su L, Chen J, Wu J. (1997). Cutinase: characteristics, preparation, and application. *Biotechnol Adv* **31**: 1754–1767.
- DeLong EF. (1992). Archaea in coastal marine environments. *Proc Natl Acad Sci USA* **89**: 5685–5689.
- DeLong EF. (2006). Archaeal mysteries of the deep revealed. *Proc Natl Acad Sci U S A* **103**: 6417–6418.
- DeLong EF, Preston CM, Mincer T, Rich V, Hallam SJ, Frigaard NU *et al.* (2006). Community genomics among stratified microbial assemblages in the ocean's interior. *Science* **311**: 496–503.
- DeLong EF, Taylor LT, Marsh TL, Preston CM. (1999). Visualization and enumeration of marine planktonic archaea and bacteria by using polyribonucleotide probes and fluorescent in situ hybridization. *Appl Environ Microbiol* **65**: 5554–5563.
- Deschamps P, Zivanovic Y, Moreira D, Rodriguez-Valera F, López-García P. (2014). Pangenome evidence for extensive inter-domain horizontal transfer affecting lineage-core and shell genes in uncultured planktonic Thaumarchaeota and Euryarchaeota. *Genome Biol Evol* **6**: 1549–1563.
- Dufresne A, Garczarek L, Partensky F. (2005). Accelerated evolution associated with genome reduction in a free-living prokaryote. *Genome Biol* **6**: R14.
- Edgar RC. (2004). MUSCLE: a multiple sequence alignment method with reduced time and space complexity. *BMC Bioinformatics* **5**: 113.
- Edgar RC. (2010). Search and clustering orders of magnitude faster than BLAST. *Bioinformatics* **26**: 2460–2461.
- Edgcomb VP, Kysela DT, Teske A, de Vera Gomez A, Sogin ML. (2002). Benthic eukaryotic diversity in the Guaymas Basin hydrothermal vent environment. *Proc Natl Acad Sci USA* **99**: 7658–7662.
- Essen LO. (2006). Photolyases and cryptochromes: common mechanisms of DNA repair and light-driven signaling? *Curr Opin Struct Biol* **16**: 51–59.
- Essen LO, Klar T. (2006). Light-driven DNA repair by photolyases. *Cell Mol Life Sci* **63**: 1266–1277.
- Fuhrman JA, Davis AA. (1997). Widespread archaea and novel bacteria from the deep sea as shown by 16S rRNA gene sequences. *Mar Ecol Prog Series* **150**: 275–285.
- Fuhrman JA, McCallum K, Davis AA. (1992). Novel major archaeobacterial group from marine plankton. *Nature* **356**: 148–149.
- Fuhrman JA, Schwalbach MS, Stingl U. (2008). Proteorhodopsins: an array of physiological roles? *Nat Rev Microbiol* **6**: 488–494.
- Galand PE, Casamayor EO, Kirchman DL, Potvin M, Lovejoy C. (2009). Unique archaeal assemblages in the Arctic Ocean unveiled by massively parallel tag sequencing. *ISME J* **3**: 860–869.
- Galand PE, Gutiérrez-Provecho C, Massana R, Gasol JM, Casamayor EO. (2010). Inter-annual recurrence of archaeal assemblages in the coastal NW Mediterranean Sea (Blanes Bay Microbial Observatory). *Limnol Oceanogr* **55**: 2117–2125.
- Ghai R, Martin-Cuadrado A, Gonzaga A, Garcia-Heredia I, Cabrera R, Martin J *et al.* (2010). Metagenome of the Mediterranean deep Chlorophyll Maximum studied by direct and fomid library 454 pyrosequencing. *ISME J* **4**: 1154–1166.
- Ghai R, McMahon KD, Rodriguez-Valera F. (2012). Breaking a paradigm: cosmopolitan and abundant freshwater actinobacteria are low GC. *Environ Microbiol Rep* **4**: 29–35.
- Giovannoni S, Nemergut D. (2014). Ecology. Microbes ride the current. *Science* **345**: 1246–1247.
- Goris J, Konstantinidis KT, Klappenbach JA, Coenye T, Vandamme P, Tiedje JM. (2007). DNA-DNA hybridization values and their relationship to whole-genome sequence similarities. *Int J Syst Evol Microbiol* **57**: 81–91.
- Gribaldo S, Lumia V, Creti R, Conway de Macario E, Sanangelantoni A, Cammarano P. (1999). Discontinuous occurrence of the hsp70 (dnaK) gene among Archaea and sequence features of HSP70 suggest a novel outlook on phylogenies inferred from this protein. *J Bacteriol* **181**: 434–443.
- Haft DH, Loftus BJ, Richardson DL, Yang F, Eisen JA, Paulsen IT *et al.* (2001). TIGRFAMs: a protein family resource for the functional identification of proteins. *Nucleic Acids Res* **29**: 41–43.
- Hallam SJ, Konstantinidis KT, Putnam N, Schleper C, Watanabe Y, Sugahara J *et al.* (2006). Genomic analysis of the uncultivated marine crenarchaeote Cenarchaeum symbiosum. *Proc Natl Acad Sci USA* **103**: 18296–18301.
- Herdnl GJ, Reinthaler T, Teira E, van Aken H, Veth C, Pernthaler A *et al.* (2005). Contribution of Archaea to total prokaryotic production in the deep Atlantic Ocean. *Appl Environ Microbiol* **71**: 2303–2309.
- Huang Y, Gilna P, Li W. (2009). Identification of ribosomal RNA genes in metagenomic fragments. *Bioinformatics* **25**: 1338–1340.
- Hyatt D, Chen GL, Locascio PF, Land ML, Larimer FW, Hauser LJ. (2010). Prodigal: prokaryotic gene recognition and translation initiation site identification. *BMC Bioinformatics* **11**: 119.
- Inoue K, Ono H, Abe-Yoshizumi R, Yoshizawa S, Ito H, Kogure K *et al.* (2013). A light-driven sodium ion pump in marine bacteria. *Nat Commun* **4**: 1678.
- Iverson V, Morris RM, Frazar CD, Berthiaume CT, Morales RL, Armbrust EV. (2012). Untangling genomes from metagenomes: revealing an uncultured class of marine Euryarchaeota. *Science* **335**: 587–590.
- Jarrell KF, Jones GM, Kandiba L, Nair DB, Eichler J. (2010). *S-layer glycoproteins and flagellins: reporters of archaeal posttranslational modifications*. Archaea 2010.
- Jarrell KF, McBride MJ. (2008). The surprisingly diverse ways that prokaryotes move. *Nat Rev Microbiol* **6**: 466–476.

- Karner MB, DeLong EF, Karl DM. (2001). Archaeal dominance in the mesopelagic zone of the Pacific Ocean. *Nature* **409**: 507–510.
- Konneke M, Bernhard AE, de la Torre JR, Walker CB, Waterbury JB, Stahl DA. (2005). Isolation of an autotrophic ammonia-oxidizing marine archaeon. *Nature* **437**: 543–546.
- Konstantinidis KT, Tiedje JM. (2005). Genomic insights that advance the species definition for prokaryotes. *Proc Natl Acad Sci USA* **102**: 2567–2572.
- Krzywinski M, Schein J, Birol I, Connors J, Gascoyne R, Horsman D et al. (2009). Circos: an information aesthetic for comparative genomics. *Genome Res* **19**: 1639–1645.
- Larsson J, Celepli N, Ininbergs K, Dupont CL, Yooseph S, Bergman B et al. (2014). Picocyanobacteria containing a novel pigment gene cluster dominate the brackish water Baltic Sea. *ISME J*.
- Lassak K, Ghosh A, Albers SV. (2012). Diversity, assembly and regulation of archaeal type IV pili-like and non-type-IV pili-like surface structures. *Res Microbiol* **163**: 630–644.
- Lassmann T, Sonnhammer EL. (2005). Kalign—an accurate and fast multiple sequence alignment algorithm. *BMC Bioinformatics* **6**: 298.
- Li H, Durbin R. (2009). Fast and accurate short read alignment with Burrows-Wheeler transform. *Bioinformatics* **25**: 1754–1760.
- Li M, Baker BJ, Anantharaman K, Jain S, Breier JA, Dick GJ. (2015). Genomic and transcriptomic evidence for scavenging of diverse organic compounds by widespread deep-sea archaea. *Nat Commun* **6**: 8933.
- Lima-Mendez G, Faust K, Henry N, Decelle J, Colin S, Carcillo F et al. (2015). Ocean plankton. Determinants of community structure in the global plankton interactome. *Science* **348**: 1262073.
- Lopez-Garcia P, Lopez-Lopez A, Moreira D, Rodriguez-Valera F. (2001a). Diversity of free-living prokaryotes from a deep-sea site at the Antarctic Polar Front. *FEMS Microbiol Ecol* **36**: 193–202.
- Lopez-Garcia P, Moreira D, Lopez-Lopez A, Rodriguez-Valera F. (2001b). A novel haloarchaeal-related lineage is widely distributed in deep oceanic regions. *Environ Microbiol* **3**: 72–78.
- Lopez-Garcia P, Philippe H, Gail F, Moreira D. (2003). Autochthonous eukaryotic diversity in hydrothermal sediment and experimental microcolonizers at the Mid-Atlantic Ridge. *Proc Natl Acad Sci USA* **100**: 697–702.
- Lopez-Garcia P, Zivanovic Y, Deschamps P, Moreira D. (2016). Bacterial gene import and mesophilic adaptation in archaea. *Nat Rev Microbiol* **13**: 447–456.
- Makarova KS, Aravind L, Galperin MY, Grishin NV, Tatusov RL, Wolf YI et al. (1999). Comparative genomics of the Archaea (Euryarchaeota): evolution of conserved protein families, the stable core, and the variable shell. *Genome Res* **9**: 608–628.
- Makarova KS, Koonin EV. (2003). Comparative genomics of Archaea: how much have we learned in six years, and what's next? *Genome Biol* **4**: 115.
- Makarova KS, Wolf YI, Koonin EV. (2015). Archaeal clusters of orthologous genes (arCOGs): an update and application for analysis of shared features between Thermococcales, Methanococcales, and Methanobacteriales. *Life (Basel)* **5**: 818–840.
- Martin-Cuadrado AB, Fontaine T, Esteban PF, del Dedo JE, de Medina-Redondo M, del Rey F et al. (2008). Characterization of the endo-beta-1,3-glucanase activity of *S. cerevisiae* Eng2 and other members of the GH81 family. *Fungal Genet Biol* **45**: 542–553.
- Martin-Cuadrado AB, Garcia-Heredia I, Molto AG, Lopez-Ubeda R, Kimes N, Lopez-Garcia P et al. (2015). A new class of marine Euryarchaeota group II from the Mediterranean deep chlorophyll maximum. *ISME J* **9**: 1619–1634.
- Martin-Cuadrado AB, Pasic L, Rodriguez-Valera F. (2014). Diversity of the cell-wall associated genomic island of the archaeon *Haloquadratum walsbyi*. *BMC Genomics* **16**: 603.
- Martin-Cuadrado AB, Rodriguez-Valera F, Moreira D, Alba JC, Ivars-Martinez E, Henn MR et al. (2008). Hindsight in the relative abundance, metabolic potential and genome dynamics of uncultivated marine archaea from comparative metagenomic analyses of bathypelagic plankton of different oceanic regions. *ISME J* **2**: 865–886.
- Massana R, DeLong EF, Pedros-Alio C. (2000). A few cosmopolitan phylotypes dominate planktonic archaeal assemblages in widely different oceanic provinces. *Appl Environ Microbiol* **66**: 1777–1787.
- Mizuno CM, Ghai R, Saghai A, Lopez-Garcia P, Rodriguez-Valera F. (2016). Genomes of abundant and widespread viruses from the deep ocean. *MBio* **7**: 4.
- Narasingarao P, Podell S, Ugalde JA, Brochier-Armanet C, Emerson JB, Brocks JJ et al. (2012). De novo metagenomic assembly reveals abundant novel major lineage of Archaea in hypersaline microbial communities. *ISME J* **6**: 81–93.
- Nawrocki EP. (2009). *Structural RNA homology search and alignment using covariance models*, PhD thesis. Washington University in Saint Louis, School of Medicine, St. Louis, MO, USA.
- Needham DM, Fuhrman JA. (2016). Pronounced daily succession of phytoplankton, archaea and bacteria following a spring bloom. *Nat Microbiol*.
- Orsi WD, Smith JM, Wilcox HM, Swalwell JE, Carini P, Worden AZ et al. (2015). Ecophysiology of uncultivated marine euryarchaea is linked to particulate organic matter. *ISME J* **9**: 1747–1763.
- Ouverney CC, Fuhrman JA. (2000). Marine planktonic archaea take up amino acids. *Appl Environ Microbiol* **66**: 4829–4833.
- Parks DH, Imelfort M, Skennerton CT, Hugenholtz P, Tyson GW. (2014). CheckM: assessing the quality of microbial genomes recovered from isolates, single cells, and metagenomes. *Genome Res* **25**: 1043–1055.
- Peng Y, Leung HC, Yiu SM, Chin FY. (2012). IDBA-UD: a de novo assembler for single-cell and metagenomic sequencing data with highly uneven depth. *Bioinformatics* **28**: 1420–1428.
- Petitjean C, Moreira D, Lopez-Garcia P, Brochier-Armanet C. (2012). Horizontal gene transfer of a chloroplast DnaJ-Fer protein to Thaumarchaeota and the evolutionary history of the DnaK chaperone system in Archaea. *BMC Evol Biol* **12**: 226.
- Qin W, Amin SA, Martens-Habbena W, Walker CB, Urakawa H, Devol AH et al. (2014). Marine ammonia-oxidizing archaeal isolates display obligate mixotrophy and wide ecotypic variation. *Proc Natl Acad Sci USA* **111**: 12504–12509.
- Quaiser A, Zivanovic Y, Moreira D, Lopez-Garcia P. (2011). Comparative metagenomics of bathypelagic plankton and bottom sediment from the Sea of Marmara. *ISME J* **5**: 285–304.

- Raes J, Korbel JO, Lercher MJ, von Mering C, Bork P. (2007). Prediction of effective genome size in metagenomic samples. *Genome Biol* **8**: R10.
- Raymann K, Forterre P, Brochier-Armanet C, Gribaldo S. (2014). Global phylogenomic analysis disentangles the complex evolutionary history of DNA replication in archaea. *Genome Biol Evol* **6**: 192–212.
- Reva O, Tummler B. (2008). Think big—giant genes in bacteria. *Environ Microbiol* **10**: 768–777.
- Rice P, Longden I, Bleasby A. (2000). EMBOSS: the European Molecular Biology Open Software Suite. *Trends Genet* **16**: 276–277.
- Rodriguez-Valera F, Martin-Cuadrado AB, Rodriguez-Brito B et al. (2009). Explaining microbial population genomics through phage predation. *Nat Rev Microbiol* **7**: 828–836.
- Romero H, Pereira E, Naya H, Musto H. (2009). Oxygen and guanine-cytosine profiles in marine environments. *J Mol Evol* **69**: 203–206.
- Rusch DB, Halpern AL, Sutton G, Heidelberg KB, Williamson S, Yooseph S et al. (2007). The Sorcerer II Global Ocean Sampling Expedition: Northwest Atlantic through Eastern Tropical Pacific. *PLoS Biol* **5**: e77.
- Scheerer P, Zhang F, Kalms J, von Stetten D, Krauss N, Oberpichler I et al. (2015). The class III cyclobutane pyrimidine dimer photolyase structure reveals a new antenna chromophore binding site and alternative photo-reduction pathways. *J Biol Chem* **290**: 11504–11514.
- Schwarz G, Mendel RR, Ribbe MW. (2009). Molybdenum cofactors, enzymes and pathways. *Nature* **460**: 839–847.
- Shannon P, Markiel A, Ozier O, Baliga NS, Wang JT, Ramage D et al. (2003). Cytoscape: a software environment for integrated models of biomolecular interaction networks. *Genome Res* **13**: 2498–2504.
- Smedile F, Messina E, La Cono V, Tsoy O, Monticelli LS, Borghini M et al. (2012). Metagenomic analysis of hadopelagic microbial assemblages thriving at the deepest part of Mediterranean Sea, Matapan-Vavilov Deep. *Environ Microbiol* **3**: 1462–2920.
- Strom SL, Brahamsha B, Fredrickson KA, Apple JK, Rodriguez AG. (2011). A giant cell surface protein in *Synechococcus* WH8102 inhibits feeding by a dinoflagellate predator. *Environ Microbiol*.
- Sunagawa S, Coelho LP, Chaffron S, Kultima JR, Labadie K, Salazar G et al. (2015). Ocean plankton. Structure and function of the global ocean microbiome. *Science* **348**: 1261359.
- Swan BK, Chaffin MD, Martinez-Garcia M, Morrison HG, Field EK, Poulton NJ et al. (2014). Genomic and metabolic diversity of Marine Group I Thaumarchaeota in the mesopelagic of two subtropical gyres. *PLoS One* **9**: e95380.
- Swan BK, Tupper B, Sczyrba A, Lauro FM, Martinez-Garcia M, Gonzalez JM et al. (2013). Prevalent genome streamlining and latitudinal divergence of planktonic bacteria in the surface ocean. *Proc Natl Acad Sci USA* **110**: 11463–11468.
- Tamura K, Stecher G, Peterson D, Filipinski A, Kumar S. (2013). MEGA6: Molecular Evolutionary Genetics Analysis version 6.0. *Mol Biol Evol* **30**: 2725–2729.
- Tyson GW, Chapman J, Hugenholtz P, Allen EE, Ram RJ, Richardson PM et al. (2004). Community structure and metabolism through reconstruction of microbial genomes from the environment. *Nature* **428**: 37–43.
- Vavourakis CD, Ghai R, Rodriguez-Valera F, Sorokin DY, Tringe SG, Hugenholtz P et al. (2016). Metagenomic insights into the uncultured diversity and physiology of microbes in four hypersaline Soda Lake Brines. *Front Microbiol* **7**: 211.
- Venter JC, Remington K, Heidelberg JF, Halpern AL, Rusch D, Eisen JA et al. (2004). *Environmental genome shotgun sequencing of the Sargasso Sea*. *Science* **304**: 66–74.

Supplementary Information accompanies this paper on The ISME Journal website (<http://www.nature.com/ismej>)

SUPPLEMENTARY INFORMATION

Supplementary Figure S1. Schematic representation of the assembly and binning procedure.

Supplementary Figure S2. Binning of the MG-III genomic fragments. **a.** Principal component analysis of tetranucleotide frequencies of the MG-III DNA fragments. Reference sequences are shown as larger circles: *Nitrosopumilus maritimus* SCM1, *Aciduliprofundum boneii* T469, MGII-GG3, MGII-Thalassoarchaea, the single amplified genome (SAG) SCGC-AAA288-E19 and the DNA fragments from Cayman92, Cayman93, Guaymas31 and Guaymas32. **b.** Heat-map of the number of reads per kilobase per gigabase of metagenome collection (rpkg) of the MG-III sequences recruiting in 33 different metagenomes (only those in which any of the MG-III sequences recruited over rpkg>3 were considered for the binning analysis).

Supplementary Figure S3. Distribution of the assembled MG-III sequences among the metagenomes of the Mediterranean series and TARA collections ordered by depth. Size fraction is indicated above each column.

Supplementary Figure S4. Average nucleotide identity (ANI) among the MG-III genome bins (in bold the sequences published in this work). Dendrogram showing the similarity among the bins is shown in the y axis.

Supplementary Figure S5. 16S and 23S-rRNA phylogeny. **a.** Maximum-likelihood 16S-rRNA gene tree showing the relationship of the MG-III with other archaea. Circles at nodes in major branches indicate bootstrap support (see legend). Scale bar represents the estimated number of substitutions per site. The different MG-III clusters are indicated by different colours and named following Galand *et al.* 2008 and this work. Sampling location is indicated in each of the sequences. Those sequences from samples from more than 500m deep are underlined. **b.** Maximum likelihood 23S-rRNA

gene tree showing the relationship of the MG-III with other archaea. (Picture features as explained before).

Supplementary Figures S6-S12. Maximum likelihood phylogenetic trees for the housekeeping genes RecA, RpoB, SecY, geranylgeranylglyceryl phosphate synthase, DnaK, GyrA and GyrB. Protein sequences from this study are indicated in bold and coloured accordingly with the sequence bin (see legend in Supplementary Figure S4). Genomic bins of MG-II and MG-III groups are indicated. Bootstrap values over 50 are indicated.

Supplementary Figure S13. Maximum likelihood phylogenetic tree of the photolyases and cryptochromes found among the MG-III bins. Protein sequences from this study are indicated in bold and coloured accordingly with their kingdom affiliation (see legend). Bootstrap values over 50 are indicated.

Supplementary Figure S14. Maximum likelihood phylogenetic tree showing the relationship of the MG-III rhodopsins with other bacterial and archaeal rhodopsins. Protein sequences from this study are indicated in bold and coloured accordingly with the sequence bin (see legend in Supplementary Figure S4). Following the nomenclature of Iverson et al. (2013), Clade A and Clade B of rhodopsins is shown. In blue are marked Pop, Pop-1, Pop-2, Pop-3 and Pop-4 euryarchaeal rhodopsins previously described. Numbers at nodes in major branches indicate bootstrap support (shown as percentages and only those >50%). Scale bar represents the estimated number of substitutions per site.

Supplementary Figure S15. Distribution of arCOG functional classes. Percentage of arCOGs predicted in the MGIII bins described in this work and MG-II marine euryarchaeal genomes MG2-GG3 and Thalasoarchaea. All genes (**a**) and genes found only in one of the MGIII bins (**b**) are indicated. Asterisks indicate categories where a significant variation was found comparing the epipelagic and pelagic MGIII.

Supplementary Figure S16. Alignment of the MG-III rhodopsins with other cloned rhodopsins sequences. Identical residues are indicated in red. Residues in blue are conserved in more than 70% of the sequences. Key amino acids for rhodopsins functionality (listed herein with *G. pallidula* numbering) are marked by colours: Lys336 (K) binds retinal, and Asp164 (D) and Glu175 (E) function as Schiff base proton acceptor and donor, respectively. Glutamine (Q) in position 172 (*) in the MG-III rhodopsins sequences indicates an absorption maxima at the blue spectrum range. Letters (G) and (B) in the name of the sequences indicate the range of the spectrum. (The GenBank accession numbers of the sequences used for the alignment are as follows: Pop-2 HF10_3D09, 82548293; Pop-3 HF70_19B12, 82548286; Pop-4 HF70_59C08, 77024964; eBAC49C08, AAY82659; HF130_81H07, 119713419; HF10_49E08, 119713779; eBAC20E09, AAS73014; HOT75m4, AAK30179; eBAC31A08 (SAR86), AAG10475; SAR86E, WP_008490645; *C. Pelagibacter ubique* HTCC1062 (SAR11), YP_266049; *Pelagibacter* sp. HTCC7211, WP_008544914; gammaproteobacteria HTCC2207 (SAR92), EAS48197; *G. pallidula*, WP_006008821; *Dokdonia donghaensis* MED134, ZP_01049273; MedDCM-JUL2012-C3793, KP211865; MedDCM-OCT2007-C1678, KP211832; MedDCM-OCT-S08-C16, ADD93192; *Exiguobacterium sibiricum* 255-15, ACB60885; *Exiguobacterium* sp. AT1b, WP_012726785; *Haloarcula marismortui* ATCC 43049, YP_136594.

Supplementary Figure S17. Classification of the DCM-metagenomes reads using the RDP (16S-rRNA) database. Only those genera which represented more than 1% were represented.

Supplementary Figure S18. Number of reads per kilobase per gigabase of metagenome collection (rpkg) for the composite genome CG-Epi1 MG-III (ordered from minus to major) compared with those obtained for the MG-II (MG2-GG3 (Iverson *et al.* 2013) and the Thalamoarchaea (Martin-Cuadrado *et al.* 2014)). Other CG MG-III were also included in the graph.

Supplementary Figure S19. Interactions (showed as percentages) calculated by Mendez-Lima *et al.*, (2015) for the MG-III with other organisms. Data extracted from Supplementary table W7 in Mendez-Lima *et al.*, (2015).

SUPPLEMENTARY TABLES

Supplementary Table S1. List of metagenomes used for recruitments in Figure 4a and Supplementary Figure 2b, sorted by temperature and depth.

Supplementary Table S2. List of sequences of each of the MG-III sequence bins.

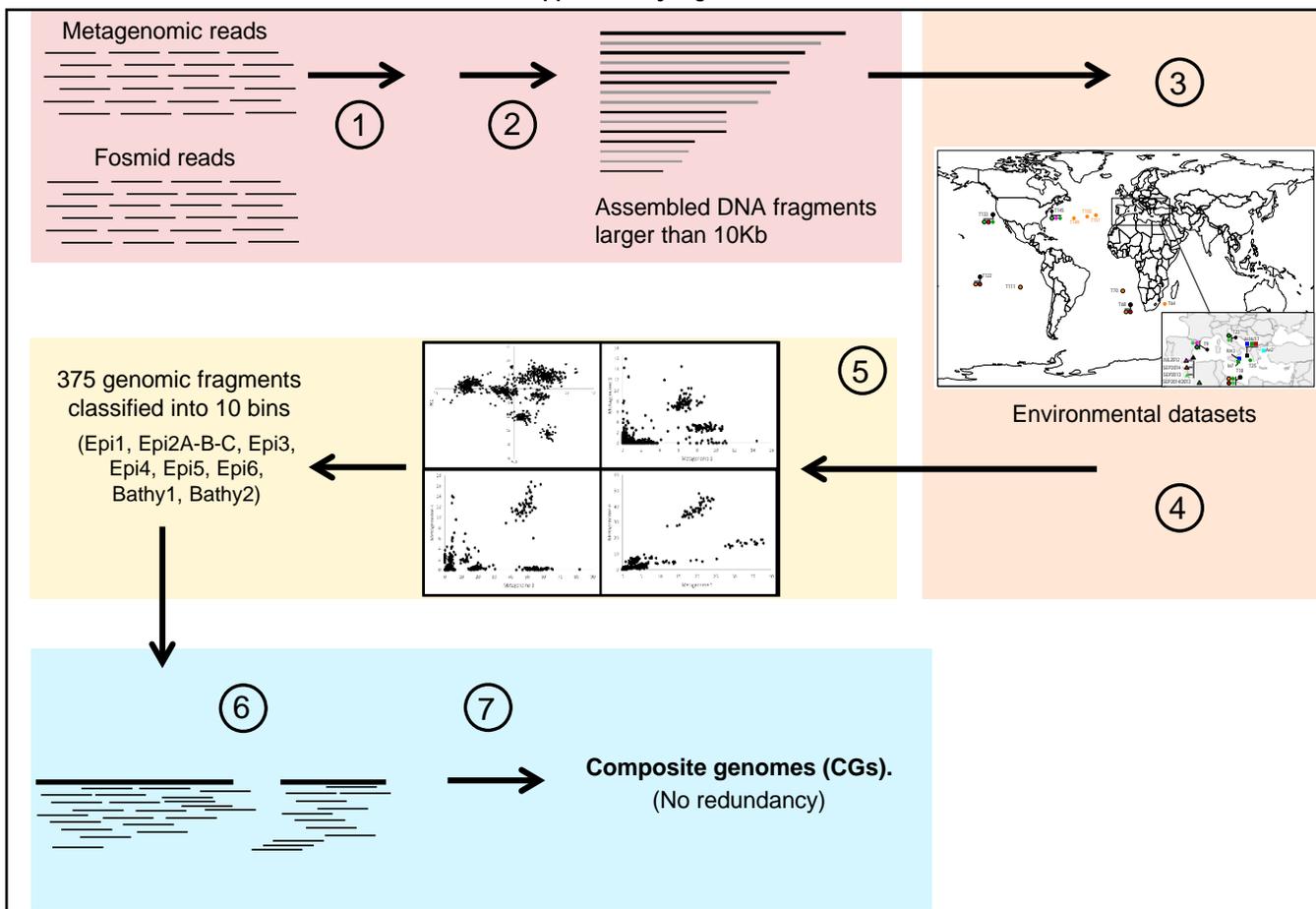
Supplementary Table S3. List of sequences of the MG-III composite genomes (CG-MGIII).

Supplementary Table S4. Housekeeping genes found in the MG-III bins and the CG-MG-III bins (as Narasingarao *et al.*, (2012).

Supplementary Table S5. CG-MGIII-protein categories based on the arCOG database.

Supplementary Table S6. Classification of the CG-MGIII unique CDSs based on the arCOG classification.

Supplementary Table S7. List of genes involved in MG-III metabolic pathways.



Assembly and annotation of euryarchaeal sequences

- 1 Assembly.** Metagenomic reads from MedDCM-JUL2012, MedDCM-SEP2014, Med-Io7-77mDCM, Med-Ae2-600mDeep and the fosmid reads from MedDCM-OCT2007, KM3 and AD1000 were independent and systematically assembled using IDBA_UD.
- 2 Annotation.** Assembled DNA fragments were annotated using the NCBI nr-database, Pfam, COGs, arCOGs and TIGRfam. Only those fragments which have more than 50% of their ORFs annotated as Euryarchaeota were taken for further analysis (in black).

Retrieving of euryarchaeal sequences

- 3 Recruitment.** Search of Euryarchaeota sequences within different marine databases. Only those metagenomes where our initial genomic fragments recruited more than 3 rpkg were selected.
- 4 Assembly and annotation** of the selected metagenomes (as described previously). DNA fragments classified as euryarchaeota were collected.

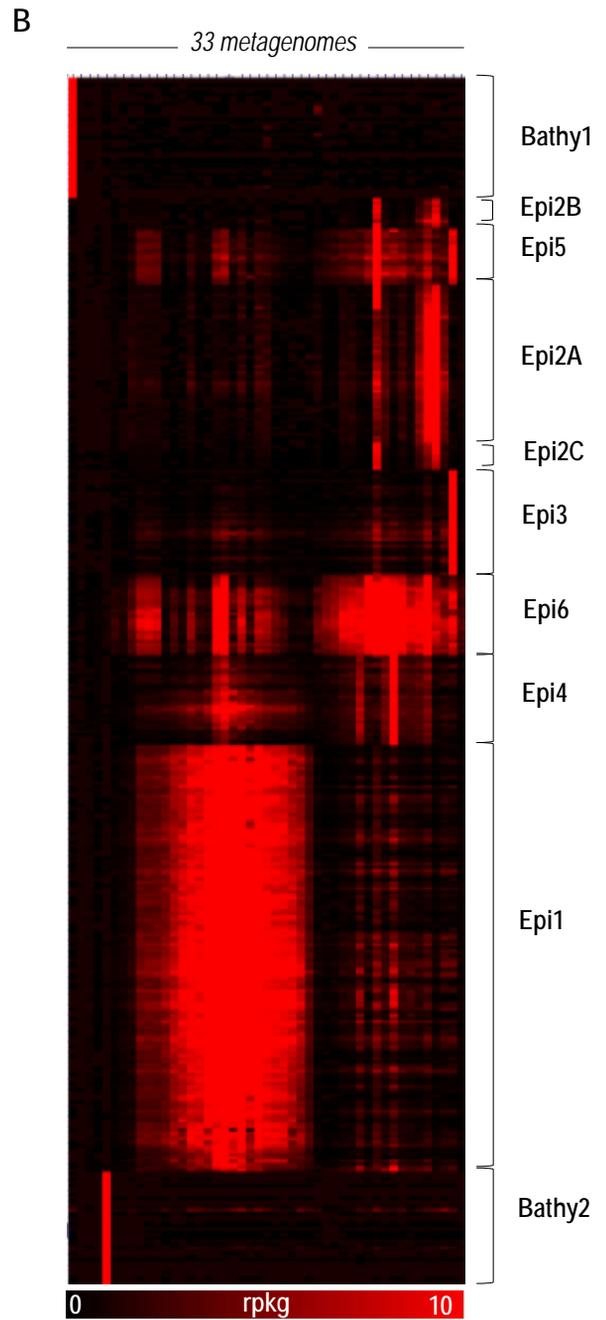
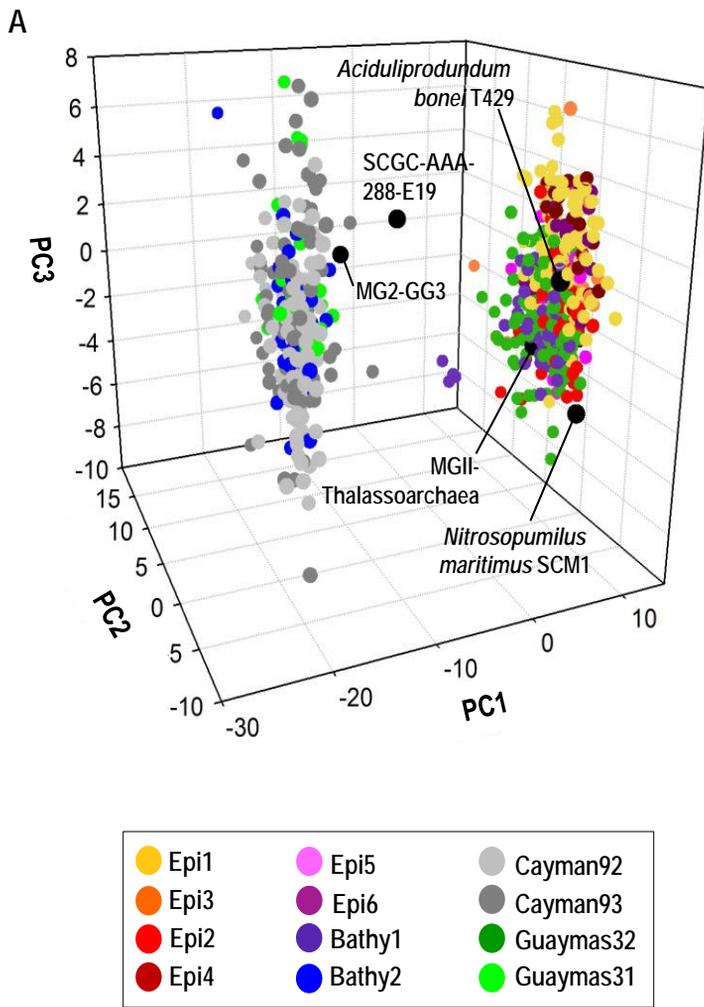
Binning of MG-III by tetranucleotide frequencies, %GC and differential coverage

- 5 Binning** of the MG-III sequences by tetranucleotide frequencies, %GC and differential coverage among 33 metagenomes.

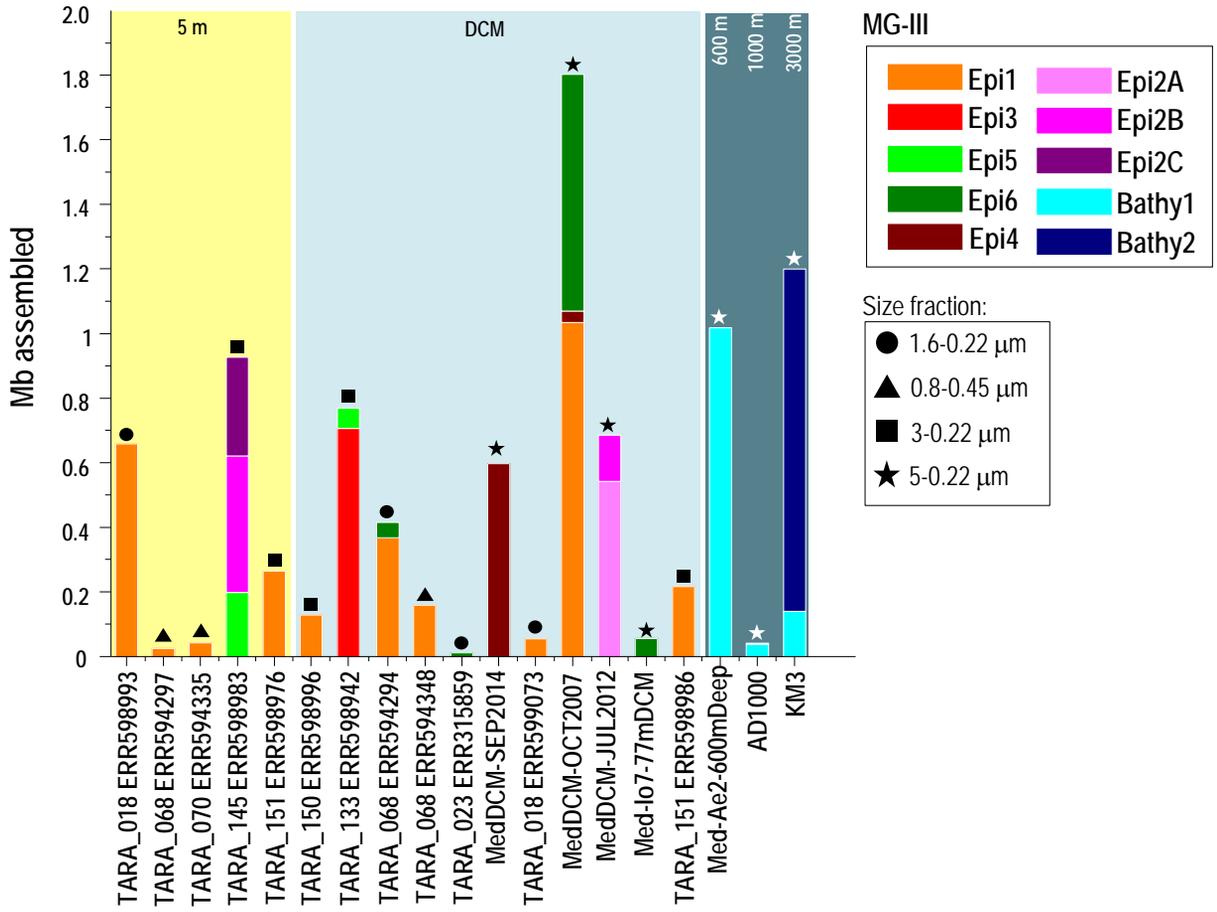
Re-assembly

- 6 Alignment** of the sequences >10 Kb of one specific bin against the metagenomic reads where those contigs came from using BWA. The process was made for all the bins. The reads extracted were used in the following step.
- 7 Assembly** of the reads with SPADES using the DNA fragments for scaffolding with the parameter `-trusted_contigs`. The re-assembly was done for all the bins and their products are called «composite genome» (CG).

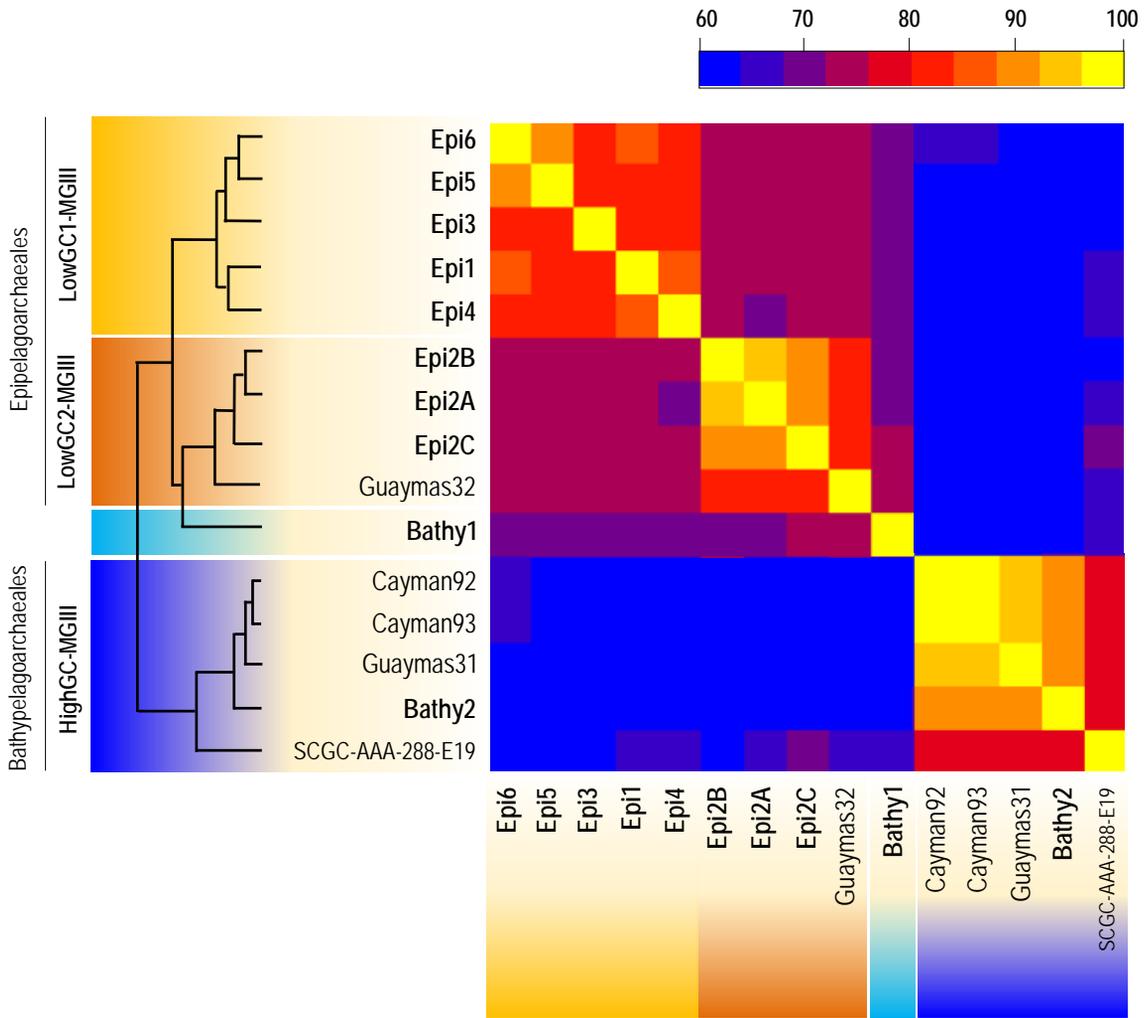
Supplementary Figure S2



Supplementary Figure S3

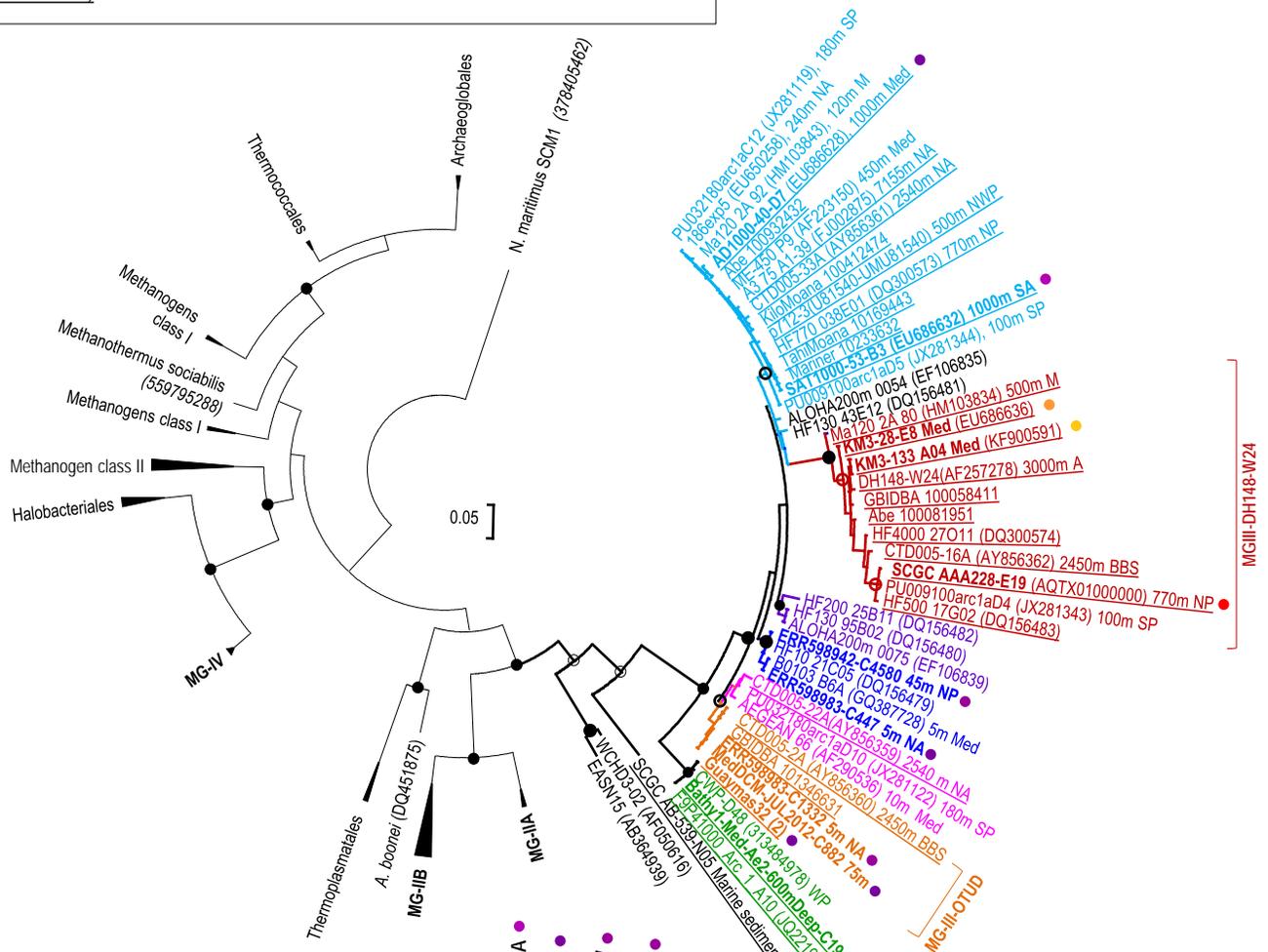


Supplementary Figure S4

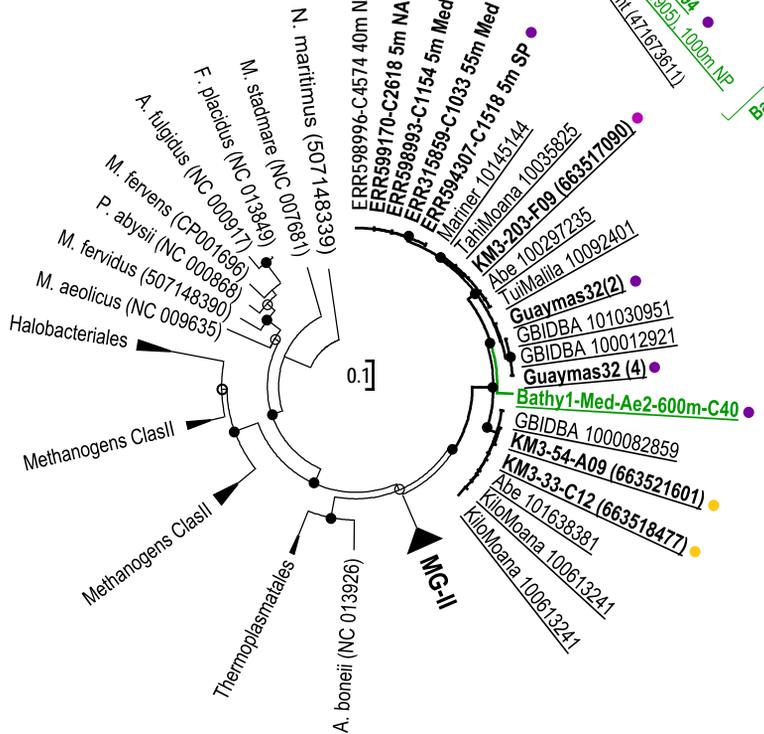




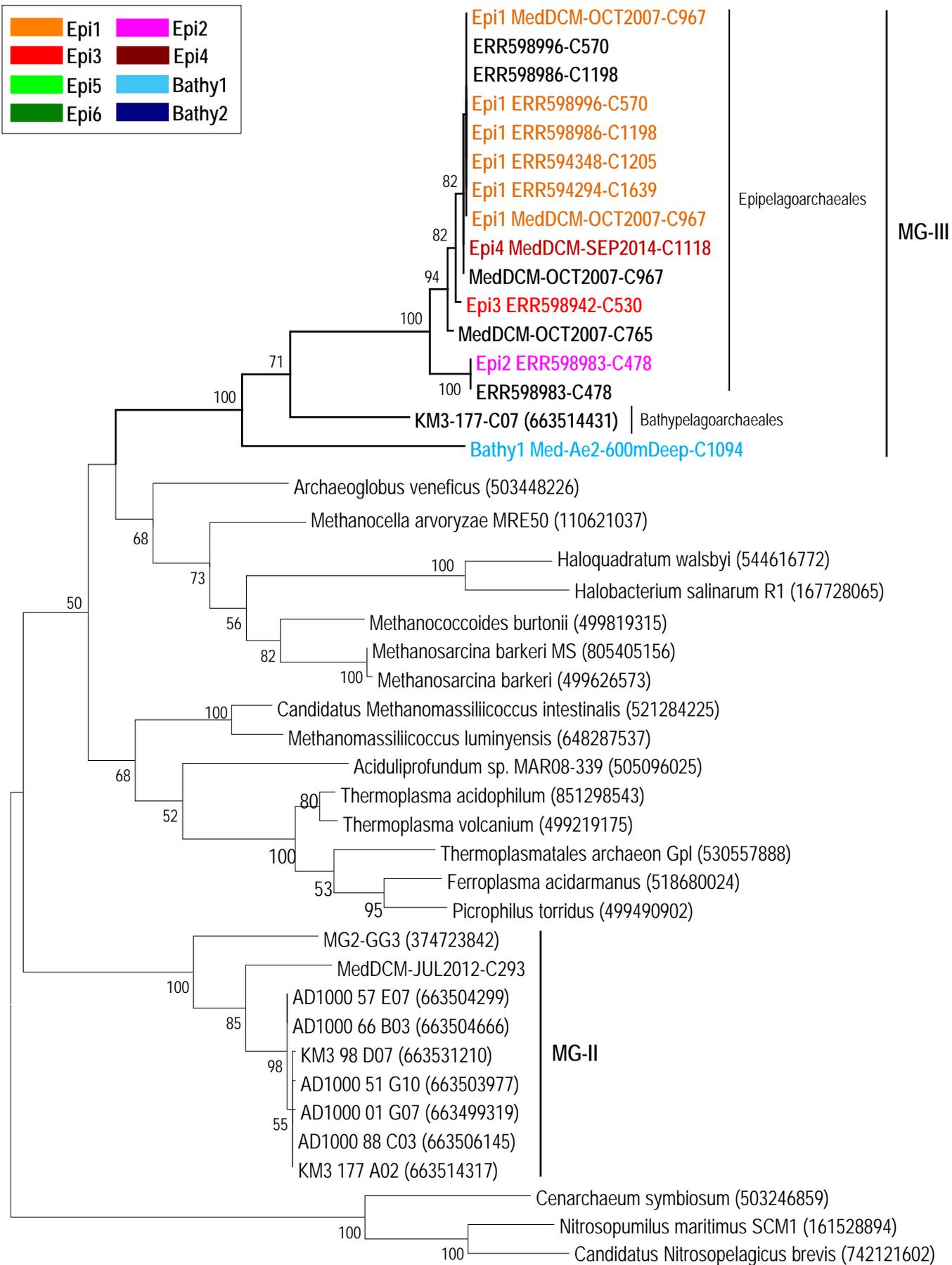
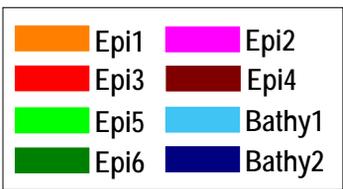
A



B

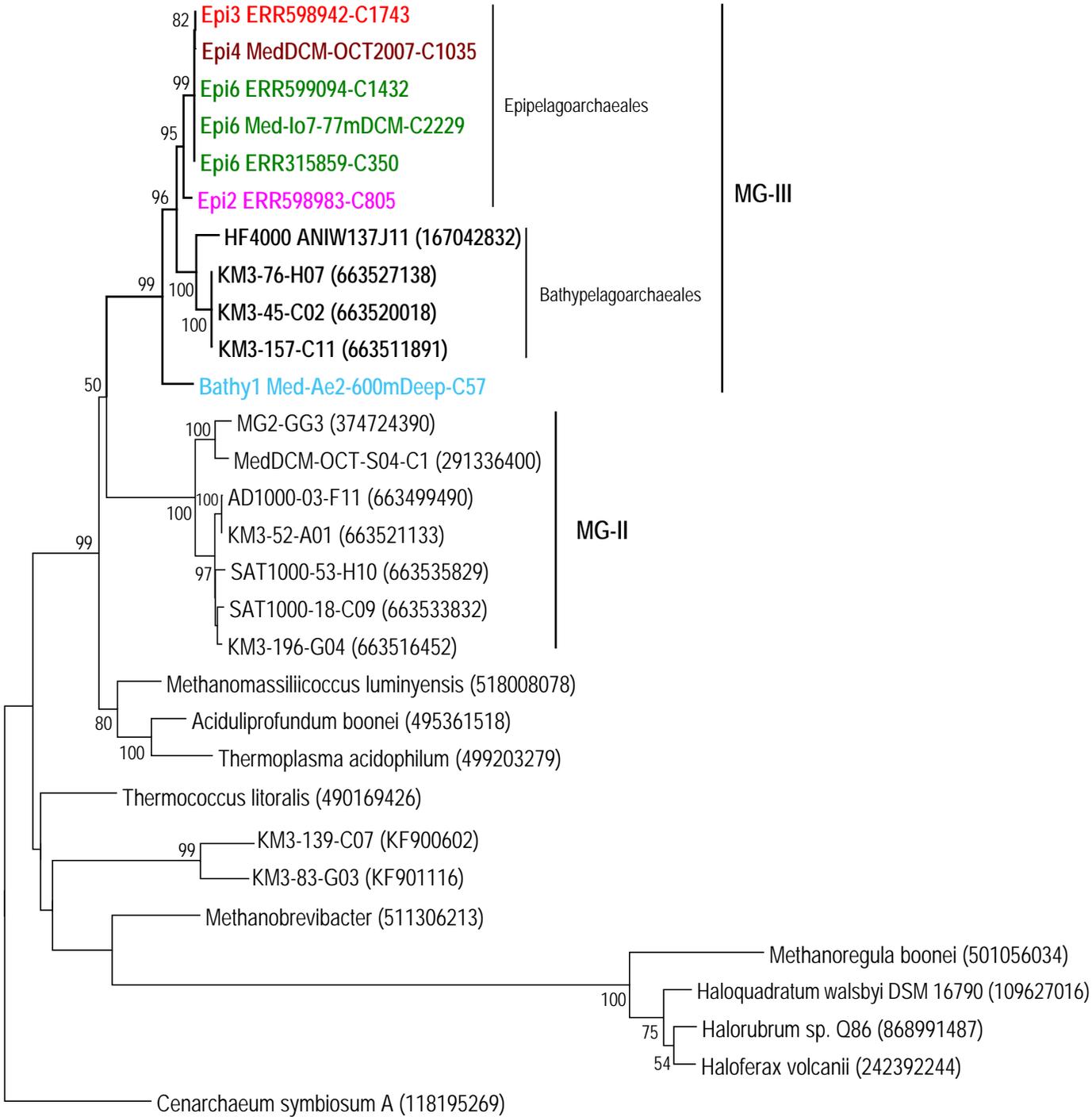


Supplementary Figure S6

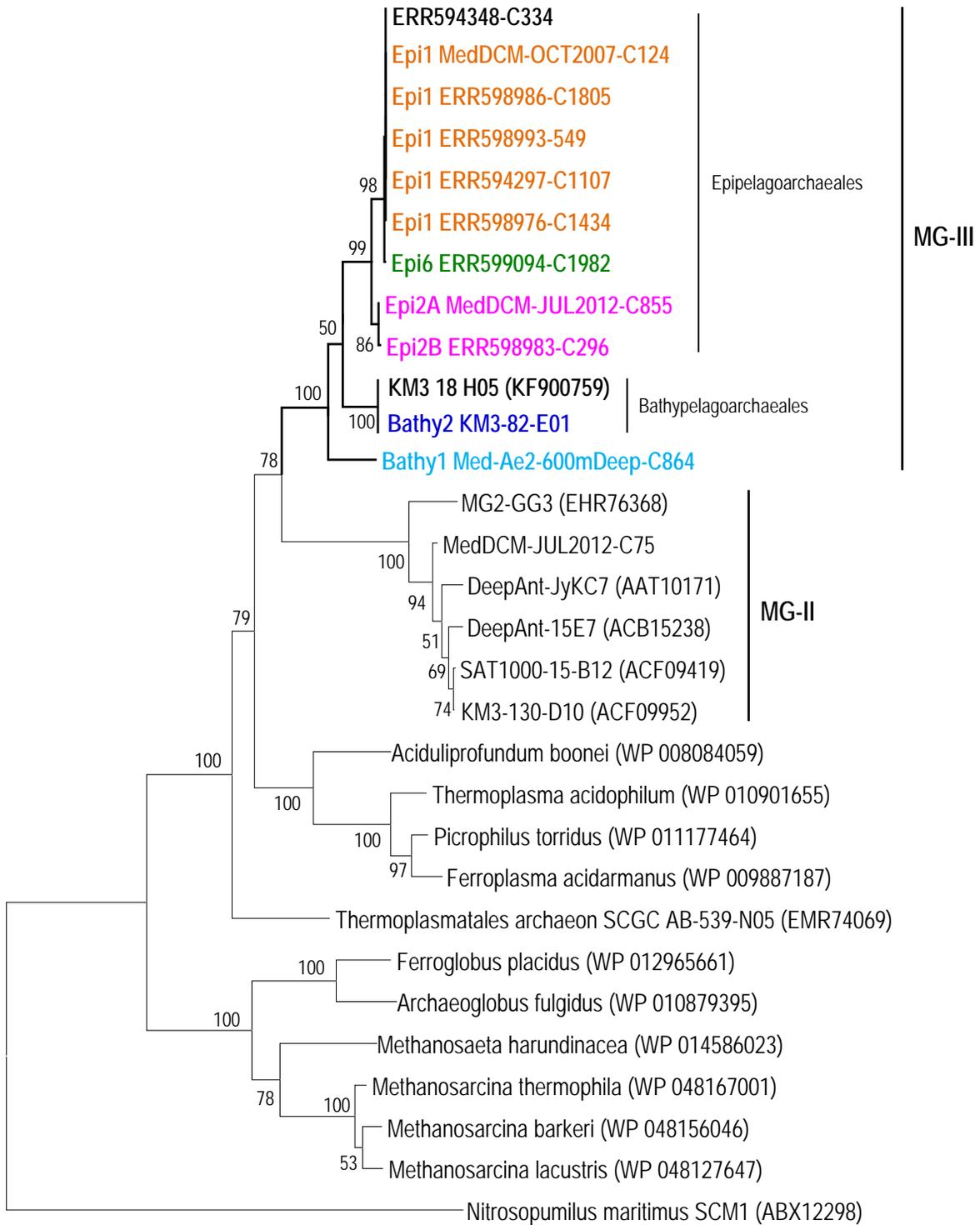


0.1

Supplementary Figure S7

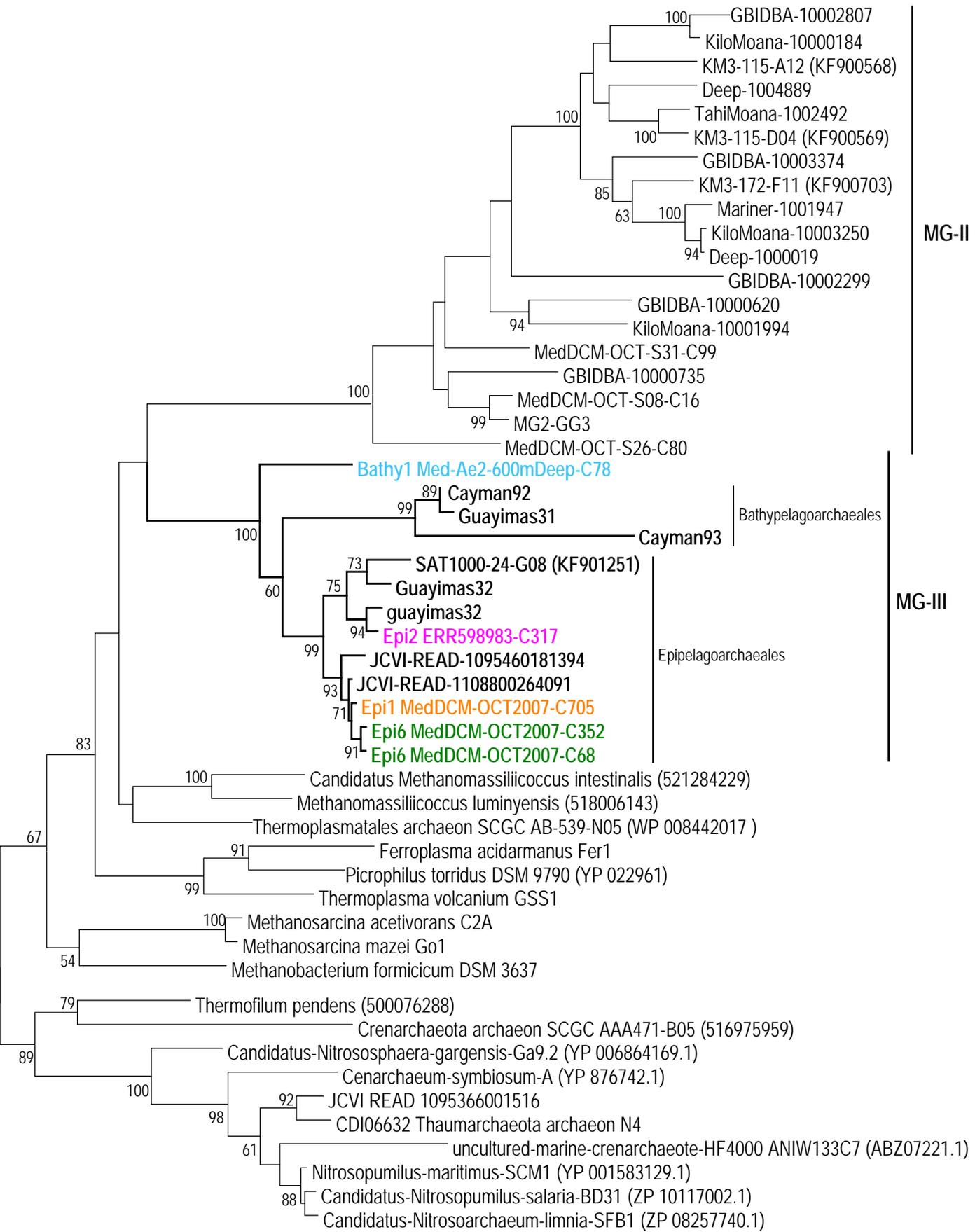


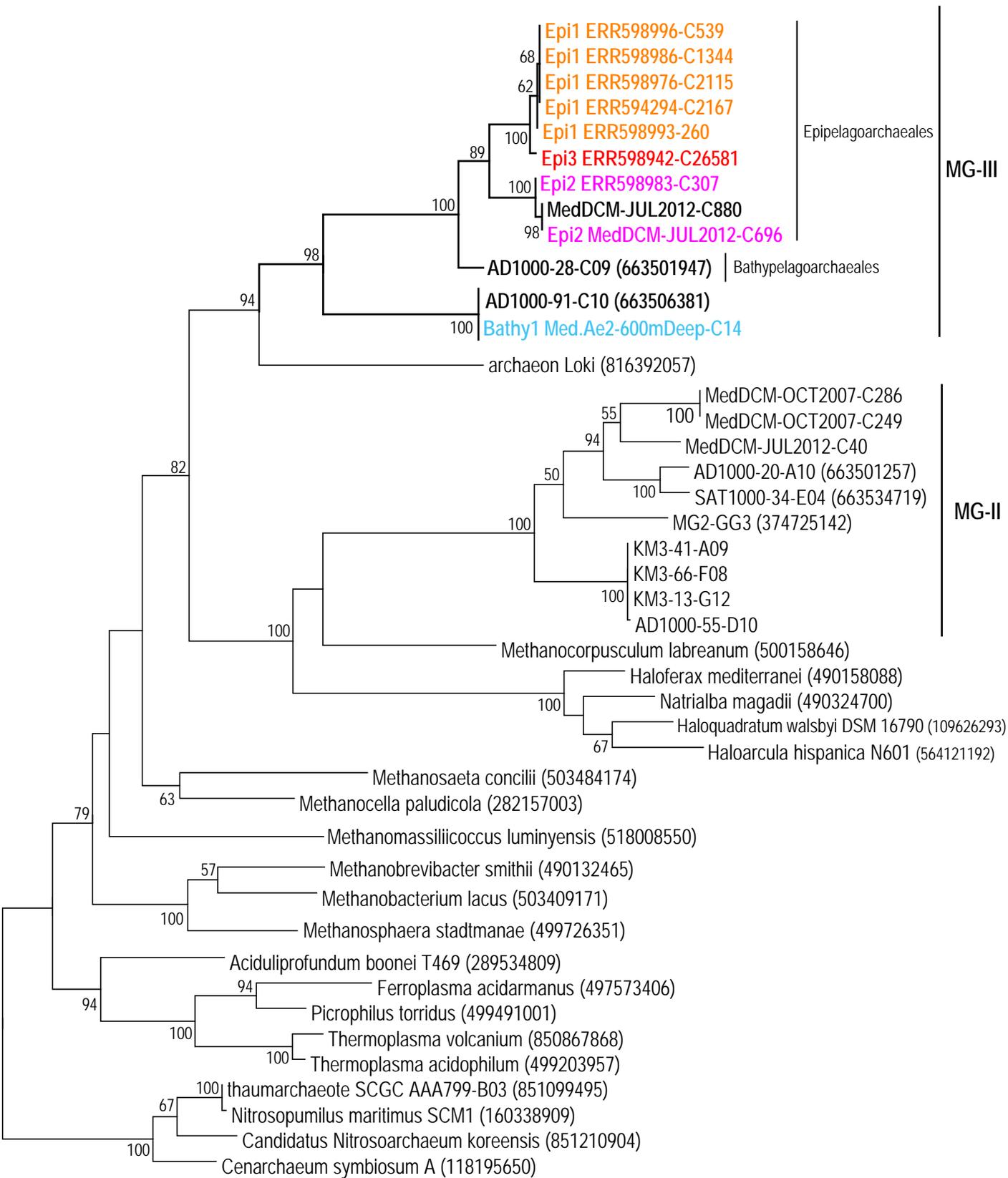
0.5



0.2

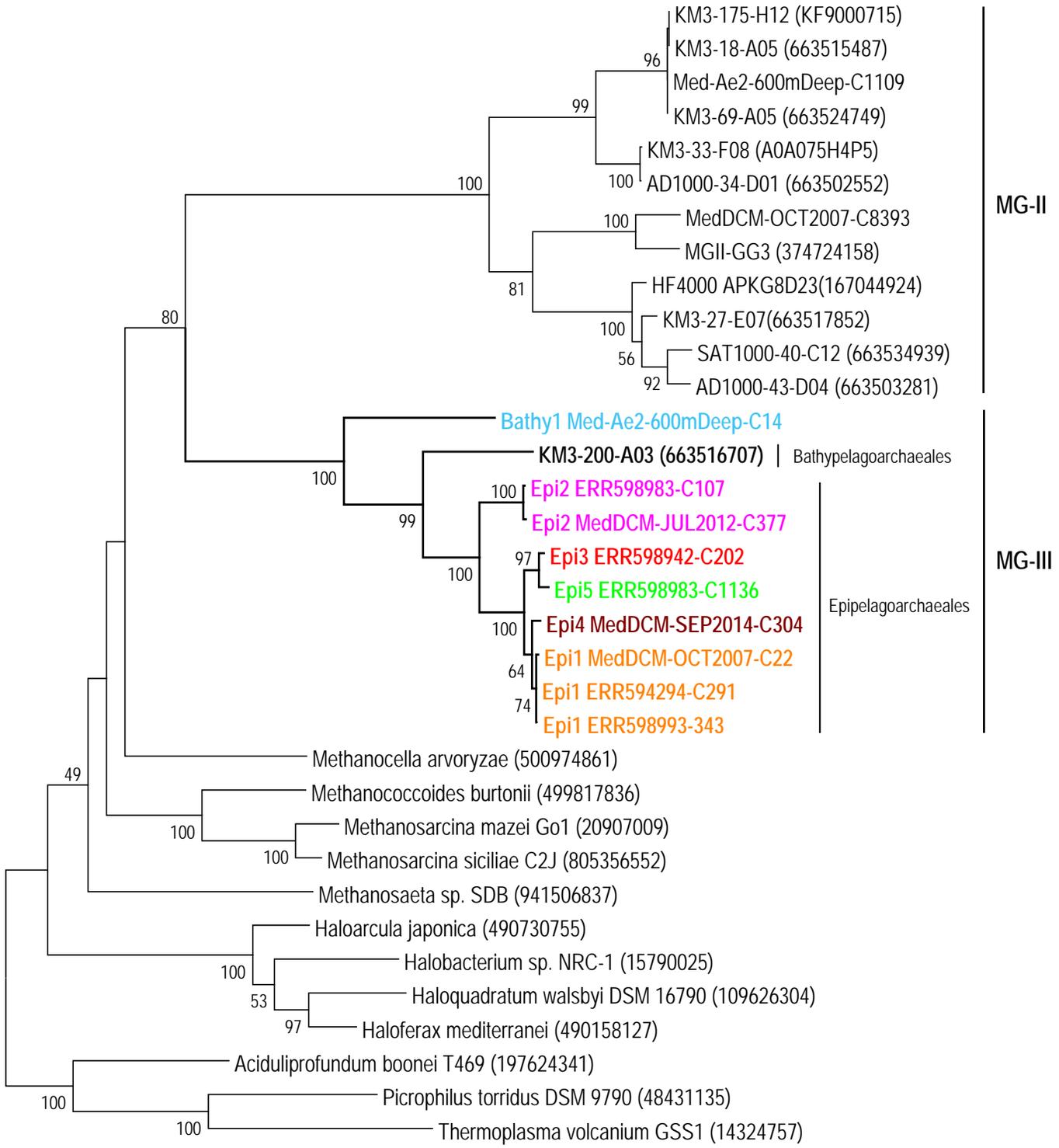
Supplementary Figure S9

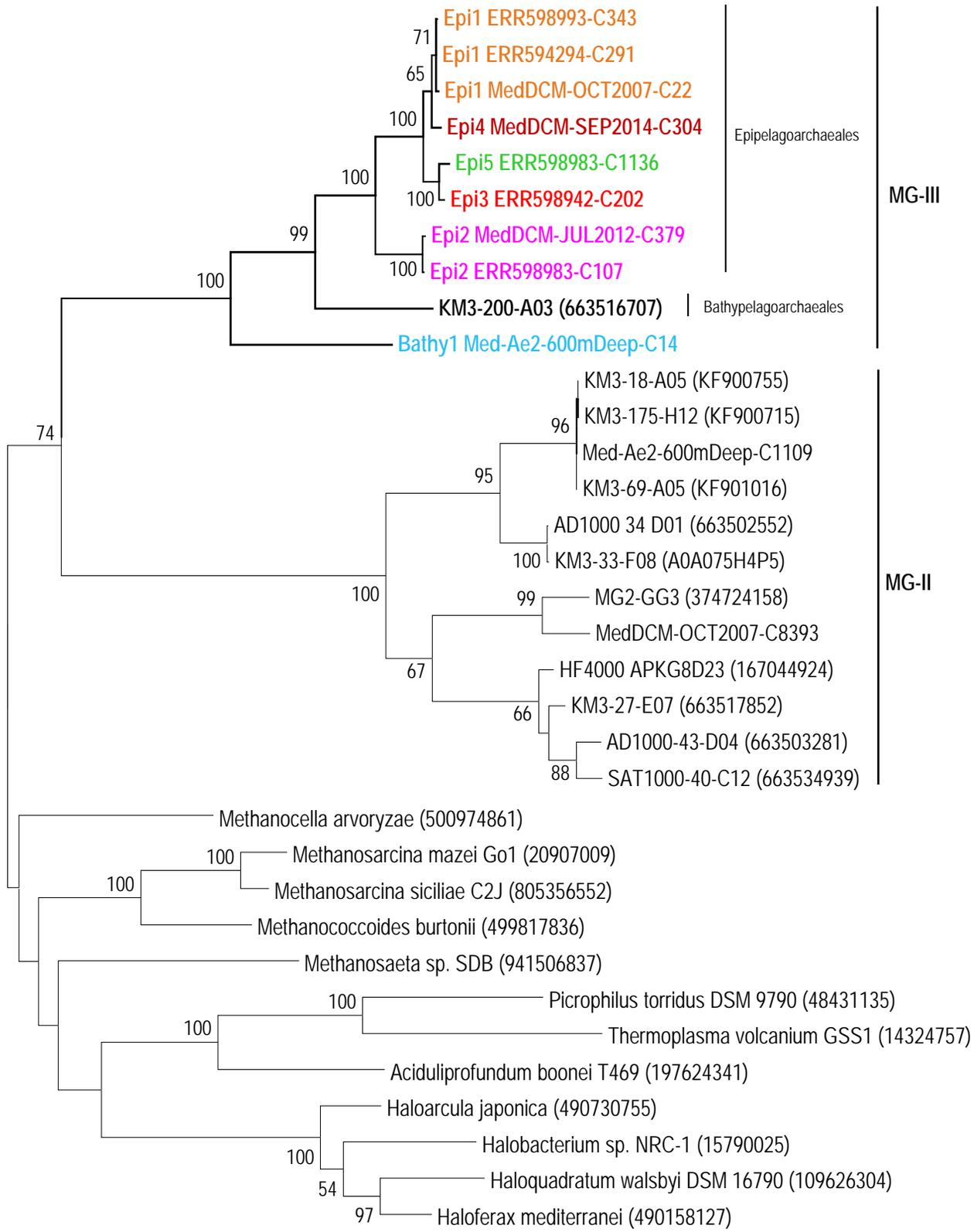




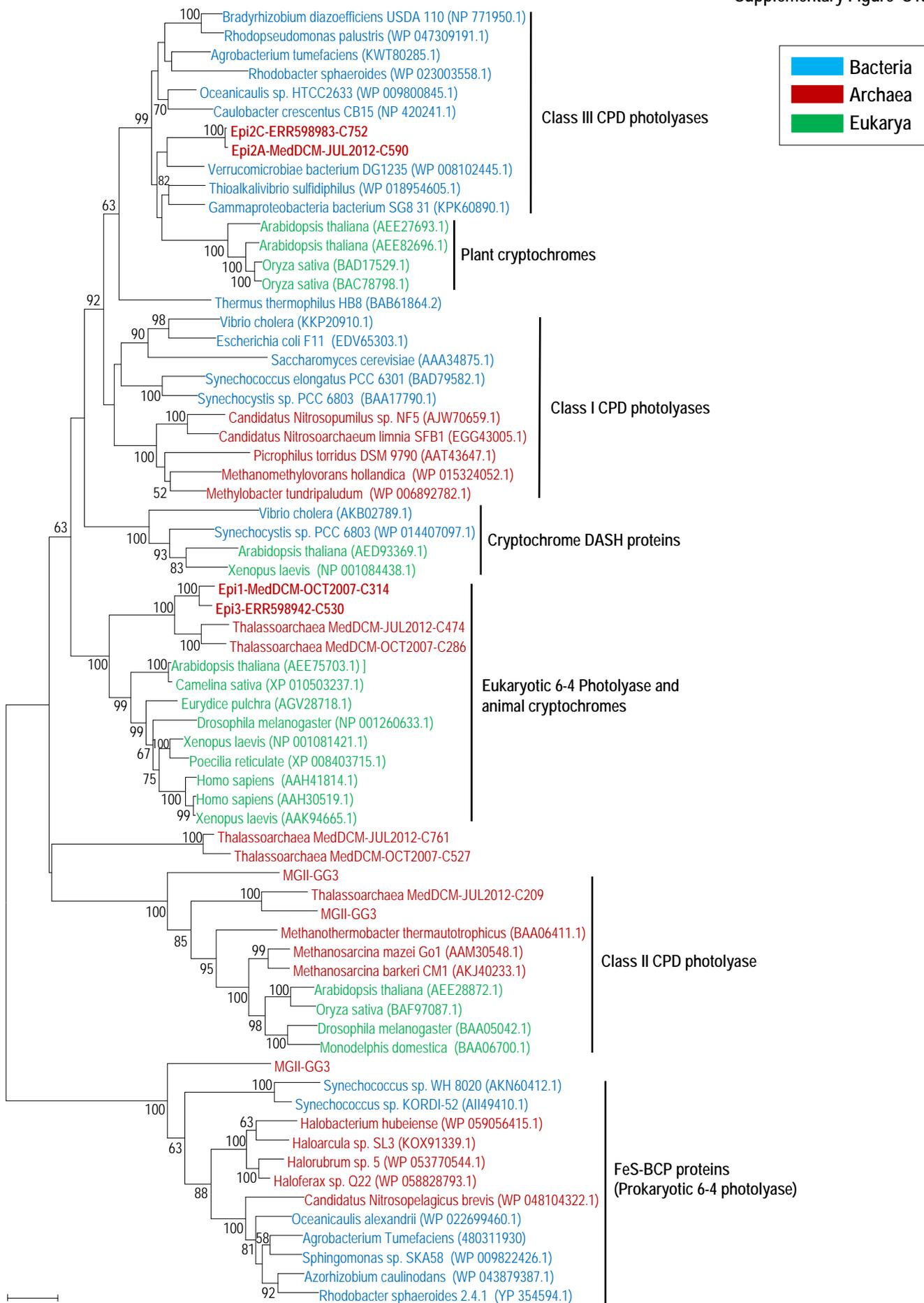
0.1

Supplementary Figure S11

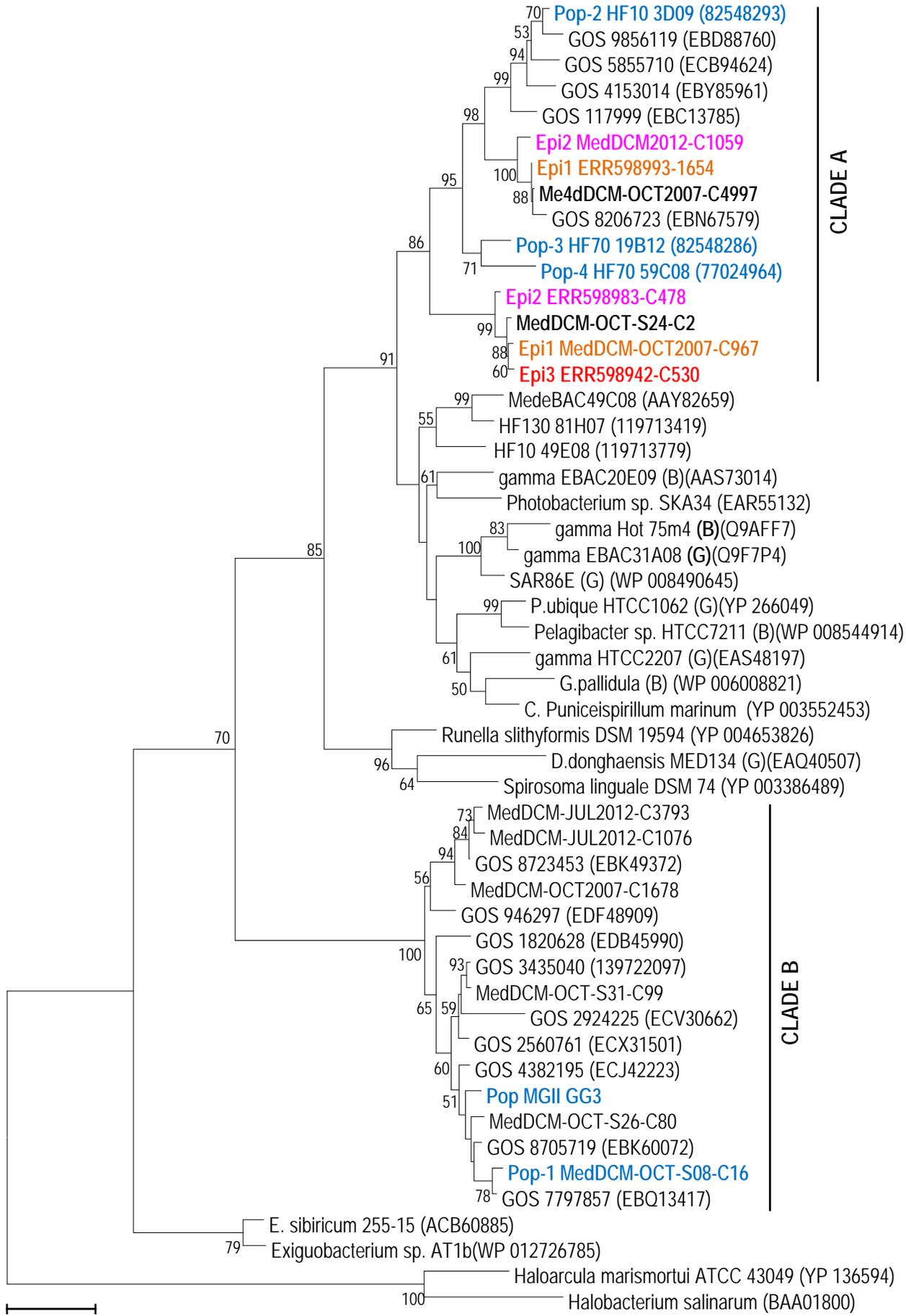




0.1

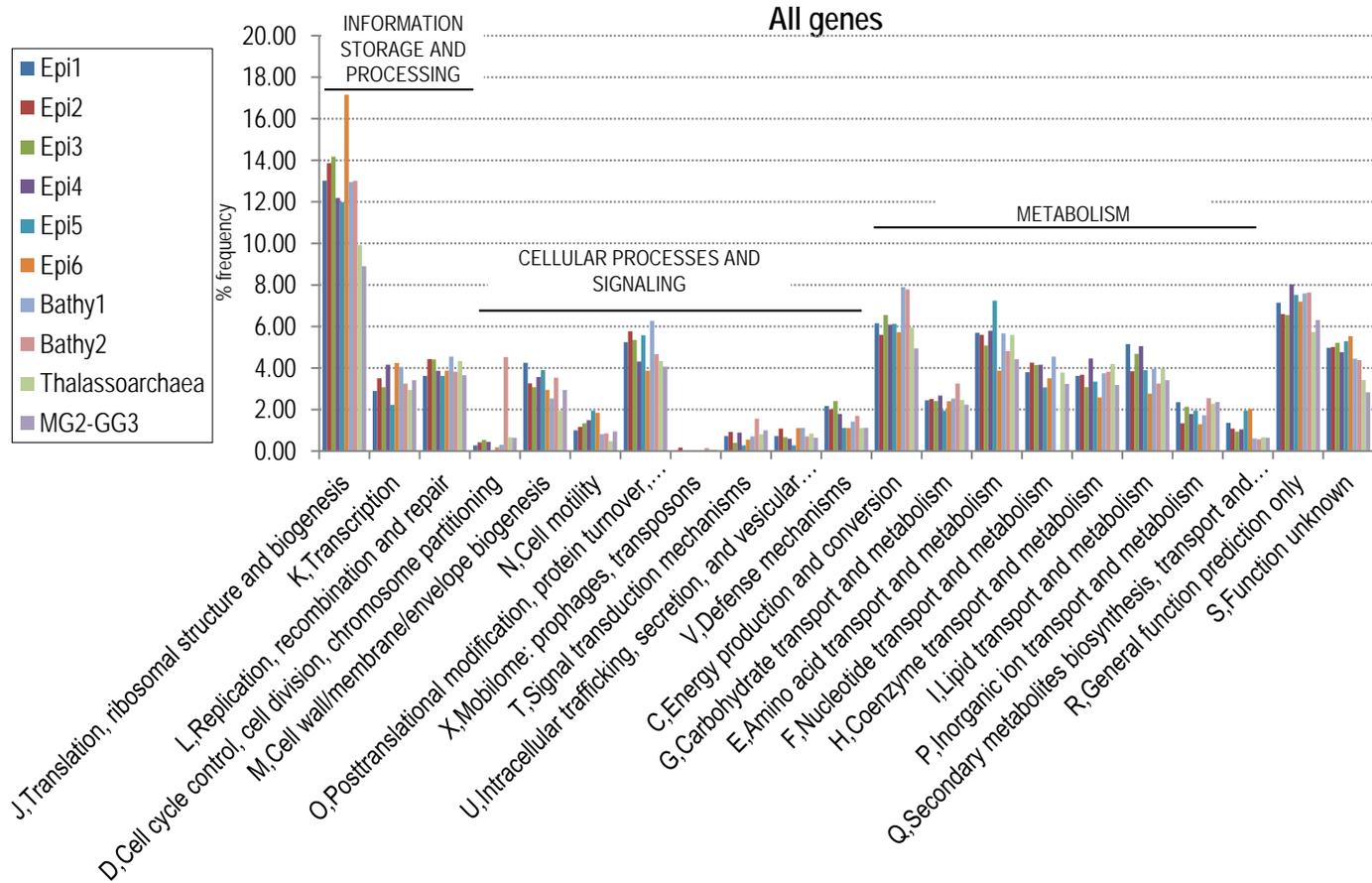


Supplementary Figure S14

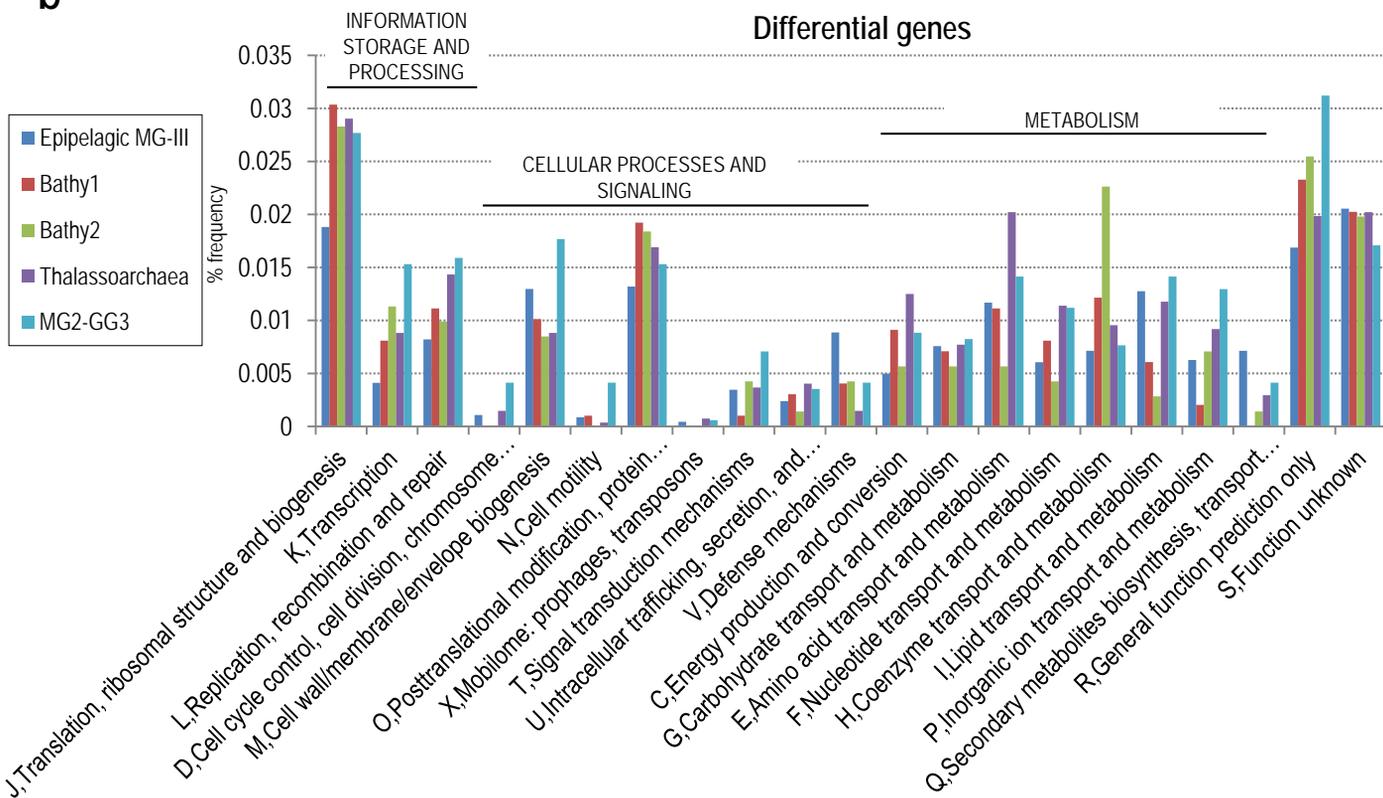


0.5

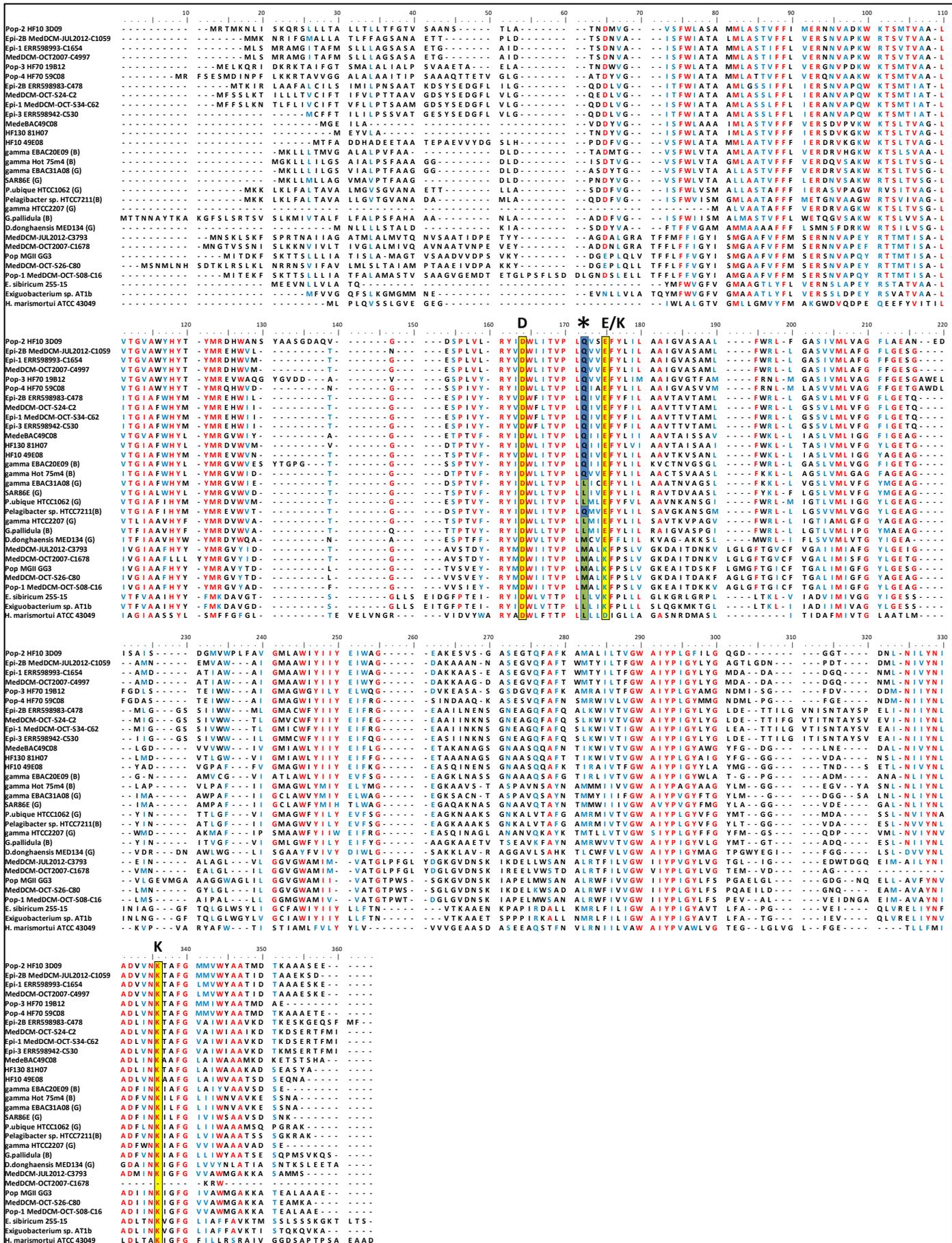
a



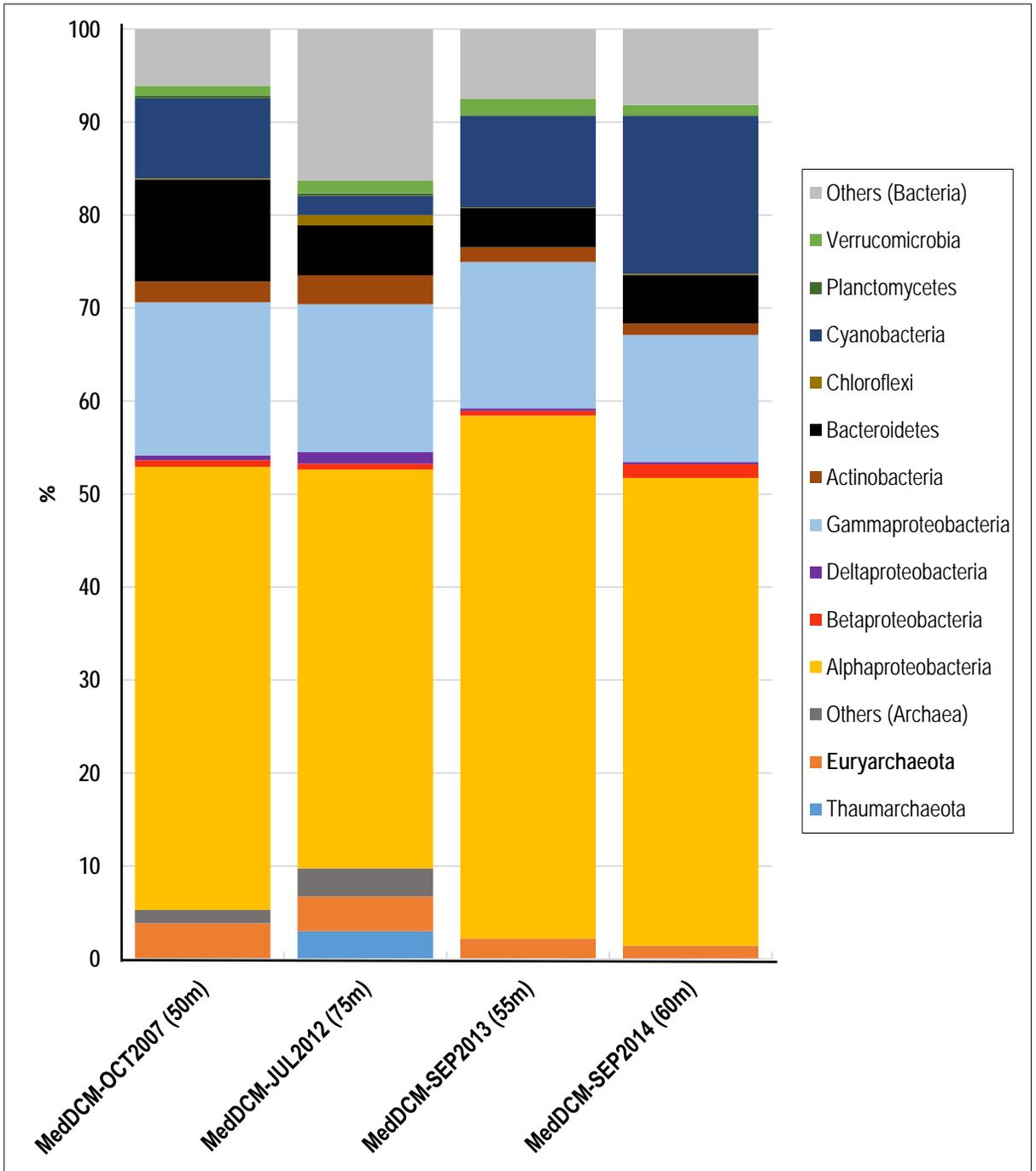
b



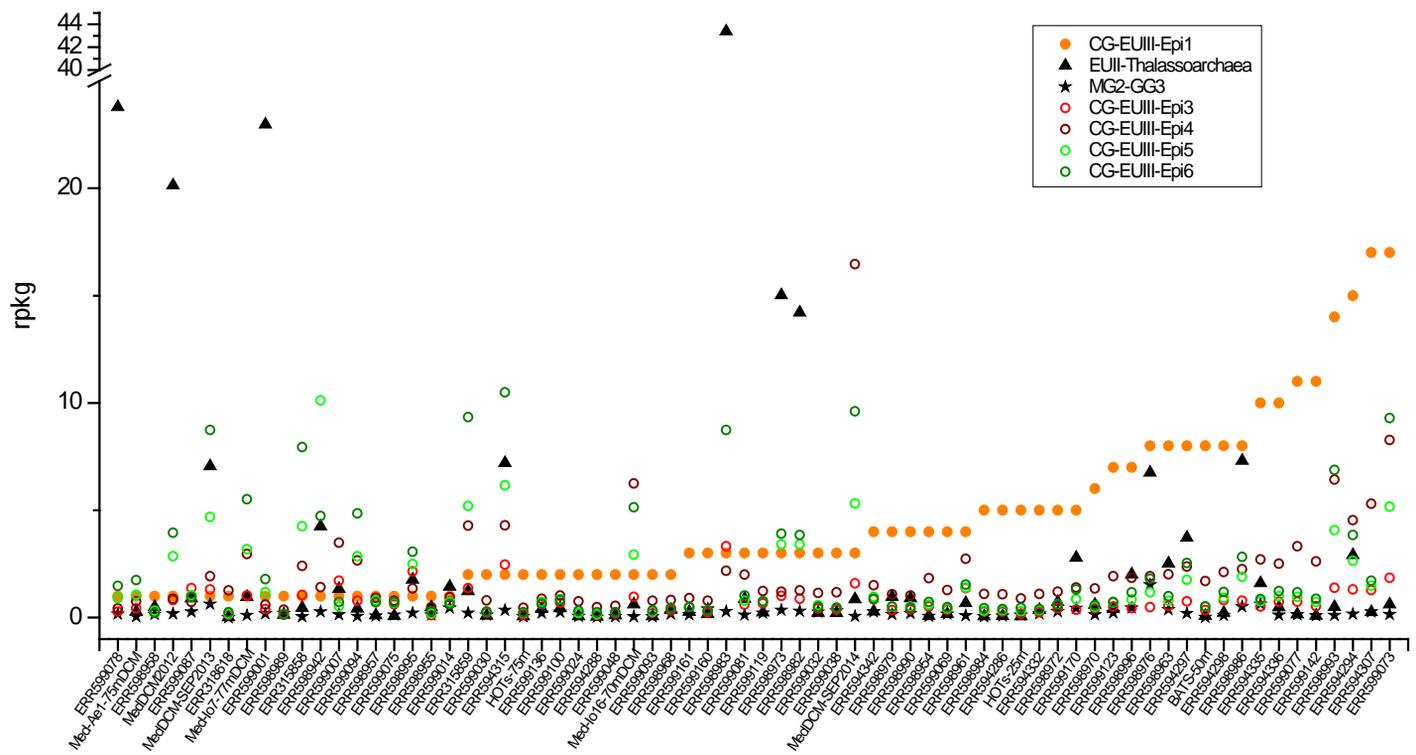
Supplementary Figure S16



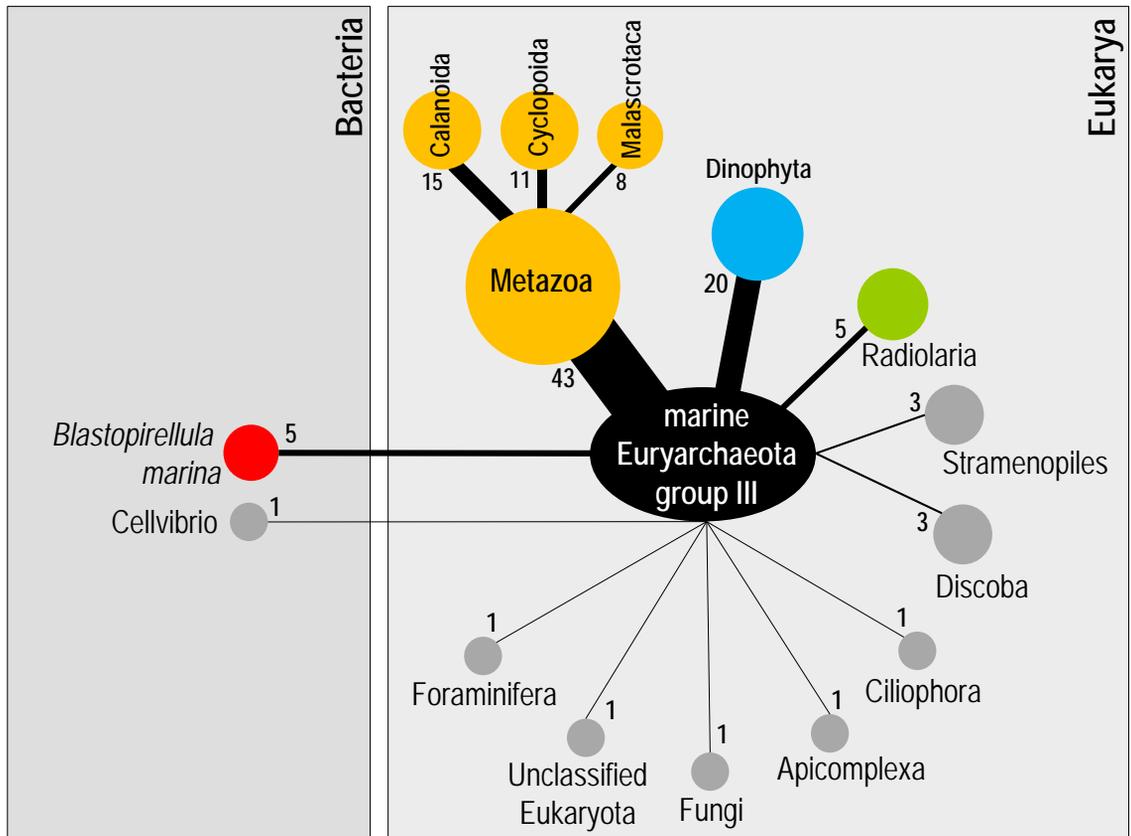
Supplementary Figure S17



Supplementary Figure S18



Supplementary Figure S19



Supplementary Table 1. List of contigs of each of the MG-III sequence bins

EPI-1			EPI-2A			EPI-3			EPI-4			EPI-5			EPI-6			BATHY-1			BATHY-2			NO CLASSIFIED CONTIGS								
Contig	GC	length (bp)	Contig	GC	length (bp)	Contig	GC	length (bp)	Contig	GC	length (bp)	Contig	GC	length (bp)	Contig	GC	length (bp)	Contig	GC	length (bp)	Contig	GC	length (bp)	Contig	GC	length (bp)	Contig	GC	length (bp)			
ERRS94294-C258	37.16	37101	ERRS98986-C1752	36.81	10318	MedDCM-JUL2012-C377	35.98	27364	ERRS98942-C113	35.54	55782	MedDCM-SEP2014-C87	37.04	47235	ERRS98942-C1146	35.6	16544	ERR315859-C350	37.38	11676	AD1000-41-D11	35.88	36746	KM3-110-C01	63.75	36614	ERR315859-C1033	41.17	7278			
ERRS94294-C291	35.19	33760	ERRS98986-C1805	37.82	10158	MedDCM-JUL2012-C368	34.94	24365	ERRS98942-C202	34.84	43429	MedDCM-SEP2014-C128	36.26	40668	ERRS98942-C2164	35.9	11461	ERRS99094-C1432	37.42	13606	AD1000-61-A07	36.68	30250	KM3-141-A08	64.58	33669	ERRS94307-C1518	40.19	11691			
ERRS94294-C495	36.13	24149	ERRS98993-C136	36.64	54729	MedDCM-JUL2012-C409	36.5	22638	ERRS98942-C302	35.53	35446	MedDCM-SEP2014-C148	37	39153	ERRS98942-C2190	35.24	11409	ERRS99094-C1899	34.8	11443	AD1000-91-C10	35.96	38736	KM3-148-H03	65.28	36104	ERRS94348-C334	37.71	21238			
ERRS94294-C597	37.63	22103	ERRS98993-C185	36.8	46411	MedDCM-JUL2012-C516	36.57	22616	ERRS98942-C339	35.82	33474	MedDCM-SEP2014-C247	36.71	31052	ERRS98942-C2311	35.88	11059	ERRS99094-C1956	35.97	11228	KM3-03-G06-C1	36.91	34695	KM3-152-H07	64.68	36691	ERRS98942-C4380	40.12	7492			
ERRS94294-C518	36.61	21634	ERRS98993-C186	36.68	38768	MedDCM-JUL2012-C603	36.14	22050	ERRS98942-C445	34.65	28224	MedDCM-SEP2014-C304	36.44	27517	ERRS98942-C2561	38.59	10664	ERRS99094-C1982	37.15	11155	KM3-03-G06-C2	35.77	33289	KM3-156-002	65.63	32803	ERRS98983-C1332	37.14	15365			
ERRS94294-C748	35.9	19337	ERRS98993-C340	36.02	32610	MedDCM-JUL2012-C602	35.56	21468	ERRS98942-C449	35.23	27959	MedDCM-SEP2014-C307	36.43	24794	ERRS98983-C594	35.52	23368	MedDCM-OCT2007-C68	36.51	111071	KM3-12-H02-C01	38.92	36194	KM3-157-C11	64.42	36794	ERRS98983-C447	36.88	27099			
ERRS94294-C624	37.01	17143	ERRS98993-C343	35.57	32391	MedDCM-JUL2012-C1228	36.1	21053	ERRS98942-C481	36.93	27084	MedDCM-SEP2014-C383	34.72	27450	ERRS98983-C718	36.85	21372	MedDCM-OCT2007-C633	34.28	55596	KM3-12-H02-C02	36.56	35952	KM3-161-F10	67.44	41692	ERRS98986-C1198	37.1	12565			
ERRS94294-C1053	36.67	15965	ERRS98993-C353	36.78	31966	MedDCM-JUL2012-C619	36.26	20185	ERRS98942-C494	35.35	26753	MedDCM-SEP2014-C411	35.59	24120	ERRS98983-C975	36.27	17947	MedDCM-OCT2007-C188	36.93	47138	KM3-147-B09	36.94	37598	KM3-164-G07	66.03	21529	ERRS98986-C1154	38.67	16689			
ERRS94294-C1574	35.19	15847	ERRS98993-C391	36.62	29994	MedDCM-JUL2012-C643	36.8	19543	ERRS98942-C530	35.95	25582	MedDCM-SEP2014-C552	35.47	20187	ERRS98983-C1136	35.76	16520	MedDCM-OCT2007-C2970	35.34	42132	Med-Ae2-600mDeep-C14	36.85	94706	KM3-176-D09	62.39	2430	ERRS98996-C4574	43.27	5775			
ERRS94294-C1114	37.11	15383	ERRS98993-C404	36.3	29492	MedDCM-JUL2012-C588	35.27	17776	ERRS98942-C531	35.88	25568	MedDCM-SEP2014-C554	37.18	20122	ERRS98983-C1174	35.36	16242	MedDCM-OCT2007-C377	36.78	41956	Med-Ae2-600mDeep-C40	38.62	67903	KM3-177-A07	60.44	30978	ERRS98996-C370	37.4	16664			
ERRS94294-C1164	37.48	15019	ERRS98993-C549	37.8	25250	MedDCM-JUL2012-C590	36.18	17749	ERRS98942-C563	34.34	24908	MedDCM-SEP2014-C667	37.41	18345	ERRS98983-C1305	36.21	15490	MedDCM-OCT2007-C3050	35.91	41814	Med-Ae2-600mDeep-C47	36.05	63835	KM3-177-C02	65.95	7771	ERRS9170-C2618	41.63	6853			
ERRS94294-C1349	36.35	14354	ERRS98993-C566	36.12	24705	MedDCM-JUL2012-C743	35.43	17605	ERRS98942-C588	36.71	24366	MedDCM-SEP2014-C672	36.21	18315	ERRS98983-C1450	36.43	14690	MedDCM-OCT2007-C824	36.05	41493	Med-Ae2-600mDeep-C50	35.64	63144	KM3-18-H05	64.03	36289	MedDCM-JUL2012-C379					
ERRS94294-C1343	36.5	13728	ERRS98993-C612	36.33	23521	MedDCM-JUL2012-C675	36.46	16175	ERRS98942-C609	36.9	22564	MedDCM-SEP2014-C690	37.48	18089	ERRS98983-C1599	36.4	13848	MedDCM-OCT2007-C352	36.98	40323	Med-Ae2-600mDeep-C53	37.02	61855	KM3-181-H05	64.58	32150	MedDCM-JUL2012-C880					
ERRS94294-C1553	38.3	12576	ERRS98993-C652	36.6	22734	MedDCM-JUL2012-C686	36.58	16035	ERRS98942-C636	35.43	19885	MedDCM-SEP2014-C703	37.68	17936	ERRS98983-C1619	37.02	13764	MedDCM-OCT2007-C449	37.06	39898	Med-Ae2-600mDeep-C57	37.81	59790	KM3-185-H03	62.49	39315	MedDCM-JUL2012-C882					
ERRS94294-C1639	36.45	12240	ERRS98993-C814	36.15	20075	MedDCM-JUL2012-C696	35.75	15875	ERRS98942-C852	33.95	19671	MedDCM-SEP2014-C793	36.1	17073	ERRS98983-C1680	35.91	13425	MedDCM-OCT2007-C1482	36.24	39690	Med-Ae2-600mDeep-C62	36.05	52612	KM3-188-A01	64.77	32963	MedDCM-OCT2007-C765					
ERRS94294-C1668	36.28	12116	ERRS98993-C863	36.95	19611	MedDCM-JUL2012-C1445	37.44	15686	ERRS98942-C899	36.04	19191	MedDCM-SEP2014-C803	36.77	16955	ERRS98983-C2504	36.19	10923	MedDCM-OCT2007-C359	37.25	37219	Med-Ae2-600mDeep-C78	36.86	47080	KM3-190-A12	64.89	34623	MedDCM-OCT2007-C967					
ERRS94294-C1732	37.13	11778	ERRS98993-C1010	35.74	18057	MedDCM-JUL2012-C1428	36.31	15645	ERRS98942-C963	36.41	18534	MedDCM-SEP2014-C851	36.55	16393	ERRS98983-C2521	35.37	10793	MedDCM-OCT2007-C359	37.25	37219	Med-Ae2-600mDeep-C83	36.31	45325	KM3-191-F05	61.01	32444						
ERRS94294-C1044	37.42	10969	ERRS98993-C1043	35.33	17827	MedDCM-JUL2012-C768	34.89	14974	ERRS98942-C1076	36.96	17164	MedDCM-SEP2014-C857	34.82	15283	ERRS98983-C2624	35.3	10525	MedDCM-OCT2007-C1276	36.23	36777	Med-Ae2-600mDeep-C97	38.33	41337	KM3-200-A03	61.24	7346						
ERRS94294-C1971	35.58	10978	ERRS98993-C1094	36	17255	MedDCM-JUL2012-C768	35.79	14911	ERRS98942-C1159	36.43	16478	MedDCM-SEP2014-C888	36.76	16025				MedDCM-OCT2007-C368	37.37	34684	Med-Ae2-600mDeep-C181	38.56	28692	KM3-202-G05	63.24	36284						
ERRS94294-C2015	36.31	10770	ERRS98993-C1183	36.43	16497	MedDCM-JUL2012-C833	34.95	14179	ERRS98942-C1332	35.61	15132	MedDCM-SEP2014-C940	37.03	15611				MedDCM-OCT2007-C360	36.86	33348	Med-Ae2-600mDeep-C194	37.74	28187	KM3-205-C10	65.19	10201						
ERRS94294-C2167	37.1	10336	ERRS98993-C1197	36.45	16346	MedDCM-JUL2012-C840	37.19	14037	ERRS98942-C1391	35.42	14753	MedDCM-SEP2014-C1047	36.5	14538				MedDCM-OCT2007-C174	36.8	32379	Med-Ae2-600mDeep-C277	36.5	23394	KM3-33-C12	64.56	14809						
ERRS94294-C2178	36.01	10029	ERRS98993-C1499	35.69	14401	MedDCM-JUL2012-C855	38.3	13838	ERRS98942-C1396	34.98	14733	MedDCM-SEP2014-C1069	36.87	14335				MedIo7-77mDCM-C2146	36.56	21038	Med-Ae2-600mDeep-C336	36.75	20947	KM3-35-H09	62.95	33996						
ERRS94294-C1107	38.74	14137	ERRS98993-C1654	35.45	13613	MedDCM-JUL2012-C643	36.84	13763	ERRS98942-C1476	36.49	14312	MedDCM-SEP2014-C1118	35.95	13922				MedIo7-77mDCM-C1113	36.16	18506	Med-Ae2-600mDeep-C344	36.81	20732	KM3-37-D11	64.49	41030						
ERRS94294-C1723	37.13	11194	ERRS98993-C1784	37.25	13048	MedDCM-JUL2012-C898	34.81	13277	ERRS98942-C1503	37.49	14168	MedDCM-SEP2014-C1286	35.57	12756				Med-Ae2-600mDeep-C1303	35.46	13394	Med-Ae2-600mDeep-C488	36.78	17189	KM3-43-F08	67.29	30905						
ERRS94348-C1415	36.67	13091	ERRS98993-C1988	37.09	12339	MedDCM-JUL2012-C743	35.98	12072	ERRS98942-C1641	36.61	13491	MedDCM-SEP2014-C1481	34.3	12843				MedIo7-77mDCM-C2049	35.01	10014	Med-Ae2-600mDeep-C599	37.9	15102	KM3-75-F08	63.04	36690						
ERRS94348-C334	37.71	21238	ERRS98993-C2355	35.73	11142	MedDCM-JUL2012-C1407	37.11	11597	ERRS98942-C1743	37.19	13056	MedDCM-SEP2014-C1485	37.54	11717				Med-Ae2-600mDeep-C2229	35.64	13869	Med-Ae2-600mDeep-C647	35.65	14260	KM3-51-F05	64.27	37422						
ERRS94348-C443	36.93	18426	ERRS98993-C2381	36.42	11076	MedDCM-JUL2012-C1485	33.85	11279	ERRS98942-C1776	38.68	12920	MedDCM-SEP2014-C1762	35.48	10580						Med-Ae2-600mDeep-C738	38.23	13111	KM3-54-A09	64.98	31009							
ERRS94348-C623	37.34	15533	ERRS98993-C2473	37.21	10870	MedDCM-JUL2012-C1587	36.42	10707	ERRS98942-C1797	35.55	12827	MedDCM-SEP2014-C1880	36.01	10193						Med-Ae2-600mDeep-C748	37.3	13028	KM3-61-H04	62.66	35580							
ERRS94348-C739	35.29	14481	ERRS98993-C2653	35.57	10434	MedDCM-JUL2012-C1294	36.93	10398	ERRS98942-C2010	35.3	11945	MedDCM-SEP2014-C1925	34.68	10057						Med-Ae2-600mDeep-C864	37.72	11932	KM3-65-G10	67.77	16442							
ERRS94348-C758	36.8	14338	ERRS98993-C2753	35.96	10196	MedDCM-JUL2012-C1295	35.14	10394	ERRS98942-C2020	35.47	11916	MedDCM-SEP2014-C1925	37.61	12697						Med-Ae2-600mDeep-C875	37.08	11813	KM3-65-H10	67.77	16442							
ERRS94348-C837	34.51	13773	ERRS98993-C2785	37.11	10145	MedDCM-JUL2012-C1698	35.26	10393	ERRS98942-C2168	38.12	11189	MedDCM-OCT2007-C1035	36.78	34544						Med-Ae2-600mDeep-C898	36.79	11640	KM3-75-F08	63.04	36690							
ERRS94348-C893	35.26	13263	ERRS98993-C2847	36.96	10045	MedDCM-JUL2012-C1741	34.99	10196	ERRS98942-C2464	35.03	10696									Med-Ae2-600mDeep-C921	36.66	11445	KM3-76-H07	64.42	34062							
ERRS94348-C1015	35.29	12441	ERRS98996-C297	35.91	23347	MedDCM-JUL2012-C1353	34.91	10030	ERRS98942-C2658	36.25	10233									Med-Ae2-600mDeep-C954	36.12	11128	KM3-79-B02	66.8	8021							
ERRS94348-C1040	37.03	12263	ERRS98996-C465	36.17	18389															Med-Ae2-600mDeep-C966	37.49	11055	KM3-82-F01	65.13	37648							
ERRS94348-C1055	37.53	12166	ERRS98996-C539	37.01	17111															Med-Ae2-600mDeep-C999	38.76	10785	KM3-89-F04</									

Supplementary Table 4. Housekeeping genes found in the MG-III bins and the CG-MG-III bins (as Naransigarao et al. 2012).

		Number of housekeeping genes found in the MG-III bins										Number of housekeeping genes found in the CG-MG-III bins								Number of housekeeping genes found in reference genomes																		
		Epi1	Epi2A	Epi2B	Epi2C	Epi3	Epi4	Epi5	Epi6	Bathy1	Bathy2	Epi1	Epi2	Epi3	Epi4	Epi5	Epi6	Bathy1	Bathy2	Cayman 92	Cayman 93	Guaymas 31	Guaymas 32															
	% Completeness estimation (Raes et al. 2007)	80	54.3	57.1	5.7	48.6	34.3	2.9	51.4	54.3	68.6	85.7	80	62.9	34.3	2.9	57.1	60	68.6	71.4	34.3	91.4	94.3															
	% Completeness estimation (Albertsen et al. 2013)	35.1	16.2	18.0	4.5	19.8	15.3	3.6	15.3	23.4	18.9	34.2	30.6	24.3	16.2	4.5	21.6	26.1	21.6	21.6	15.3	33.3	37.8															
	% Completeness estimation (Naransigarao et al. 2012)	83.0	45.3	54.7	5.7	45.3	39.6	7.6	54.7	60.4	58.5	84.9	75.2	62.3	43.4	9.4	60.4	64.2	58.5	67.9	35.9	92.5	90.6															
	# of genome-species inside the bin	3.07	1.08	1.03	1.00	1.00	1.00	1.00	1.48	1.09	2.32	1.18	1.43	1	1	1	1.0385	1.14	1	1	1	1	1.86															
Ribosomal genes	16S RNA	-	-	-	-	-	-	-	-	1	-	-	-	-	-	-	1	-	-	-	-	-	3															
	23S RNA	-	-	-	-	-	-	-	-	1	-	-	-	-	-	-	1	-	-	-	-	-	3															
COG	COG classification	Function																																				
	COG0008	GlnS COG0008 472	Glutamyl- and glutamyl-tRNA synthetases	3	1	1	-	-	-	-	-	1	-	2	2	-	1	1	-	1	-	1	-	1	1													
	COG0012	Predicted GTPase, probable translation factor	1	-	-	-	-	-	-	-	1	-	1	-	-	-	-	-	2	-	-	-	1	1														
	COG0013	AlaS COG0013 879	Alanyl-tRNA synthetase	1	1	-	-	1	1	-	-	2	1	1	2	1	1	-	-	1	1	-	-	1	1													
	COG0016	PheS COG0016 335	Phenylalanyl-tRNA synthetase alpha subunit	3	1	-	1	1	-	-	-	1	1	1	2	1	-	-	-	1	1	1	-	1	2													
	COG0018	ArgS COG0018 577	Arginyl-tRNA synthetase	2	-	-	-	1	1	1	1	1	-	2	-	1	1	1	1	1	1	1	1	1	2													
	COG0024	Map COG0024 255	Methionine aminopeptidase	5	1	1	-	1	1	1	1	2	-	1	2	1	1	1	1	3	-	1	-	1	2													
	COG0048	RpsL COG0048 129	Ribosomal protein S12	2	-	1	-	-	1	-	2	1	-	1	1	1	1	-	1	1	1	1	-	1	2													
	COG0049	RpsG COG0049 148	Ribosomal protein S7	2	-	1	-	-	1	-	2	1	-	1	1	1	1	-	1	1	1	1	-	1	2													
	COG0051	RpsJ COG0051 104	Ribosomal protein S10	1	-	1	-	-	-	-	2	1	-	1	1	1	-	-	1	1	1	1	-	1	2													
	COG0060	IleS COG0060 933	Isoleucyl-tRNA synthetase	2	-	-	-	-	-	-	1	-	-	1	-	-	-	-	1	-	-	-	-	1	2													
	COG0071	HspA COG0071 146	Molecular chaperone (small heat shock protein)	2	-	-	-	-	1	-	1	1	2	1	-	-	1	-	1	1	1	1	-	1	2													
	COG0080	RplK COG0080 141	Ribosomal protein L11	2	1	-	-	-	1	-	1	1	-	1	2	1	1	-	1	1	1	1	-	1	2													
	COG0081	RplA COG0081 228	Ribosomal protein L1	1	-	1	-	-	-	-	-	1	1	1	1	-	-	-	1	1	1	1	1	1	1													
	COG0085	RpoB COG0085 1060	DNA-directed RNA polymerase, beta subunit/140 kD subunit	-	-	1	-	1	1	-	3	1	3	-	1	1	1	-	1	1	1	1	1	1	2													
	COG0086	RpoC COG0086 808	DNA-directed RNA polymerase, beta subunit/160 kD subunit	-	-	1	-	1	1	-	3	1	3	-	1	1	1	-	1	1	1	1	1	1	1													
	COG0087	RplC COG0087 218	Ribosomal protein L3	5	-	1	-	-	-	-	-	3	1	1	1	1	-	-	-	1	1	1	1	1	2													
	COG0088	RplD COG0088 214	Ribosomal protein L4	5	-	1	-	1	-	-	-	3	1	1	1	-	-	-	-	1	1	1	1	1	2													
	COG0090	RplB COG0090 275	Ribosomal protein L2	5	1	1	-	1	-	-	-	3	1	1	1	1	-	-	-	1	1	1	1	1	1													
	COG0091	RplV COG0091 120	Ribosomal protein L22	5	1	1	-	1	-	-	-	3	1	1	1	-	-	-	-	1	1	1	1	1	2													
	COG0092	RpsC COG0092 233	Ribosomal protein S3	5	1	1	-	1	-	-	-	3	1	1	1	1	-	-	-	1	1	1	1	1	2													
	COG0093	RplN COG0093 122	Ribosomal protein L14	6	1	1	-	1	-	-	1	-	3	1	2	1	-	-	1	-	1	1	1	1	2													
	COG0094	RplE COG0094 180	Ribosomal protein L5	6	1	1	-	1	-	-	1	1	3	1	2	1	-	-	1	1	1	1	1	1	2													
	COG0096	RpsH COG0096 132	Ribosomal protein S8	6	1	1	-	1	-	-	1	1	3	1	2	1	-	-	1	1	1	1	1	1	2													
	COG0097	RplF COG0097 178	Ribosomal protein L6/P/L9E	6	1	1	-	1	-	-	1	1	3	1	2	1	-	-	1	1	1	1	1	1	2													
	COG0098	RpsE COG0098 181	Ribosomal protein S5	6	1	1	-	1	-	-	1	1	3	1	2	1	-	-	1	1	1	1	1	1	2													
	COG0099	RpsM COG0099 121	Ribosomal protein S13	2	-	-	-	-	1	-	-	-	1	2	-	-	1	-	-	1	-	-	-	1	2													
	COG0100	RpsK COG0100 129	Ribosomal protein S11	2	-	-	-	-	1	-	-	-	2	2	-	-	1	-	-	1	1	1	1	1	2													
	COG0102	RplM COG0102 148	Ribosomal protein L13	1	1	-	-	-	1	-	1	-	3	1	1	1	-	1	1	1	1	-	-	1	2													
	COG0103	RplS COG0103 130	Ribosomal protein S9	1	1	-	-	-	1	-	1	-	3	1	1	1	-	1	1	1	1	-	-	1	2													
	COG0124	HisS COG0124 429	Histidyl-tRNA synthetase	-	-	-	-	-	-	2	1	-	1	-	-	-	-	-	1	-	1	-	-	1	2													
	COG0130	TruB COG0130 271	Pseudouridine synthase	-	-	-	-	-	-	-	1	-	-	-	-	-	-	-	1	-	-	-	1	1	2													
	COG0143	MetG COG0143 558	Methionyl-tRNA synthetase	2	1	1	-	-	-	-	1	-	2	1	-	1	-	-	1	-	1	1	-	1	1													
	COG0164	RnhB COG0164 199	Ribonuclease HII	2	2	-	1	1	-	-	-	2	-	1	1	1	-	-	2	-	-	-	-	1	2													
	COG0177	Nth COG0177 211	Predicted EndoII-related endonuclease	1	-	-	1	1	1	-	-	1	1	1	1	1	-	-	1	1	1	1	1	1	2													
	COG0180	TrpS COG0180 314	Tryptophanyl-tRNA synthetase	1	-	1	-	1	1	1	1	1	-	3	1	1	1	1	1	1	1	-	1	1	1													
	COG0186	RpsQ COG0186 87	Ribosomal protein S17	6	1	1	-	1	-	-	1	-	3	1	2	1	-	-	1	-	1	1	1	1	2													
	COG0197	RplP COG0197 146	Ribosomal protein L16/L10E	5	2	-	-	1	1	-	-	1	-	1	1	1	1	-	-	1	-	-	-	1	2													
	COG0200	RplO COG0200 152	Ribosomal protein L15	6	1	1	-	1	-	-	1	1	3	1	2	1	-	-	1	1	1	1	-	1	2													
	COG0201	SecY COG0201 436	Preprotein translocase subunit SecY	5	1	1	-	-	-	-	1	1	3	1	2	1	-	-	-	1	1	1	1	-	1	2												
	COG0250	NusG COG0250 178	Transcription antiterminator	1	1	-	-	-	1	-	1	-	-	1	2	1	1	-	1	1	1	-	-	1	2													
	COG0256	RplR COG0256 125	Ribosomal protein L18	6	1	1	-	1	-	-	1	1	3	1	2	1	-	-	-	1	1	1	1	-	1	1												
	COG0441	ThrS COG0441 589	Threonyl-tRNA synthetase	1	-	1	-	-	-	-	3	1	-	1	1	-	-	-	1	1	-	1	1	1	1	2												
	COG0459	GroL COG0459 524	Chaperonin GroEL (HSP60 family)	1	-	-	-	1	1	-	1	1	1	2	1	1	1	-	1	2	1	1	1	1	2	4												
	COG0468	RecA COG0468 279	RecA/RadA recombinase	4	-	2	-	1	1	1	1	1	1	1	2	1	1	1	2	1	1	1	1	1	1	4												
	COG0480	FusA COG0480 697	Translation elongation factors (GTPases)	2	-	1	-	-	1	-	2	1	-	1	1	1	1	-	1	1	-	1	-	-	1	1												
	COG0495	LeuS COG0495 814	Leucyl-tRNA synthetase	1	1	-	-	-	-	-	-	-	-	1	1	-	-	-	-	-	1	1	1	1	1	2												
	COG0522	RpsD COG0522 205	Ribosomal protein S4 and related proteins	2	-	-	-	-	1	-	-	-	1	2	-	-	1	-	-	-	1	1	-	-	1	2												
	COG0525	ValS COG0525 877	Valyl-tRNA synthetase	-	-	1	-	-	-	-	-	-	3	1	1	1	1	-	-	1	1	-	-	1	2													
	COG0532	InfB COG0532 509	Translation initiation factor 2 (IF-2; GTPase)	1	-	1	-	-	-	-	-	1	1	1	2	1	1	1	-	1	1	-	-	1	1													

Supplementary Table 5. Protein categories based on arCOG database.

arCOG classification	gene	product	COG classification	pFAM domain	cdc	TIGR classification	Epipelagic CG-MGIII bins					Pelagic CG-MGIII bins		Other Euryarchaea					
							Epi1	Epi2	Epi3	Epi4	Epi5	Epi6	Bathy1	Bathy-2	A.boneii T469	MG2-GG3	Thalassosarchaea		
arCOG00415	L	Replication, recombination and repair	RecA	RecA/RadA recombinase	COG00468	pfam14520.pfam0842	cd01123	TIGR02236	1	1	1	1	1	1	1	1	1	1	1
arCOG04143	L	Replication, recombination and repair	-	DNA topoisomerase VI, subunit A	COG01697	pfam04406	cd00223		1	1	1	1	1	1	1	1	1	1	5
arCOG04455	L	Replication, recombination and repair	HYS2	Archaeal DNA polymerase II, small subunit/DNA polymerase delta, subunit B	COG01311	pfam01336.pfam0404	cd04490,cd07386		1	1	1	1	1	1	1	1	1	1	1
arCOG00459	L	Replication, recombination and repair	Nth	EndoIII-related endonuclease	COG00177	pfam00730.pfam1057	cd00056	TIGR01083	1	1	1	1	1	1	1	2	1	1	1
arCOG00417	L	Replication, recombination and repair	RecA	RecA/RadA recombinase	COG00468		cd01394	TIGR02237	1	1	1	1	1	2	1	1	1	1	1
arCOG04367	L	Replication, recombination and repair	GyrA	Type IIA topoisomerase (DNA gyrase/topo II, topoisomerase IV), A subunit	COG00188	pfam00521.pfam0398	cd00187	TIGR01063	1	2	1	1	1	1	1	1	1	1	3
arCOG00872	L	Replication, recombination and repair	MPH1	ERCC4-like helicase	COG01111	pfam00270.pfam0027	cd00046,cd120	TIGR00643,TIGR	1	2	1	1	1	1	1	1	1	1	2
arCOG04447	L	Replication, recombination and repair	-	Archaeal DNA polymerase II, large subunit	COG01933	pfam03833.pfam09845		TIGR00354	1	2	1	1	1	1	1	1	1	1	1
arCOG00551	L	Replication, recombination and repair	-	DNA replication initiation complex subunit, GINS15 family	COG01711		cd11714		1		1	1	1	1	1	1	1	1	1
arCOG04990	L	Replication, recombination and repair	-	Predicted endonuclease, contains HTH and PD-DEK nuclease domains		pfam14811			1		1	1	1	1	1	1	1	1	2
arCOG00467	L	Replication, recombination and repair	CDC6	Cdc6-related protein, AAA superfamily ATPase	COG01474	pfam13401.pfam0907	cd00009,cd087	TIGR02928	2	1	1	1	1	1	1	1	1	1	2
arCOG02610	L	Replication, recombination and repair	ScpA	Chromatin segregation and condensation protein Rec8/ScpA/Sccl1, kleisin fam	COG01354	pfam02616				1				1	1	1	1	1	2
arCOG00439	L	Replication, recombination and repair	MCM2	Predicted ATPase involved in replication control, Cdc46/Mcm family	COG01241	pfam14551.pfam0049	cd00009				1	1	1	1	1	1	1	1	2
arCOG00427	L	Replication, recombination and repair	RecJ/Cdc45	Single-stranded DNA-specific exonuclease RecJ	COG00608									1	1	1	1	1	2
arCOG02258	L	Replication, recombination and repair	-	RPA family protein, a subunit of RPA complex in P.furiosus	COG03390				1	1	1	1	1	1	1	1	1	1	3
arCOG04582	L	Replication, recombination and repair	Dpo4/DinP	Family Y DNA polymerase	COG00389	pfam00817.pfam1179	cd03586		1	1	1	1	1	1	1	1	1	1	1
arCOG01166	L	Replication, recombination and repair	MutL	DNA mismatch repair enzyme (predicted ATPase)	COG00323	pfam13589.pfam0111	cd00075,cd007	TIGR00585	1	1	1	1	1	1	1	1	1	1	2
arCOG01165	L	Replication, recombination and repair	-	DNA topoisomerase VI, subunit B	COG01389	pfam02518.pfam0348	cd00075,cd008	TIGR01052	1	1	1	1	1	1	1	1	1	1	4
arCOG01486	L	Replication, recombination and repair	RnmV	5S rRNA maturation endonuclease (Ribonuclease M5), contains TOPRIM dom	COG01658	pfam01751	cd01027		1	1	1	1	1	1	1	1	1	1	1
arCOG04121	L	Replication, recombination and repair	RnhB	Ribonuclease HII	COG00164	pfam01351	cd07180	TIGR00729	1	1	1	1	1	1	1	1	1	1	2
arCOG00470	L	Replication, recombination and repair	HolB	ATPase involved in DNA replication HolB, large subunit	COG00470	pfam00004	cd00009	TIGR02397	1	2	1	1	1	1	1	1	1	1	1
arCOG04371	L	Replication, recombination and repair	GyrB	Type IIA topoisomerase (DNA gyrase/topo II, topoisomerase IV), B subunit	COG00187	pfam02518.pfam0020	cd00075,cd008	TIGR01059	1	2	1	1	1	1	1	1	1	1	3
arCOG04110	L	Replication, recombination and repair	PR1	Eukaryotic-type DNA primase, catalytic (small) subunit	COG01467	pfam01896	cd04860	TIGR00335	1	2	2	2	1	1	1	1	1	2	5
arCOG00488	L	Replication, recombination and repair	DnaN	DNA polymerase sliding clamp subunit (PCNA homolog)	COG00592	pfam00705.pfam0274	cd00577	TIGR00590	1	1	1	1	1	1	1	1	1	1	2
arCOG01078	L	Replication, recombination and repair	-	NUDX1 family hydrolase	COG00494	pfam00293	cd03428			1	1	1	1	1	1	2	1	1	1
arCOG00787	L	Replication, recombination and repair	-	UvrD/Rep family helicase fused to exonuclease family domain	COG02887	pfam12705	cd09637	TIGR01249,TIGR00372			1		1	1	1	1	1	1	1
arCOG01527	L	Replication, recombination and repair	TopA	Topoisomerase IA	COG00550	pfam01751.pfam0113	cd03362,cd001	TIGR01057	1	1	1	1	1	1	1	1	1	1	2
arCOG04050	L	Replication, recombination and repair	FEN1	5'-3' exonuclease	COG00258	pfam00752.pfam0086	cd09867	TIGR03674	1	1	1	1	1	1	1	1	1	1	2
arCOG00558	L	Replication, recombination and repair	SrmB	Superfamily II DNA and RNA helicase	COG00513	pfam00270.pfam0027	cd00268,cd000	TIGR01389	1	1	1	1	1	1	1	3	3	3	3
arCOG00129	L	Replication, recombination and repair	-	DNA modification methylase	COG00863	pfam01555.pfam01555		TIGR01177	1							1	1	1	1
arCOG00328	L	Replication, recombination and repair	PolB3	DNA polymerase PolB3	COG00417	pfam03104.pfam0013	cd05781,cd055	TIGR00592	1	1					2	1	2	1	4
arCOG00905	L	Replication, recombination and repair	-	Uracil-DNA glycosylase	COG01573	pfam03167	cd10031	TIGR00758	1						2	1	2	1	1
arCOG01510	L	Replication, recombination and repair	RPA1	Single-stranded DNA-binding replication protein A (RPA), large (70 kD) subunit	COG01599		cd04491,cd04491		2	3	2	2	1	2	2	2	3	2	3
arCOG01072	L	Replication, recombination and repair	-	NUDX1 family hydrolase	COG00494	pfam00293	cd03426		1	1	1	1	1	1	1	1	1	1	1
arCOG03013	L	Replication, recombination and repair	PR2	Eukaryotic-type DNA primase, large subunit	COG02219	pfam04104	cd06560		1	1	1	1	1	1	1	1	1	1	1
arCOG00469	L	Replication, recombination and repair	HolB	ATPase involved in DNA replication HolB, small subunit	COG00470	pfam13177.pfam0854	cd00009	TIGR02397	1	1	1	1	1	1	1	1	1	2	2
arCOG00553	L	Replication, recombination and repair	BRR2	Replicative superfamily II helicase	COG01204	pfam00270.pfam0027	cd00046,cd000	TIGR04121	2	3	1	2	1	3	3	1	1	1	4
arCOG01894	L	Replication, recombination and repair	Nfo	Endonuclease IV	COG00648	pfam01261	cd00019	TIGR00587	1	1	1	1	1	1	1	1	1	1	4
arCOG01526	L	Replication, recombination and repair	TopG2	Reverse gyrase	COG01110	pfam00270.pfam0175	cd00046,cd033	TIGR01054	1	2	1	1	1	1	1	1	1	1	2
arCOG00464	L	Replication, recombination and repair	AlkA	3-methyladenine DNA glycosylase/8-oxoguanine DNA glycosylase	COG00122	pfam07934.pfam0073	cd00056	TIGR00588	1		1	1	1	1	1	1	1	1	1
arCOG03142	L	Replication, recombination and repair	-	Nuclease of RNase H fold, RuvC/Ygf family					1	1	1	1	1	1	1	1	1	1	1
arCOG00368	L	Replication, recombination and repair	SbcC	ATPase involved in DNA repair, SbcC	COG00419	pfam13476.pfam1351	cd03240,cd001	TIGR00611,TIGR02168			1			1	1	1	1	1	3
arCOG02897	L	Replication, recombination and repair	MutS	Mismatch repair ATPase (MutS family)	COG00249	pfam01624.pfam0518	cd03284	TIGR01070			1			2	1	1	1	1	1
arCOG02724	L	Replication, recombination and repair	Ada	Methylated DNA-protein cysteine methyltransferase	COG00350	pfam01035	cd06445	TIGR00589			1				1	1	1	1	1
arCOG00397	L	Replication, recombination and repair	SbcD	DNA repair exonuclease, SbcD	COG00420	pfam00149	cd00840								2	1	1	1	1
arCOG02257	L	Replication, recombination and repair	-	RPA family protein, a subunit of RPA complex in P.furiosus	COG03390														1
arCOG08649	L	Replication, recombination and repair	-	Topoisomerase IB	COG03569	pfam02919.pfam0102	cd00660,cd00659		1	1		1							1
arCOG04281	L	Replication, recombination and repair	DnaG	DNA primase (bacterial type)	COG00358	pfam13662	cd01029	TIGR01391	1	2						1	1	1	2
arCOG01073	L	Replication, recombination and repair	-	NUDX1 family hydrolase	COG00494	pfam00293	cd03424	TIGR00052	1		1					1	1	1	1
arCOG01347	L	Replication, recombination and repair	CDC9	ATP-dependent DNA ligase	COG01793	pfam04675.pfam0106	cd07901,cd079	TIGR000574	2							1	1	1	1
arCOG02840	L	Replication, recombination and repair	PhrB	Deoxyribodipyrimidine photolyase	COG00415	pfam00875.pfam03441		TIGR03556	1	3	1					2	2	7	7
arCOG05109	L	Replication, recombination and repair	DnaQ	DNA polymerase III, epsilon subunit or related 3'-5' exonuclease	COG00847	pfam00929	cd06127	TIGR00573	1							1	1	1	1
arCOG00890	L	Replication, recombination and repair	-	DNA modification methylase	COG00863	pfam01555				1									1
arCOG01898	L	Replication, recombination and repair	Uve	UV damage repair endonuclease	COG04294	pfam03851		TIGR00629			1								1
arCOG00115	L	Replication, recombination and repair	-	DNA modification methylase	COG00863	pfam01555											1	1	1
arCOG00792	L	Replication, recombination and repair	-	Superfamily I DNA/RNA helicase	COG01112	pfam13086.pfam13087		TIGR00376									1	1	1
arCOG00919	L	Replication, recombination and repair	-	Holliday junction resolvase, archaeal type	COG01591	pfam01870	cd00523										1	1	2
arCOG02207	L	Replication, recombination and repair	XthA	Exonuclease III	COG00708	pfam03372	cd09073	TIGR00633									1	1	2
arCOG00048	L	Replication, recombination and repair	RlmL	23S rRNA G2445 N2-methylase RlmL	COG00116	pfam02926.pfam0117	cd11715	TIGR01177									1	1	2
arCOG00426	L	Replication, recombination and repair	RecJ	DH1 superfamily phosphohydrolase/exonuclease	COG00608	pfam01368											1	1	1
arCOG00463	L	Replication, recombination and repair	-	Uri superfamily endonuclease	COG01833	pfam01986	cd10441										1	1	1
arCOG00928	L	Replication, recombination and repair	-	Endonuclease V homolog	COG01628	pfam01949											1	1	1
arCOG01074	L	Replication, recombination and repair	-	NUDX1 family hydrolase	COG00494	pfam00293	cd03427	TIGR02705									1	1	1
arCOG04206	L	Replication, recombination and repair	MUS81	ERCC4-type nuclease	COG01948	pfam02732.pfam12826		TIGR00596									1	1	1
arCOG04295	L	Replication, recombination and repair	Mpg	3-methyladenine DNA glycosylase	COG02094	pfam02245	cd00540	TIGR00567									1	1	1
arCOG04357	L	Replication, recombination and repair	ENDO3c	Thermostable 8-oxoguanine DNA glycosylase	COG01059	pfam00730	cd00056												

arCOG04099	J	Translation, ribosomal structure and biogenesis	RpsS	Ribosomal protein S19	COG00185	pfam00203		TIGR01025	1	1	1	1	1	1	1	1	1	2
arCOG00678	J	Translation, ribosomal structure and biogenesis	Rrp4	Exosome complex RNA-binding protein Rrp4, contains S1 and KH domains	COG01097		cd05789		1	1	1	1	1	1	1	1	1	1
arCOG01574	J	Translation, ribosomal structure and biogenesis	Rrp42	Exosome complex RNA-binding protein Rrp42, RNase PH superfamily	COG02123	pfam01138, pfam0372	cd11365	TIGR01966	1	1	1	1	1	1	1	1	1	2
arCOG04131	J	Translation, ribosomal structure and biogenesis	RsmA	16S rRNA A1518 and A1519 N6-dimethyltransferase RsmA/KsgA/DIM1	COG00030	pfam00398		TIGR00755	1	1	1	1	1	1	1	1	1	1
arCOG00973	J	Translation, ribosomal structure and biogenesis	RsmB	16S rRNA C967 or C1407 C5-methylase, RsmB/RsmF family	COG00144	pfam01189		TIGR00446	1	1	1	1	1	1	1	1	1	3
arCOG00975	J	Translation, ribosomal structure and biogenesis	RsmB	16S rRNA C967 or C1407 C5-methylase, RsmB/RsmF family	COG00144	pfam01189	cd02440	TIGR00446	1	1	1	1	1	1	1	1	1	3
arCOG01239	J	Translation, ribosomal structure and biogenesis	RsmE	RNA base methyltransferase family enzyme	COG01901	pfam04013			1	2	1	1	1	1	1	1	1	1
arCOG04246	J	Translation, ribosomal structure and biogenesis	RtcB	RNA 3'-P ligase, RtcB family protein	COG01690	pfam01139		TIGR03073	1	1	1	1	1	1	1	1	1	1
arCOG04187	J	Translation, ribosomal structure and biogenesis	Sdo1	Ribosome maturation protein Sdo1	COG01500	pfam01172, pfam09377		TIGR00291	1	1	1	1	1	1	1	1	1	1
arCOG01564	J	Translation, ribosomal structure and biogenesis	SeIB	Selenocysteine-specific translation elongation factor or SeIB-II domain	COG03276		cd03696		1	1	1	1	1	1	1	1	1	3
arCOG01701	J	Translation, ribosomal structure and biogenesis	SEN2	tRNA splicing endonuclease	COG01676	pfam02778, pfam01974		TIGR00324	1	1	1	1	1	1	1	1	1	5
arCOG00403	J	Translation, ribosomal structure and biogenesis	SerS	Seryl-tRNA synthetase	COG00172	pfam02403, pfam0058	cd00770	TIGR00414	1	1	1	1	1	1	1	1	1	1
arCOG01923	J	Translation, ribosomal structure and biogenesis	SIK1	RNA processing factor Prp31, contains Nop domain	COG01498				1	1	1	1	1	1	1	1	1	2
arCOG01952	J	Translation, ribosomal structure and biogenesis	SUA5	tRNA A37 threonylcarbamoyladenosine synthetase subunit TsaC/SUA5/YrdC	COG00009	pfam01300		TIGR00057	1	2	1	1	1	1	2	1	1	1
arCOG04223	J	Translation, ribosomal structure and biogenesis	SUI1	Translation initiation factor 1 (eIF-1/SUI1)	COG00023	pfam01253	cd11567	TIGR01158	1	2	1	1	1	1	1	1	1	2
arCOG04107	J	Translation, ribosomal structure and biogenesis	SUI2	Translation initiation factor 2, alpha subunit (eIF-2alpha)	COG01093	pfam00575, pfam0754	cd04452	TIGR00717	1	1	1	1	1	1	1	1	1	2
arCOG00056	J	Translation, ribosomal structure and biogenesis	Tan1	tRNA(Ser,Leu) C12 N-acetylase TAN1, contains THUMP domain	COG01818	pfam02926, pfam1441	cd11718, cd061	TIGR00342	1	1	1	1	1	1	1	1	1	2
arCOG01630	J	Translation, ribosomal structure and biogenesis	TdcF	Translation initiation inhibitor, yjvF family	COG00251	pfam01042	cd00448	TIGR00004	2	2	2	2	2	1	3	2	2	4
arCOG01561	J	Translation, ribosomal structure and biogenesis	TEF1	Translation elongation factor eF-1 alpha, GTPase	COG05256	pfam00009, pfam0314	cd01883, cd036	TIGR00483	1	1	1	1	1	1	1	1	1	5
arCOG00989	J	Translation, ribosomal structure and biogenesis	Tgt	Queuine/archaeosine tRNA-ribosyltransferase	COG00343	pfam01702		TIGR00432	1	1	1	1	1	1	1	1	1	1
arCOG00038	J	Translation, ribosomal structure and biogenesis	Thil	tRNA S(4)U 4-thiouridine synthase	COG00301	pfam02926, pfam0256	cd11716, cd017	TIGR00342, TIGR04271	1	1	1	1	1	1	1	1	2	2
arCOG00401	J	Translation, ribosomal structure and biogenesis	ThrS	Threonyl-tRNA synthetase	COG00441	pfam00587, pfam0312	cd00771, cd008	TIGR00418	1	1	1	1	1	1	1	1	1	4
arCOG01115	J	Translation, ribosomal structure and biogenesis	TiaS	tRNA(Lie2) 2-azagmatinylcytidine synthetase; containing Zn-ribbon domain and	COG01571	pfam04849, pfam0728	cd04482	TIGR03280	1	1	1	1	1	1	1	1	1	1
arCOG04176	J	Translation, ribosomal structure and biogenesis	TIF6	Translation initiation factor 6 (eIF-6)	COG01976	pfam01912	cd00527	TIGR00323	1	2	1	1	1	1	1	1	1	1
arCOG00042	J	Translation, ribosomal structure and biogenesis	TiIS	tRNA(Lie)-lysine synthase TiIS/MesI	COG00037	pfam01171	cd01993	TIGR02432	1	1	1	1	1	1	1	1	2	3
arCOG00985	J	Translation, ribosomal structure and biogenesis	Tma20	Predicted RNA-binding protein, contains PUA domain	COG02016	pfam09183, pfam01472		TIGR03684	1	1	1	1	1	1	1	1	1	2
arCOG01951	J	Translation, ribosomal structure and biogenesis	TmcA	tRNA(Met) C34 N-acetyltransferase TmcA	COG01444	pfam08351, pfam05127, pfam13718			1	1	1	1	1	1	1	1	1	2
arCOG01219	J	Translation, ribosomal structure and biogenesis	TRM1	N2, N2-dimethylguanosine tRNA methyltransferase	COG01867	pfam02005		TIGR00308	1	2	1	1	1	1	2	1	1	1
arCOG00047	J	Translation, ribosomal structure and biogenesis	Trm11	tRNA G10 N-methylase Trm11	COG01041	pfam01170		TIGR01177	1	1	1	1	1	1	1	1	1	2
arCOG00033	J	Translation, ribosomal structure and biogenesis	Trm5	Wybutosine (yW) biosynthesis enzyme, Trm5 methyltransferase	COG02520	pfam02475			2	1	1	2	2	1	1	2	1	2
arCOG01018	J	Translation, ribosomal structure and biogenesis	TrmJ	tRNA C32_U32 (ribose-2'-O)-methylase TrmJ or a related methyltransferase	COG00565	pfam00588		TIGR00050	1	2	1	1	1	2	1	1	2	2
arCOG01887	J	Translation, ribosomal structure and biogenesis	TrpS	Tryptophanyl-tRNA synthetase	COG00180	pfam00579	cd00806	TIGR00233	1	1	1	1	1	1	1	1	1	3
arCOG04449	J	Translation, ribosomal structure and biogenesis	TruA	Pseudouridylylase synthase	COG00101	pfam01416, pfam0141	cd02866	TIGR00071	1	1	1	1	1	1	1	1	1	2
arCOG00987	J	Translation, ribosomal structure and biogenesis	TruB	Pseudouridine synthase	COG00130	pfam08068, pfam0150	cd02572	TIGR00425	1	1	1	1	1	1	1	1	1	1
arCOG04252	J	Translation, ribosomal structure and biogenesis	TruD	tRNA(Glu) U13 pseudouridine synthase TruD	COG00585	pfam01142	cd02577	TIGR00094	1	2	1	1	1	1	1	1	1	1
arCOG00761	J	Translation, ribosomal structure and biogenesis	TsaA	tRNA (Trp-GGU) A37 N-methylase	COG01720	pfam01980	cd09281	TIGR00104	1	1	1	1	1	1	1	1	1	1
arCOG04733	J	Translation, ribosomal structure and biogenesis	Tsr3	Ribosome biogenesis protein Tsr3, contains Fer4-like metal-binding domain	COG02042	pfam04034			1	1	1	1	1	1	1	1	1	2
arCOG01886	J	Translation, ribosomal structure and biogenesis	TyrS	Tyrosyl-tRNA synthetase	COG00162	pfam00579	cd00805	TIGR00234	1	1	1	1	1	1	1	1	1	2
arCOG04174	J	Translation, ribosomal structure and biogenesis	TYW1	Wybutosine (yW) biosynthesis enzyme, Fe-S oxidoreductase	COG00731	pfam04055, pfam0860	cd01335	TIGR03972	1	2	1	1	1	1	1	1	1	3
arCOG10124	J	Translation, ribosomal structure and biogenesis	TYW2	Wybutosine (yW) biosynthesis enzyme, TYW2 transferase	COG02520	pfam02475	cd02440	TIGR01444	1	1	1	1	1	1	1	1	1	2
arCOG04156	J	Translation, ribosomal structure and biogenesis	TYW5	Wybutosine (yW) biosynthesis enzyme	COG01590	pfam02676			1	1	1	1	1	1	1	1	1	2
arCOG00808	J	Translation, ribosomal structure and biogenesis	ValS	Valyl-tRNA synthetase	COG00525	pfam00133, pfam0826	cd00817, cd079	TIGR00422	1	1	1	1	1	1	1	1	2	6
arCOG04225	J	Translation, ribosomal structure and biogenesis	YmdB	O-acetyl-ADP-ribose deacetylase (regulator of RNase III), contains Macro dom	COG02110	pfam01661	cd02907		1	1	1	1	1	1	1	1	1	1
arCOG00541	J	Translation, ribosomal structure and biogenesis	YSH1	Predicted exonuclease of the beta-lactamase fold involved in RNA processing	COG01236	pfam00753, pfam10996	pfam07521	TIGR03675	1	1	1	1	1	1	1	1	1	6
arCOG00545	J	Translation, ribosomal structure and biogenesis	YSH1	Predicted exonuclease of the beta-lactamase fold involved in RNA processing	COG01236			TIGR04122	1	1	1	1	1	2	1	1	1	6

CELLULAR PROCESSES AND SIGNALING																		
arCOG02263	D	Cell cycle control, cell division, chromosome partitioning	-	Predicted cell division protein, SepF homolog	COG02450	pfam04472			1	1	1	1	1	1	1	1	1	6
arCOG11012	D	Cell cycle control, cell division, chromosome partitioning	ATS1	Alpha-tubulin suppressor and related RCC1 domain-containing proteins	COG05184	pfam13540, pfam00415, pfam00415, pfam00415, pfam00415, pfam00415, pfam00415			1	2	1	1	1	1	1	1	7	3
arCOG04701	D	Cell cycle control, cell division, chromosome partitioning	CrcB/FEX	Integral membrane protein possibly involved in fluoride export and chromosome partitioning	COG00239	pfam02537		TIGR00494	1	1	1	1	1	1	1	1	1	3
arCOG02201	D	Cell cycle control, cell division, chromosome partitioning	FtsZ	Cell division GTPase	COG00206	pfam00091, pfam1232	cd02201	TIGR00065	2	3	1	2	1	1	1	1	2	1
arCOG05007	D	Cell cycle control, cell division, chromosome partitioning	Maf	Nucleotide-binding protein implicated in inhibition of septum formation	COG00424	pfam02545	cd00555	TIGR00172	1	1	1	1	1	1	1	1	2	3
arCOG03061	D	Cell cycle control, cell division, chromosome partitioning	MreB	Actin-like ATPase involved in cell morphogenesis	COG01077	pfam06723	cd10227	TIGR00904	1	1	1	1	1	1	1	1	1	1
arCOG00585	D	Cell cycle control, cell division, chromosome partitioning	Mrp	Mrp family protein, ATPase, contains iron-sulfur cluster	COG00489	pfam10609	cd02037	TIGR01969	1	1	1	1	1	1	1	1	1	3
arCOG00371	D	Cell cycle control, cell division, chromosome partitioning	Smc	Chromosome segregation ATPase	COG01196	pfam02463	cd03278, cd032	TIGR02169	1	1	1	1	1	1	1	1	3	1
arCOG00586	D	Cell cycle control, cell division, chromosome partitioning	Soj	ATPase involved in chromosome partitioning, ParA family	COG01192	pfam01656	cd02042	TIGR03453	1	1	1	1	1	1	1	1	1	1
arCOG02416	N	Cell motility	-	Pilin/Flagellin, FlaG/FlaF family	COG03430	pfam07790			1	1	1	1	1	1	1	1	3	1
arCOG00434	N	Cell motility	-	AAA+ ATPase of MoxR-like family, a component of a putative secretion system	COG00714	pfam07726	cd00009	TIGR02031	2	1	1	2	1	1	1	2	2	3
arCOG02079	N	Cell motility	-	S-layer protein, possibly associated with type IV pili like system	COG01361				1	1	1	1	1	1	1	1	1	1
arCOG02423	N	Cell motility	-	Pilin/Flagellin, FlaG/FlaF family	COG03430	pfam07790			1	1	1	1	1	1	2	1	2	1
arCOG02911	N	Cell motility	-	Predicted pilin/flagellin	SC_00343				1	1	1	1	1	1	1	1	1	1
arCOG02382	N	Cell motility	CheB	Chemotaxis response regulator containing a CheY-like receiver domain and a	COG02201	pfam00072, pfam0133	cd00156	TIGR02875	1	1	1	1	1	1	1	1	1	1
arCOG01819	N	Cell motility	CpaF	Pilus assembly protein, ATPase of CpaF family	COG04962	pfam00437	cd01130	TIGR03819	1	2	1	1	1	1	1	1	1	1
arCOG01829	N	Cell motility	FlaB	Archaeal flagellins	COG01681				1	1	1	1	1	1	1	1	3	1
arCOG02964	N	Cell motility	FlaD	Archaeum protein D/E	COG03351	pfam05377, pfam04659			1	1	1	1	1	1	1	1	2	1
arCOG01824	N	Cell motility	FlaF	Archaeum protein F, flagellin of FlaG/FlaF family	COG03353				1	1	1	1	1	1	1	1	1	1
arCOG01822	N	Cell motility	FlaG	Archaeum protein G, flagellin of FlaG/FlaF family	COG03354				1	1	1	1	1	1	1	1	1	1
arCOG04148	N	Cell motility	FlaH	ATPase involved in biogenesis of archaeum	COG02874	pfam06745	cd01394	TIGR03881	1	1	1	1	1	1	1	1	1	1
arCOG01809	N	Cell motility	FlaJ	Archaeum assembly protein J, TadC family	COG01955				1	1	1	1	1	1	1	1	1	1
arCOG02298	N	Cell motility	Flak/PuLO	Peptidase A24A, prelin protein IV	COG01989	pfam01478, pfam06847			1	1	1	1	1	1	1	2	1	1
arCOG01808	N	Cell motility	TadC	Pilus assembly protein TadC	COG02064	pfam00482, pfam00482			2	2	2	2	2	2	2	2	2	4
arCOG01811	N	Cell motility	TadC	Pilus assembly protein TadC	COG02064				1	1	1	1	1	1	1	1	1	1
arCOG01812	N	Cell motility	TadC	Pilus assembly protein TadC	COG02064				1	3	1	1	1	1	1	1	1	1
arCOG01817	N	Cell motility	VirB11	ATPase involved in archaeum/pili biosynthesis	COG00630	pfam00437	cd01130	TIGR03819	1	1	1	1	1	1	1	1	3	2
arCOG02488	M	Cell wall/membrane/envelope biogenesis	-	Cell surface protein, a component of a putative secretion system	SC_00293				1	1	1	1	1	1	1	1	1	1
arCOG01385	M	Cell wall/membrane/envelope biogenesis	-	Glycosyl transferase family 2	COG00463	pfam00535	cd02522	TIGR04283	1	1	1	1	1	1	1	1	2	3
arCOG05978	M	Cell wall/membrane/envelope biogenesis	-	Extracellular protein containing Kelch and FN3 domains	-	pfam07081			1	2	1	1	1	1	1	1	8	1
arCOG00894	M	Cell wall/membrane/envelope biogenesis	-	Glycosyl transferase family														

Supplementary Table 6. Classification of the unique genes based on the arCOG classification.

arCOG	arCOG classification	gene	product	LUG classification	pFAM domain	cDC	TIGR classification	Number of genes									
								EMBL/CCDS	MGII	BATHY1	BATHY2	chaos	MG2-GG3				
arCOG00415	L	RecA	RecA/RadA recombinase	CG00468	pfam14520.pfam	cd01123	TIGR0236	1									
arCOG00439	L	MCM2	Predicted ATPase involved in replication control, Cdc46/Mcm family	CG01241	pfam14551.pfam	cd00009		1									
arCOG04110	L	PRI1	Eukaryotic-type DNA primase, catalytic (small) subunit	CG01467	pfam01896	cd04860	TIGR0335	1				1		1			
arCOG00787	L	-	UvrD/Rep family helicase fused to exonuclease family domain	CG00287	pfam12705	cd09637	TIGR01249,TIGR0372	1									
arCOG05109	L	DnaQ	DNA polymerase III, epsilon subunit or related 3'-5' exonuclease	CG00847	pfam00929	cd06127	TIGR0573	1									1
arCOG01058	L	Uvr	UV endonuclease	CG00494	pfam13851	cd00056	TIGR0428	1									
arCOG00469	L	HolB	ATPase involved in DNA replication HolB, small subunit	CG00470	pfam13177.pfam	cd00009	TIGR0297	2									1
arCOG01894	L	Nfo	Endonuclease IV	CG00648	pfam01261	cd00019	TIGR0587	2									
arCOG01073	L	-	NUDX family hydrolase	CG00494	pfam00293	cd03424	TIGR0052	2									
arCOG01347	L	CDC9	ATP-dependent DNA ligase	CG01793	pfam04675.pfam	cd07901,cd079	TIGR00574	2									
arCOG00284	L	PhrB	Deoxyribopyrimidine photolase	CG00415	pfam00875.pfam	cd03441	TIGR0556	2									1
arCOG01078	L	-	NUDX family hydrolase	CG00494	pfam00293	cd03428		3		1							1
arCOG00464	L	AlkA	3-methyladenine DNA glycosylase/8-oxoguanine DNA glycosylase	CG00212	pfam07934.pfam	cd00056	TIGR0058	3									1
arCOG01342	L	-	Nuclease of RNase H fold, RuvC/YagG family	CG00468	pfam01751	cd01027		3									1
arCOG01486	L	RnmV	5S rRNA maturation endonuclease (Ribonuclease M5), contains TOPRIM domain	CG00158	pfam01751	cd01027		4		1							1
arCOG00849	L	-	Topoisomerase IIb	CG03569	pfam02919.pfam	cd00660,cd00659		4									1
arCOG00417	L	RecA	RecA/RadA recombinase	CG00468	pfam01751	cd01027		5									
arCOG04367	L	Gyrase	Type IIA topoisomerase (DNA gyrase/Topo II, topoisomerase IV), A subunit	CG00188	pfam00521.pfam	cd00187	TIGR01063	5									2
arCOG00872	L	MPH1	ERCC4-like helicase	CG00187	pfam02158.pfam	cd00075,cd000	TIGR01059	5									2
arCOG00251	L	DnaN	DNA replication initiation complex subunit, GINS15 family	CG01711	pfam00720.pfam	cd00046,cd012		5									1
arCOG00427	L	RecJ/Cdc	Single-stranded DNA-specific exonuclease RecJ	CG00608	-	cd11714		5									1
arCOG00258	L	-	RPA family protein, a subunit of RPA complex in P. furiosus	CG00390	-			5									1
arCOG01166	L	MutL	DNA mismatch repair enzyme (predicted ATPase)	CG00323	pfam13589.pfam	cd00075,cd007	TIGR0585	5									2
arCOG04211	L	RohB	Ribonuclease HII	CG00164	pfam01351	cd07180	TIGR00729	5									2
arCOG00470	L	HolB	ATPase involved in DNA replication HolB, large subunit	CG00470	pfam00004	cd00009	TIGR02397	5									1
arCOG04371	L	Gyrase	Type IIA topoisomerase (DNA gyrase/Topo II, topoisomerase IV), B subunit	CG00187	pfam02158.pfam	cd00075,cd000	TIGR01059	5									1
arCOG00408	L	DnaN	DNA polymerase III, epsilon subunit (PCNA homolog)	CG01711	pfam00720.pfam	cd00057	TIGR0058	5									2
arCOG01527	L	TopA	Topoisomerase IA	CG00550	pfam01751.pfam	cd03362,cd000	TIGR01057	5									1
arCOG04050	L	FEN1	5'-3' exonuclease	CG00258	pfam00752.pfam	cd09867	TIGR03674	5									1
arCOG00558	L	SrmB	Superfamily II DNA and RNA helicase	CG00513	pfam00270.pfam	cd00268,cd000	TIGR01389	5									1
arCOG00328	L	PoIB3	DNA polymerase PoIB3	CG00417	pfam03104.pfam	cd05781,cd055	TIGR00592	5									1
arCOG01510	L	RPA1	Single-stranded DNA-binding replication protein A (RPA), large (70 kD) subunit	CG00159	-	cd04491,cd04491		5									2
arCOG01072	L	-	NUDX family hydrolase	CG00494	pfam00293	cd03426		5									2
arCOG00213	L	PRI2	Eukaryotic-type DNA primase, large subunit	CG00219	pfam01896	cd00056		5									1
arCOG00553	L	RRF2	Release factor superfamily II helicase	CG01204	pfam00270.pfam	cd00046,cd000	TIGR01121	5									3
arCOG01526	L	TopG2	Reverse gyrase	CG00110	pfam00270.pfam	cd00046,cd003	TIGR01054	5									1
arCOG00368	L	SbcC	ATPase involved in DNA repair, SbcC	CG00419	pfam13476.pfam	cd03240,cd001	TIGR00611,TIGR02168	5									1
arCOG00274	L	Ada	Methylated DNA-protein cysteine methyltransferase	CG00150	pfam01035	cd06445	TIGR00589	5									1
arCOG00397	L	SbcD	DNA repair exonuclease, SbcD	CG00420	pfam00149	cd00840		5									1
arCOG00329	L	PoIB2	DNA polymerase PoIB2, inactivated	CG00417	pfam03106	cd05531	TIGR00592	5									1
arCOG00802	L	RecB	ATP-dependent helicase (exonuclease V) beta subunit (contains helicase)	CG00171	pfam00504.pfam	cd01381	TIGR00785	5									2
arCOG02895	L	MutS2	DNA structure-specific ATPase involved in suppression of recombination, MutS2	CG01153	pfam04048	cd03243	TIGR01069	5									1
arCOG04694	L	UvrA	Excinuclease ABC subunit A, ATPase	CG00178	-	cd03271,cd032	TIGR00630	5									3
arCOG00462	L	MuY	A/G-specific DNA glycosylase	CG01194	pfam00730	cd00056	TIGR01084	5									1
arCOG03646	L	XseB	Exonuclease VII small subunit	CG01722	pfam02609		TIGR01280	5									1
arCOG04513	L	XseA	Exonuclease VII, large subunit	CG01570	pfam13742.pfam	cd04489	TIGR00237	5									1
arCOG04754	L	Lig	NAD-dependent DNA ligase	CG00272	pfam1655.pfam	cd00114,cd000	TIGR00575	5									1
arCOG07300	L	-	Uncharacterized protein associated with inactivated PoIB-like polymerase	CG00494	pfam00293	cd02885		5									1
arCOG01082	L	-	NUDX family hydrolase	CG00494	pfam00293	cd02885		5									1
arCOG01305	L	-	Topoisomerase DNA binding C4 zinc finger fused to uncharacterized N-term	CG001637	-			5									1
arCOG02896	L	MutS	Mismatch repair ATPase (MutS family)	CG00249	pfam01624.pfam	cd03284	TIGR01070	5									1
arCOG01981	K	SUA7	Transcription initiation factor TFIIB, Bf1 subunit/Transcription initiation factor	CG01405	pfam08271.pfam	cd00043		5		1							1
arCOG01863	K	-	Predicted transcription factor, homolog of eukaryotic MBF1	CG01813	pfam01381	cd00093	TIGR00270	5									1
arCOG02811	K	-	Predicted transcriptional regulator, contains two HTH domains	CG00398	pfam13412.pfam	cd00090,cd00090		5									2
arCOG07361	K	-	Predicted menkane-associated transcriptional regulator	CG00212	-			5									2
arCOG00770	K	Dmg	Rad3-related DNA helicase	CG01199	pfam06733.pfam	cd13307	TIGR00604	5									2
arCOG09571	K	CsgD	Transcriptional regulator LuxR family	CG002771	-			5									2
arCOG01680	K	ArxR	Transcriptional regulator containing HTH domain, ArxR family	CG00640	pfam01022	cd00090		5									1
arCOG04280	K	NagC	Transcriptional regulator/sugar kinase	CG01940	pfam00480	cd00012	TIGR00744	5									1
arCOG01753	K	Ssh10b	Archaeal DNA-binding protein	CG01581	pfam01918		TIGR00285	5									1
arCOG00579	K	RBP9	DNA-directed RNA polymerase, subunit M/Transcription elongation factor	CG001594	-		TIGR01384	5									1
arCOG01084	K	RBP7	DNA-directed RNA polymerase, subunit E/Rbp7	CG00177	pfam01022	cd00090,cd00090		5									3
arCOG00675	K	RBP8	DNA-directed RNA polymerase, subunit E'/Rbp8	CG01095	pfam01876.pfam	cd04331,cd044	TIGR00448	5									1
arCOG04258	K	RBP5	DNA-directed RNA polymerase, subunit H, RpoH/RBP5	CG002012	pfam01191			5									3
arCOG01580	K	-	DNA-binding transcriptional regulator, Lrp family	CG001522	pfam13412.pfam	cd00090		5									1
arCOG05161	K	WecD	Acetyltransferase (GNAT) family	CG00454	-			5									1
arCOG04111	K	RBP11	DNA-directed RNA polymerase, subunit L	CG001761	pfam13656	cd06927		5									1
arCOG01764	K	SPT15	TATA-box binding protein (TBP), component of TFIID and TFIIB	CG002101	pfam00352.pfam	cd04518		5									1
arCOG02099	K	Tro1	Nuclease-dependent transcriptional regulator (DlxR family)	CG001212	pfam1321.pfam	cd01742,pfam04023		5									1
arCOG02421	K	RpoA/Rpo	DNA-directed RNA polymerase subunit D	CG002020	pfam1193	cd07030		5									1
arCOG02038	K	-	Sugar-specific transcriptional regulator TrmB	CG001378	-			5									1
arCOG02037	K	-	Sugar-specific transcriptional regulator TrmB	CG001378	pfam01978			5									1
arCOG01057	K	HvIR	DNA-binding transcriptional regulator, HvIR family	CG001733	pfam01638	cd00090		5									3
arCOG00608	K	-	Predicted transcriptional regulator with C-terminal CBS domains	CG003620	pfam01381.pfam	cd00093,cd048	TIGR03070,TIGR01137	5									1
arCOG04248	K	SIR2	NAD-dependent protein deacetylase, SIR2 family	CG00846	pfam01246	cd01413		5									1
arCOG04177	K	-	Predicted component of the ribosome quality control (RQC) complex, YbaK	CG004738	-			5									1
arCOG00826	K	WecD	Acetyltransferase (GNAT) family	CG00454	pfam00583	cd04301	TIGR01575	5									1
arCOG02844	K	AcrR	Transcriptional regulator, TetR/AcrR family	CG001309	pfam00440		TIGR03613	5									1
arCOG05152	K	-	Transcriptional regulator, contains HTH domain	-	-			5									1
arCOG02271	K	-	Transcriptional regulator, contains HTH domain	CG003413	pfam04967			5									2
arCOG02274	K																

arCG001308	O	Posttranslational modification, protein turnover, chaperones	Cdc48	ATPase of the AAA-class, CDC48 family	CGG0464	pfam0004.pfam0004	cd00009,cd00009	TIGR01243						3	1
arCG000605	O	Posttranslational modification, protein turnover, chaperones	cSdA	Selenocysteine lyase/Cysteine desulfurase	CGG00250	pfam00266	cd06453	TIGR01979							1
arCG003103	O	Posttranslational modification, protein turnover, chaperones	CtAA	Uncharacterized protein required for cytochrome oxidase assembly	CGG01812	pfam02628			1						1
arCG006880	O	Posttranslational modification, protein turnover, chaperones	DnaI	DnaI-type Zn finger domain	CGG04884								3	1	
arCG002846	O	Posttranslational modification, protein turnover, chaperones	DnaI	DnaI-class molecular chaperone	CGG04884	pfam00226	cd06257	TIGR02349							1
arCG004142	O	Posttranslational modification, protein turnover, chaperones	DYS1	Deoxyhypusine synthase	CGG01899	pfam01916		TIGR00321					1		
arCG004712	O	Posttranslational modification, protein turnover, chaperones	ECM4	Predicted glutathione S-transferase	CGG00435	pfam13409.pfam013409	cd03190								1
arCG001341	O	Posttranslational modification, protein turnover, chaperones	GIM5	Predicted prefoldin, molecular chaperone implicated in de novo protein fold	CGG01730	pfam02996	cd00584	TIGR00293					1	1	
arCG005154	O	Posttranslational modification, protein turnover, chaperones	GroEL	Chaperonin GroEL (HSP60 family)	CGG04549	pfam00118	cd03344	TIGR02348					5		
arCG001257	O	Posttranslational modification, protein turnover, chaperones	GroEL	Chaperonin GroEL, HSP60 family	CGG04549	pfam00118	cd03344	TIGR02339							7
arCG004772	O	Posttranslational modification, protein turnover, chaperones	GrpE	Heat shock chaperone GrpE (heat shock protein)	CGG04549	pfam00118	cd03344	TIGR02348							2
arCG002066	O	Posttranslational modification, protein turnover, chaperones	GrpE	Heat shock chaperone GrpE (heat shock protein)	CGG04549	pfam00118	cd03344	TIGR02348							1
arCG002067	O	Posttranslational modification, protein turnover, chaperones	GrpE	Heat shock chaperone GrpE (heat shock protein)	CGG04549	pfam00118	cd03344	TIGR02348							1
arCG001915	O	Posttranslational modification, protein turnover, chaperones	HHC	Membrane protease subunit, stomatin/prohibitin homolog	CGG00330	pfam01145	cd08826	TIGR01933							1
arCG002959	O	Posttranslational modification, protein turnover, chaperones	Iap	Zn-dependent amino- or carboxypeptidase, M28 family	CGG02334	pfam04389	cd05643								3
arCG004560	O	Posttranslational modification, protein turnover, chaperones	IscA	Fe-S cluster assembly iron-binding protein IscA	CGG00316	pfam01521		TIGR00049							2
arCG002443	O	Posttranslational modification, protein turnover, chaperones	IscY	ABC-type transport system involved in multi-copper enzyme maturation, per	CGG01277	pfam12679			1						1
arCG002438	O	Posttranslational modification, protein turnover, chaperones	IscY	ABC-type transport system involved in multi-copper enzyme maturation, per	CGG01277	pfam12679			1						1
arCG001846	O	Posttranslational modification, protein turnover, chaperones	IscY	ABC-type transport system involved in multi-copper enzyme maturation, per	CGG01277	pfam12679			1						1
arCG000976	O	Posttranslational modification, protein turnover, chaperones	IscY	ABC-type transport system involved in multi-copper enzyme maturation, per	CGG01277	pfam12679			1						1
arCG005850	O	Posttranslational modification, protein turnover, chaperones	IscY	ABC-type transport system involved in multi-copper enzyme maturation, per	CGG01277	pfam12679			1						1
arCG004767	O	Posttranslational modification, protein turnover, chaperones	IscY	ABC-type transport system involved in multi-copper enzyme maturation, per	CGG01277	pfam12679			1						1
arCG001306	O	Posttranslational modification, protein turnover, chaperones	RPT1	ATP-dependent 26S proteasome regulatory subunit	CGG01222	pfam00004	cd00009	TIGR01242							1
arCG000609	O	Posttranslational modification, protein turnover, chaperones	RspP	Membrane-associated protease RspP, regulator of RpoE activity in bacteria	CGG00750	pfam02183	cd06160			1					1
arCG004664	O	Posttranslational modification, protein turnover, chaperones	RspP	Membrane-associated protease RspP, regulator of RpoE activity in bacteria	CGG00750	pfam02183	cd06160			1					1
arCG005081	O	Posttranslational modification, protein turnover, chaperones	Sjpa	FKBP-type peptidyl-prolyl cis-trans isomerase 2	CGG01047	pfam00254	cd00446	TIGR00115							2
arCG005090	O	Posttranslational modification, protein turnover, chaperones	Sjpa	FKBP-type peptidyl-prolyl cis-trans isomerase 2	CGG01047	pfam00254	cd00446	TIGR00115							2
arCG002784	O	Posttranslational modification, protein turnover, chaperones	SRAP	Putative SOS response-associated peptidase YedK	CGG02135	pfam02586									1
arCG003580	O	Posttranslational modification, protein turnover, chaperones	STE14	Putative protein-5-isoprenylcysteine methyltransferase	CGG02020	pfam04191			2						1
arCG001715	O	Posttranslational modification, protein turnover, chaperones	SufB	Cysteine desulfurase activator SufB	CGG00719	pfam01458		TIGR01981					3	1	
arCG007441	O	Posttranslational modification, protein turnover, chaperones	SUR4	Parvulin-like peptidyl-prolyl isomerase	CGG00740	pfam00639									1
arCG002021	O	Posttranslational modification, protein turnover, chaperones	TldD	ATP-dependent protease component of TldD/TldE system	CGG00312	pfam01533									1
arCG003032	O	Posttranslational modification, protein turnover, chaperones	TldE	Inactivated Zn-dependent protease, component of TldD/TldE system	CGG00312	pfam01533									1
arCG006181	O	Posttranslational modification, protein turnover, chaperones	TrxA	Thiol-disulfide isomerase or thioredoxin	CGG00526	pfam00578	cd02966						3	1	
arCG001972	O	Posttranslational modification, protein turnover, chaperones	TrxA	Thiol-disulfide isomerase or thioredoxin	CGG00526	pfam00578	cd02966								1
arCG001929	O	Posttranslational modification, protein turnover, chaperones	XdhC	Xanthine and CO dehydrogenase maturation factor, XdhC/CoxF family	CGG01975	pfam13478									1
arCG002985	T	Signal transduction mechanisms	-	Membrane protein of CAAX superfamily, regulator of anti-sigma factor	CGG02339	pfam13367							3	1	
arCG002967	T	Signal transduction mechanisms	-	NACHT family NTPase fused to HEAT repeats domain	CGG05635	pfam13646.pfam13646							3	1	
arCG001460	T	Signal transduction mechanisms	ROQ1	Serine/threonine kinase involved in cell cycle control	CGG01718	pfam11633	cd05145	TIGR03724							1
arCG004620	T	Signal transduction mechanisms	-	SQU1 heme-binding protein	CGG01718	pfam04832									3
arCG006193	T	Signal transduction mechanisms	-	Signal transduction histidine kinase and PAS domains	CGG00642	pfam1426.pfam0130.cd00130.cd00130	cd00130.cd00130	TIGR00229,TIGR00229,TIGR01386							2
arCG004425	T	Signal transduction mechanisms	Wzb	Protein-tyrosine-phosphatase	CGG00394	pfam01451	cd00115	TIGR02689							1
arCG005374	T	Signal transduction mechanisms	-	GAF domain-containing protein	CGG01956	pfam11385									1
arCG001173	T	Signal transduction mechanisms	RAD55	RecA-superfamily ATPase implicated in signal transduction	CGG04667	pfam06745	cd01124	TIGR03877							2
arCG004453	T	Signal transduction mechanisms	DISA_N	Dialanyl-lysine cyclase (c-di-AMP synthetase), DISA_N domain	CGG01624	pfam02457									1
arCG003798	T	Signal transduction mechanisms	HisG	GAF, PAS/PAC domain containing signal transduction protein	CGG00202	pfam02643									2
arCG001143	T	Signal transduction mechanisms	Apaf1	Serine/threonine protein phosphatase PP2A family	CGG00639	pfam00149	cd00144								1
arCG002391	T	Signal transduction mechanisms	CheY	Rec domain	CGG00784	pfam00072	cd00156	TIGR02154							3
arCG003413	T	Signal transduction mechanisms	CDCL4	Protein-tyrosine phosphatase	CGG02453	pfam00782	cd00047								1
arCG003517	T	Signal transduction mechanisms	-	Formylglycine-generating sulfatase enzyme	CGG01262	pfam12867.pfam03781									1
arCG001992	T	Signal transduction mechanisms	SiXa	Phosphohistidine phosphatase SiXa	CGG02062	pfam00300	cd07067	TIGR00249							2
arCG006801	T	Signal transduction mechanisms	SrKx	Ser/Thr protein kinase RdoA involved in Cpx stress response, Maf Antagonist	CGG02334	pfam01636	cd05153								3
METABOLISM															
arCG002767	E	Amino acid transport and metabolism	-	Metal-dependent membrane protease, CAAX family	CGG01266	pfam02517									3
arCG003600	E	Amino acid transport and metabolism	-	Transglutaminase-like cysteine protease	CGG01305										2
arCG014875	E	Amino acid transport and metabolism	-	Aspartyl protease	-	pfam05618									2
arCG003611	E	Amino acid transport and metabolism	-	Peptidase C1A subfamily	-		cd08546,cd14254								2
arCG007760	E	Amino acid transport and metabolism	-	Peptidase family C25	-	pfam01364									2
arCG004335	E	Amino acid transport and metabolism	-	Aspartate/tyrosine/aromatic aminotransferase	CGG00436	pfam01515	cd00609	TIGR03947							1
arCG001301	E	Amino acid transport and metabolism	-	Aspartate/tyrosine/aromatic aminotransferase	CGG00436	pfam01515	cd00609	TIGR03540							2
arCG002163	E	Amino acid transport and metabolism	-	Transglutaminase-like cysteine protease	CGG01305	pfam01841									1
arCG001131	E	Amino acid transport and metabolism	-	Aspartate/tyrosine/aromatic aminotransferase	CGG00436	pfam01515	cd00609	TIGR01265							1
arCG004044	E	Amino acid transport and metabolism	-	2-amino-3,7-dideoxy-D-threo-6-ulosonic acid synthase, DhnA-aldolase	CGG01830	pfam01791	cd00958	TIGR01949							2
arCG001888	E	Amino acid transport and metabolism	AmpS	Leucyl aminopeptidase (aminopeptidase T)	CGG02309	pfam02073									2
arCG001890	E	Amino acid transport and metabolism	AmpS	Leucyl aminopeptidase (aminopeptidase T)	CGG02309	pfam02073									2
arCG001124	E	Amino acid transport and metabolism	AnaB	L-asparaginase/chaecolysin-III/HRNAIII amidotransferase subunit D	CGG00252	pfam00710	cd08962	TIGR02153							1
arCG008063	E	Amino acid transport and metabolism	Arc	Asparagine synthase (glutamine hydrolyzing)	CGG00367	pfam00733	cd04235	TIGR00746							2
arCG001107	E	Amino acid transport and metabolism	Arc	Asparagine synthase (glutamine hydrolyzing)	CGG00367	pfam00733	cd04235	TIGR01910							1
arCG000912	E	Amino acid transport and metabolism	ArgF	Ornithine carbamoyltransferase	CGG00078	pfam02729.pfam00185		TIGR00658							3
arCG004134	E	Amino acid transport and metabolism	AroA	5-enolpyruvylshikimate-3-phosphate synthase	CGG00275	pfam00275	cd01556	TIGR01356							1
arCG001033	E	Amino acid transport and metabolism	AroE	Shikimate 5-dehydrogenase	CGG00169	pfam08501.pfam01065		TIGR00507							2
arCG001025	E	Amino acid transport and metabolism	AroK2	Archaeal shikimate kinase	CGG01685	pfam00288		TIGR01920							2
arCG000494	E	Amino acid transport and metabolism	Asd	Aspartate-semialdehyde dehydrogenase	CGG00136	pfam1116.pfam02774		TIGR00978							1
arCG001121	E	Amino acid transport and metabolism	AsnB	Asparagine synthase (glutamine hydrolyzing)	CGG00367	pfam00733	cd04235	TIGR01336							1
arCG000771	E	Amino acid transport and metabolism	AsnB	Asparagine synthase (glutamine hydrolyzing)	CGG00367	pfam00733	cd01991	TIGR01536							1
arCG001594	E	Amino acid transport and metabolism	CarB	Carbamoylphosphate synthase large subunit	CGG00458	pfam00289.pfam02786.pfam02786		TIGR01369							2
arCG000073	E	Amino acid transport and metabolism	CysH	PAPS reductase related enzyme fused to RNA-binding PUA domain and ferredoxin	CGG00175	pfam01507	cd01713	TIGR00434							1
arCG001430	E	Amino acid transport and metabolism	CysK	Cysteine synthase	CGG00031	pfam00291	cd01561	TIGR01136							1
arCG000755	E	Amino acid transport and metabolism	DadA	Glycine/D-amino acid oxidase (deaminating)	CGG00665	pfam01266									2
arCG001646	E	Amino acid transport and metabolism	DAD2	Dipeptidyl aminopeptidase/acylaminoacyl-peptidase	CGG01506	pfam07859	cd00312								8
arCG001089	E	Amino acid transport and metabolism	DadH	Diaminopyruvate decarboxylase or related enzyme	CGG02274	pfam02274		TIGR01078							1
arCG005395	E	Amino acid transport and metabolism	FtdC	Forminostyrylhydrolase/cyclodextrinase	CGG03404										1
arCG000915	E	Amino acid transport and metabolism	GabT	4-aminobutyrate aminotransferase or related aminotransferase	CGG00160	pfam00202	cd00610	TIGR00707							1
arCG001303	E	Amino acid transport and metabolism	GcvH	Glycine cleavage system H protein (lipoate-binding)	CGG00509	pfam01597	cd06848	TIGR00527							

Supplementary Table S7. Genes found in MG-III Metabolic Pathways

	Epipelagic MG-III	Bathy1	Bathy2
Glycolysis			
hexokinase (glk)	--	--	--
phosphoglucosomerase (pgi)	X	X	X
phosphofruktokinase (pfkA)	X	--	--
aldolase (fba/dhnA)	X	X	X
triosephosphate isomerase (tpi)	X	X	--
glyceraldehyde 3-phosphate dehydrogenase (gapA)	X	X	X
3-phosphoglycerate kinase (pgk)	X	X	X
phosphoglyceromutase (pgm/yibO)	X	X	--
enolase (eno)	X	X	--
pyruvate kinase (pykA)	--	--	--
Gluconeogenesis			
phosphoenolpyruvate synthase (ppsA)	X	X	X
enolase (eno)	X	X	--
phosphoglyceromutase (pgm)	X	--	--
3-phosphoglycerate kinase (pgk)	X	X	X
glyceraldehyde 3-phosphate dehydrogenase (gapA)	X	X	X
triosephosphate isomerase (tpi)	X	X	--
aldolase (fba/dhnA)	X	X	X
fructose bisphosphatase (suhB)	X	X	X
phosphoglucosomerase (pgi)	X	X	X
Pentose phosphate shunt and pentose biosynthesis			
glucose-6-phosphate dehydrogenase (zwf)	--	--	--
6-phosphogluconate dehydrogenase (gnd)	--	--	--
transketolase (tktA)	X	X	X
transaldolase (talA)	--	--	--
pentose-5-phosphate-3-epimerase (yhfD)	X	X	--
ribose 5-phosphate isomerase (rpiA)	X	X	X
deoxyribose-phosphate aldolase (deoC)	--	--	--
Entner–Doudoroff pathway			
glucose-6-phosphate dehydrogenase (zwf)	--	--	--
6-phosphogluconate dehydratase (edd)	--	--	--
2-keto-3-deoxy-6-phosphogluconate aldolase (eda)	--	--	--
TCA cycle			
citrate synthase (gltA)	X	X	--
aconitase (acnA)	X	X	X
isocitrate dehydrogenase (icd)	X	--	--
a-ketoglutarate dehydrogenase (sucA, sucB)	X	--	--
succinyl-CoA synthase (sucC, sucD)	X	X	--
fumarate reductase (frdA, frdB)	X	--	--
fumarase (fumA)	X	X	X
malate dehydrogenase (mdh)	X	X	--
Purine biosynthesis			
phosphoribosylpyrophosphate synthase (prsA)	X	X	X
amidophosphoribosyltransferase (purF)	X	X	X
GAR synthase (purD)	X	X	--
GAR transformylase (purN/purT)	X	X	X
FGAM synthase (purL)	X	X	X
AIR synthase (purM)	X	X	X
NCAIR synthase (purK)	--	--	--
NCAIR mutase (purE)	X	--	X
SAICAR synthase (purC)	X	X	--
adenylosuccinate lyase (purB)	X	X	X
AICAR transformylase (purH2)	X	X	X
IMP cyclohydrolase (purH1)	X	X	X
adenylosuccinate synthase (purA)	X	X	--
IMP dehydrogenase (guaB)	X	--	X
GMP synthase (guaA)	X	X	--
Pyrimidine biosynthesis			
carbamoylphosphate synthase (carA, carB)	X	--	X
aspartate carbamoyltransferase (pyrB)	X	X	--
dihydroorotase (pyrC/ygeZ)	--	--	--
dihydroorotate dehydrogenase (pyrD)	X	X	X
orotate phosphoribosyl-transferase (pyrE)	X	X	X
orotidine-5'-phosphate decarboxylase (pyrF)	X	--	--
UMP kinase (pyrH)	--	--	--

	NDP kinase (ndk)	X	X	X
	CTP synthase (pyrG)	X	X	--
Histidine biosynthesis				
	phosphosphoribosylpyrophosphate synthase (prsA)	X	X	X
	ATP-phosphoribosyltransferase (hisG)	--	--	--
	phosphoribosyl-ATP pyrophosphatase (hisI2)	--	--	--
	phosphoribosyl-AMP cyclohydrolase(hisI1)	--	--	--
	58-ProFAR isomerase (hisA)	--	--	--
	imidazoleglycerol phosphate synthase (hisH, hisF)	--	--	--
	imidazoleglycerol phosphate dehydratase (hisB2)	--	--	--
	histidinoll phosphate aminotransferase (hisC)	X	X	--
	histidinol phosphatase (hisB1)	--	--	--
	histidinol dehydrogenase (hisD)	--	--	--
Branched chain amino acids biosynthesis				
	threonine deaminase (ilvA)	X	--	X
	acetoxyhydroxyacid synthase (ilvB, ilvN)	--	X	--
	acetoxyhydroxyacid isomeroeductase (ilvC)	--	--	--
	dihydroxyacid dehydratase (ilvD)	--	--	--
	2-isopropylmalate synthase (leuA)	--	--	--
	isopropylmalate isomerase (leuC, leuD)	--	--	--
	3-isopropyl-malate dehydrogenase (leuB)	--	--	--
	glutamate transaminase (ilvE)	X	X	--
Aromatic amino acids biosynthesis				
	3-deoxyheptulosonate 7-phosphate synthase (aroG/kdsA)	--	--	--
	3-dehydroquininate synthase (aroB)	--	--	--
	3-dehydroquininate dehydratase (aroD)	--	--	--
	shikimate dehydrogenase (aroE)	--	--	--
	shikimate kinase (aroK)	--	--	--
	5-enolpyruvoylshikimate 3-phosphate synthase (aroA)	--	--	--
	chorismate synthase (aroC)	--	--	--
	chorismate mutase (pheA1)	--	--	--
	prephenate dehydratase (pheA2)	--	--	--
	prephenate dehydrogenase (tyrA2)	--	--	--
	tyrosine aminotransferase (tyrB)	--	--	--
	antranilate synthase (trpD1, trpE)	--	--	--
	antranilate phosphoribosyl-transferase (trpD2)	--	--	--
	phosphoribosylantranilate isomerase (trpC2)	--	--	--
	indole-glycerol phosphate synthase (trpC1)	--	--	--
	tryptophan synthase (trpA, trpB)	X	--	--
Threonine biosynthesis				
	aspartokinase (thrA1)	--	--	--
	aspartate semialdehyde dehydrogenase (asd)	--	--	--
	homoserine dehydrogenase (thrA2)	--	--	--
	homoserine kinase (thrB)	--	--	--
	threonine synthase (thrC)	--	--	--
Methionine biosynthesis				
	aspartokinase (metL1)	--	--	--
	aspartate semialdehyde dehydrogenase (asd)	--	--	--
	homoserine dehydrogenase (metL2)	--	--	--
	homoserine transsuccinylase (metA)	--	--	--
	cystathionine g-synthase (metB)	X	X	X
	b-cystathionase (metC)	--	--	--
	methionine synthase (metE/metH)	--	--	--
Arginine biosynthesis				
	acetylglutamate synthase (argA2)	--	--	--
	acetylglutamate kinase (argB)	X	--	--
	acetylglutamate phosphate reductase (argC)	--	--	--
	acetylornithine aminotransferase (argD)	X	--	--
	acetylornithinase (argE)	X	--	--
	ornithine carbamoyltransferase (argF)	X	X	--
	argininosuccinate synthase (argG)	--	--	--
	argininosuccinate lyase (argH)	--	--	--
NAD biosynthesis				
	aspartate oxidase (nadB)	--	--	--
	quinolinate synthase (nadA)	X	X	--
	quinolinate phosphoribosyltransferase (nadC)	X	X	--
	nicotinic acid mononucleotide adenyltransferase (nadD)	--	--	--
	deamido-NAD ammonia ligase (nadE)	X	X	X

Riboflavin biosynthesis				
	GTP cyclohydrolase II (ribA)	X	X	--
	pyrimidine deaminase (ribD1)	--	--	--
	pyrimidine reductase (ribD2)	X	X	X
	3,4-dihydroxybutanone-4-phosphate synthase (ribB)	X	X	--
	6,7-dimethyl-8-ribityllumazine synthase (ribE)	X	X	--
	riboflavin synthase (ribC)	X	X	--
Siroheme biosynthesis				
	Glutamyl-tRNA reductase (hemA)	--	--	--
	glutamate 1-semialdehyde aminotransferase (hemL)	--	--	--
	probilinogen III synthase (hemB)	--	--	--
	hydroxymethylbilane synthase (hemC)	--	--	--
	uroporphyrinogen III synthase (hemD)	--	--	--
	uroporphyrinogen methyltransferase (cysG2)	--	--	--
	dimethyluroporphyrinogen III dehydrogenase (cysG1)	--	--	--
Cobalamin biosynthesis				
	uroporphyrinogen III methylase (cysG2)	--	--	--
	precorrin-2 methylase (cbiL)	--	--	--
	precorrin-3B methylase (cbiH)	--	--	--
	precorrin-4 methylase (cbiF)	--	--	--
	precorrin-6A reductase (cbiJ)	--	--	--
	precorrin 6B methylase (cbiE)	--	--	--
	precorrin 6B decarboxylase (cbiT)	--	--	--
	precorrin-8x isomerase (cbiC)	--	--	--
	cobyric acid a,c-diamide synthase (cbiA)	--	--	--
	cobalt insertion protein (cobN)	--	--	--
	cob(I)alamin adenosyltransferase (cobA)	--	--	--
	cobyric acid synthase (cbiP)	--	--	--
	cobyric acid aminotransferase (cobD)	--	--	--
	cobinamide synthase (cbiB)	--	--	--
	nicotinate-nucleotide:dimethylbenzimidazole phosphoribosyltransferase (cobT)	--	--	--
	cobalamin synthase (cobS)	--	--	--
Biotin biosynthesis				
	pimeloyl-CoA synthetase (bioW)	--	--	--
	7-keto-8-aminopelargonate synthetase (bioF)	X	X	--
	7,8-diaminopelargonate aminotransferase (bioA)	--	--	--
	dethiobiotin synthetase (bioD)	--	--	--
	biotin synthetase (bioB)	--	--	--
	biotin-[acetyl-CoA carboxylase] holoenzyme synthetase (birA)	X	X	X

Cells marked with a "X" means that the protein was found.